

Combined few-body and mean-field model for nuclei

D Hove¹, E Garrido^{2,‡}, P. Sarriguren², D.V. Fedorov¹, H.O.U. Fynbo¹, A.S. Jensen¹, N.T. Zinner^{1,3}

¹ Department of Physics and Astronomy, Aarhus University, DK-8000 Aarhus C, Denmark

² Instituto de Estructura de la Materia, IEM-CSIC, Serrano 123, E-28006 Madrid, Spain

³ Aarhus Institute of Advanced Studies, Aarhus University, DK-8000 Aarhus C, Denmark

E-mail: e.garrido@csic.es

Abstract. The challenging nuclear many-body problem is discussed along with classifications and qualitative descriptions of existing methods and models. We present detailed derivations of a new method where cluster correlations co-exist with an underlying mean-field described core-structure. The variation of an antisymmetrized product of cluster and core wave functions and a given nuclear interaction, provide sets of self-consistent equations of motion.

First we test the technique on the neutron dripline nucleus ^{26}O , considered as ^{24}O surrounded by two neutrons. We choose Skyrme effective interactions between all pairs of nucleons. To ensure correct asymptotic behavior we modify the valence neutron-neutron interaction to fit the experimental scattering length in vacuum. This is an example of necessary considerations both of effective interactions between in-medium and free pairs, and renormalizations due to restrictions in allowed Hilbert space.

Second, we investigate the heavier neutron dripline nucleus ^{72}Ca , described as ^{70}Ca plus two neutrons. We continuously vary the strength of the Skyrme interaction to fine-tune the approach to the dripline. Halo structure in the s -wave is observed followed by the tendency to form Efimov states. Occurrence of Efimov states are prevented by the exceedingly unfavorable system of two light and one heavy particle. Specifically the neutron-neutron scattering length is comparable to the spatial extension of a possible Efimov state, and scaling would place the next of the states outside our galaxy.

Our third application is on the proton dripline nucleus ^{70}Kr , described as ^{68}Se plus two protons, which is a prominent waiting point for the astrophysical rp -process. We calculate radiative capture rates and discuss the capture mechanism as being either direct, sequential, virtual sequential or an energy dependent mixture of them. We do not find any 1^- resonance and therefore no significant $E1$ transition. This is consistent with the long waiting time, since both $E2$ and background transitions are very slow.

After the applications on dripline nuclei we discuss perspectives with improvements and applications. In the conclusion we summarize while emphasizing the merits of consistently treating both short- and large-distance properties, few- and many-body correlations, ordinary nuclear structure, and concepts of halos and Efimov states.

Submitted to: *J. Phys. G: Nucl. Part. Phys.*

‡ Author to whom any correspondence should be addressed

1. Introduction

The present report describes methods formulated for applications on the low-energy nuclear many-body problem. Many techniques have over the years been developed for that purpose. Some methods were designed before computers were available, while some are recent creations using powerful computers. The physical insight obtained over the years from simple analytical models are now used in extensive numerical calculations. We shall here first recall a number of the challenges of the multifaceted many-body nuclear physics. Then get down to the somewhat more dedicated purpose of the present work, and finally describe the report structure.

1.1. Status of the nuclear challenge

The constituents of nuclei are first of all neutrons and protons, which throughout this report shall be treated as either structureless point-like particles or equivalently with frozen inert intrinsic structure. Nuclear physics is concerned with the many-body nucleon problem. The properties are basically governed by the short-range strong interaction [1, 2], which in turn originates and is characterized through the non-perturbative theory of low-energy quantum chromodynamics (QCD) [3]. One (often minor) complication is that the protons are charged implying modification from the associated long-range Coulomb interaction [4]. Another implication is that the energy must be relatively low to avoid intrinsic nucleonic excitations occurring at 140 MeV when the pion can be created. Thus, we shall consider here low-energy properties [5] only.

The meaning of “many nucleons” is a number between 2 and 300 for the more or less ordinary nuclei of interest in the present report, up to about 1000 if non-stable exotic toroidal systems are also considered, and 10^{55} if also nuclear structure in neutron stars are included. Clearly then few-body physics must be part of our complete descriptions. In addition, our many-body treatment has to apply for the relatively low number of a few hundred, somewhat in contrast to the genuine many-body physics problems in solid state and condensed matter physics.

The basic theoretical tool is quantum theory which is unavoidable due to the microscopic characteristics. On top the fermionic nature of neutrons and protons requires quantum statistics to obey the Pauli exclusion principle for each of these types of nucleons [6]. Nuclear physics with these two non-identical, but very similarly interacting, constituents is unique and gives rise to the concept of isospin. The corresponding symmetry is slightly broken in nuclei but used abundantly in particle physics.

Many nuclear properties can surprisingly be explained by macroscopic physics concepts, like the liquid drop model or similar elaborate extended modifications [7]. The level of accuracy from these models is roughly between 5% and 10%, whereas the remaining few percents are overwhelmingly decisive for both the present level of understanding and the derived properties. The mixture of micro- and macroscopic properties extends even further, since nuclear densities fall off from maximum to zero

over surface widths of about 2 fm corresponding roughly to the range of the strong interaction. Such leptodermous (thin skin) systems [7] are characteristic for mesoscopic systems where the surface and finite size have significant influence on the acquired properties.

The models to account for all these features can be searched for by measuring the nucleon mean-free path at low energy within nuclei. The result of roughly 5 fm is comparable with the radii of medium heavy nuclei, and therefore almost explicitly announcing that neither mean-field nor strongly correlated structures can alone be responsible for nuclear properties [2]. Thus, efficient nuclear models must be able to describe mean-field single particle motion, macroscopic collective modes, and various correlated structures. These requirements are further emphasized by noting that nuclear reaction and decay times vary from the age of the Universe and down to 10^{-22} seconds [8].

The status at present in the few-body limit is that full and accurate ab-initio calculations are possible and carried out for nucleon numbers less than 10–15. Even here co-existing correlations are exceedingly difficult to describe, like cluster structure within disparate background structure exemplified by the Hoyle state in ^{12}C [9, 10, 11, 12]. The efficient first principle methods known from quantum chemistry [13, 14] can not be directly adopted, as they are built around the idea of a perturbative description of the relevant effective interactions. This is a huge difference as the strong nuclear interaction originates in the low-energy QCD, where, however, the inherent non-perturbativity only is the tip of the iceberg with regards to complications.

Treating heavier nuclei with more than 20 particles requires more assumptions and approximations. The simplest description of average properties is obtained by use of preferentially self-consistent mean-field calculations. More elaborate and perhaps more ambitious theories are abundantly formulated, but implementations always rely on various types of approximations, where almost all can be referred to a restriction on the available Hilbert space. A general description of such approximations is that some of the particles are constrained in frozen cluster structures while others are allowed to move freely.

It is clear that nuclear physics poses daunting challenges, and great ingenuity is needed to make any progress within the subject. However, as a reward for attempting to overcome these challenges, nuclear physics also provides a unique insight into the fields of many-body quantum physics, as well as the nature of both the strong and the weak interaction. Furthermore, due to the general nature of the problem, the lessons can also be useful in other subfields of physics. In any case we shall in this report describe our own scheme of approximations dedicated to our immediate goals, that is especially to describe cluster correlations emerging from a background of uncorrelated nucleons.

1.2. Requirements and purpose

Given the many facets of nuclear physics, it is not surprising that no single theory can encompass all the complexities of the field. As such the various methods for approaching and describing nuclear systems more often complements, than replaces, each other. However, one can propose a number of characteristics that an ideal model should possess based on the fundamental challenges within the field. We limit ourselves to low-energy properties where the building blocks are assumed to be nucleons. The model should be able to describe single-particle properties and cluster correlations, as well as being scalable and computational efficient to allow applications on both light and heavier nuclei.

In addition, as any observation will be at large distances compared to the size of the system, it is also vitally important to associate the observed and necessarily large-distance behavior reliably and consistently with the short-distance nature of the system in question. In other words, it is necessary to have a wave function consistently describing from spatially compact to extended configurations. In particular, the long-range, observable, asymptotic behavior (scattering length, energy levels, and so on) must be correct. Ideally such a wave function should be found with an interaction derived from basic nucleon-nucleon properties, but not necessarily the same although still also obeying the decisive phenomenologically observed properties.

In this connection, the importance of spatially extended and weakly bound configurations are in particular apparent in relation to the concept of universality in connection with halo formation and decay, and the extreme of Efimov physics. Both phenomena appear in nuclei and nuclear astrophysics, as well as in cold atomic and molecular gases. To describe properties of such weakly bound nuclear systems is currently one of the prevailing limitations for many models. Not only in relation to halo [15] and Efimov physics [16], but also in relation to dripline nuclei. In addition, computational requirements are also a significant constraint for many of the more popular methods. Of course, these problems are closely related, as the size of the needed basis drastically increases with the nucleon number. The more complicated the description of the small-distance structure, the more computationally demanding the extension to larger distances becomes. A desirable method would provide a fairly simple consistent and detailed description of both small and large distances

The purpose of this report is to present the details of a new method, which incorporates several of these requirements, and which is particularly well suited for describing weakly bound, extended systems. A new, efficient, and flexible method for combining few- and many-body treatments of relative and intrinsic degrees-of-freedom of the constituent particles in a complex system is derived in detail and applied to several topical nuclear systems. A structure consisting of a few potentially many-body clusters is imposed, and a wave function for the entire system based on the individual clusters and the overarching few-body structure is established. By performing a variation of the energy with respect to both cluster and three-body wave functions, a series of

coupled Schrödinger equations can be derived. They consist of a many-body equation for each cluster, which can be solved self-consistently, and a few-body equation where the traditionally phenomenological two-body potentials instead are derived from the many-body equations combined with the related effective nucleon-nucleon interaction.

This implementation has the advantage of being conceptually very simple. In principle, all that is needed is to settle on a many-body and a few-body formalism, and perform a variation. This technical implementation of few- and many-body formalisms including the necessary interactions are related but not separate. The benefit of this, from a practical point of view, is that the flexibility and versatility of the few-body approach is maintained, along with the detailed insight provided by the many-body model, while the computational complexity is not significantly greater than the sum of the parts. In addition, the ambiguity often associated with phenomenological few-body methods is eliminated, or at least pushed to the next level of the hierarchy, as all interactions in principle are produced within the same framework.

1.3. Report structure

The previous subsections outlined the general challenges inherent to the field of nuclear physics, and it also gave an outline of some desirable characteristics in a model applicable to the low-energy nuclear many-body problem. In addition, our general purpose for introducing a new method was stated, along with a short overview of how this method is formulated. This should enable the reader to place the present method among the many variants within the myriads of other attempts to formulate the techniques to solve (aspects of) the nuclear many-body problem.

Sec. 2 contains classifications and qualitative outlines of several already existing methods and models. The focus is on selected few methods, which are either distinguished by their historical significance, general popularity, or accuracy and usability. An in-depth review of each will not be presented, instead the key concepts and assumptions will be presented and discussed along with the primary strengths and weaknesses. Even such a review can never be fully exhaustive, but the intention is that it should provide the interested reader with a general overview, along with key references for origin and further explorations.

Afterwards, in Sec. 3, the detailed derivation of our method is presented. This is divided in two parts, where the first part in Sec. 3.1 contains a general derivation, where as few choices and assumptions as possible are made. This is continued in Sec. 3.2 by specific derivation with more assumptions, where selected mean-field and three-body formalisms are chosen along with a specific type of nucleon-nucleon interaction.

The technicalities of the implementation are presented in Sec. 4. This includes both the method of solving the main equations, along with the differences of this work from the more traditional many-body and few-body methods. Practical considerations and the crucial implementation of the Pauli principle are described. In addition, some of the subtleties related to incorporating the new effective interactions in the three-body

formalism are discussed.

The implementation on realistic examples is crucial and used to test applicability, accuracy, and efficiency. In Secs. 5 to 7 the focus is on the neutron dripline nuclei ^{26}O and ^{72}Ca , as well as the proton dripline nucleus ^{70}Kr . The ^{26}O -nucleus is an ideal initial test case on the neutron dripline due to its double magic structure [17] with a spherical ^{24}O -core surrounded by two valence neutrons [18, 19, 20]. This is also at the limit of what is currently experimentally feasible, and it has received much attention recently [19, 18, 21].

However, the method is not limited to light nuclei, and in the present formulation is directly applicable to any system where a mean-field calculation can produce a self-consistent solution. The application illustrated by ^{72}Ca in Sec. 6 is of special interest. The s -state near the unbound threshold provides optimal conditions for pronounced halo structures and possibly Efimov states. This potential occurrence of Efimov states, or very large halo states, has caused the heavy calcium isotopes to receive increased attention recently [22]. For such heavy systems, traditional clusterized few-body techniques seem problematic, as they tend to neglect the internal structure of the clusters. This is not in any way a problem here, where the internal core structure is fully incorporated.

Practical astrophysical applications are demonstrated in Sec. 7 by application to the ^{70}Kr ($^{68}\text{Se} + p + p$) nucleus, where the primary focus is on the two-proton radiative capture on ^{68}Se . This has a significant influence on the effective lifetime of ^{68}Se in stellar environments, and is therefore central to the understanding of the rapid proton (rp) capture process.

The specific applications described in details are supplemented with a discussion of possible future improvements and generalizations in Sec. 8. Particular attention is devoted to achieve full consistency between core and cluster interactions as well as improvements of both the mean-field core-description and the adiabatic few-body expansion related to the cluster-core potential. The many detailed derivations and formula are relegated to appendices. Finally, Sec. 9 briefly summarizes the report and presents our conclusions from the work.

2. The nuclear many-body problem for pedestrians

The theories are necessarily microscopic and quantum mechanical, that is, based on the Schrödinger equation. The properties of the systems are contained in the resulting wave function and derived through expectation values. Nuclear properties require an underlying interaction which on some level has to be phenomenologically determined. This corresponds immediately to an uncertainty in the initial input. Addressing the many-body problem implies that approximations to the ideal procedure must be adopted. These two points of input and method are intertwined in the sense that a given approximate procedure dictates, or at least constrains, the parameterization or form of the interaction.

We shall here mostly be concerned with the design of a suitable method, while the interaction is chosen to match the method in each of the formulations. We shall first discuss how interactions and degrees-of-freedom are related. Then we shall qualitatively sketch how the nuclear many-body problem has been attempted to be solved in previous formulations. Assuming the interaction is known, at least two approaches have been tried. One is to formulate a brute force method, which along with progress has been approximated to allow practical implementation. The principle example is the shell model in various formulations and approximations.

Another approach is to focus on the physics quantities of interest and select and treat the corresponding much fewer degrees-of-freedom. Improvements are then achieved iteratively by adding, perhaps approximately, more degrees-of-freedom. The two approaches (from few towards many and vice versa) should ideally coincide in some region of parameter space. Combinations of (approximate) full treatment and selected degrees-of-freedom are both possible and desirable in nuclear physics. An example could be cluster models where relative and intrinsic degrees-of-freedom are treated differently.

We shall sketch some methods in a little more detail. This provides perspective on advantages and disadvantages as well as prizes for the efforts of different methods. We shall point out a number of places for improvements of the methods and the related interactions. However, first we address the crucial issue of how interaction and Hilbert space are tied together.

2.1. Interaction versus Hilbert space

The focus on selected degrees-of-freedom must be the first consideration in investigations of a physics problem. This is almost equivalent, or at least immediately leads, to choice of Hilbert space in the subsequent theoretical formulation. The next question in low-energy hamiltonian based quantum mechanics is to find the interactions between the constituents described by the chosen degrees-of-freedom.

2.1.1. Basic ideas. The obvious starting point is to isolate two constituents from the environment in the total system of interest, and find the interaction by experimental or theoretical phenomenological considerations. Direct use of such interactions for many particles in the restricted Hilbert space can unfortunately be a very misguided suggestion. The actual interactions are influenced by space restrictions as seen by considering motion in an accelerated coordinate system or on a curved surface in ordinary three dimensional space. The general acceptance of effects arising from motion in a restricted Hilbert space leads to the concept of effective interactions [23, 24]. The formulation due to Feshbach is to eliminate undesired parts of the Hilbert space and in the remaining space obtain a more complicated interaction perhaps even with an imaginary (non-unitary) part.

It can be mathematically demonstrated that appropriately renormalized effective interactions in the restricted space formally provide the same correct solution of

energy and wave function as unrestricted interactions in the complete Hilbert space [23, 24]. It is then a matter of using the effective interaction corresponding precisely to the chosen restricted Hilbert space. The problem is that the proper transformation between complete and restricted solutions only is fully defined in terms of the complete (unknown) solution. However, approximations, guesses or iterations in the procedures have over the years been successfully employed to get closer to the correct answers. The same approximately known transformation operators must be applied to calculate observable quantities. The procedures are easily very elaborate and often too complicated to be fully implemented, and truncations become unavoidable.

These rather abstract considerations can be illustrated by well known examples like a nuclear few-body system with valence particles(s) outside a spherical nuclear core [2]. The Coulomb interaction between the core and the valence particle should be either absent for neutrons or determined by the known charge for the protons. However, the core is in reality polarized by the short-range nuclear interaction. The effect in the restricted (core-nucleon) space can be parameterized through a finite non-negligible effective charge of the valence neutron(s) and a modified charge of the protons [2]. Another well-known example is the Skyrme-type of effective interactions used in mean-field Slater determinantal restricted solutions, as we shall see throughout this article.

2.1.2. Effective field theory. The phenomenological parameterization of the effects is in many cases replaced by formal and systematic derivations with much more controllable errors. The prominent example is effective field theory [25, 26, 27], where the overall key properties again are that the physics of interest is related to degrees-of-freedom, approximately decoupled from all other sets. This has always been used throughout physics as evidenced by examples ordered in hierarchies: molecules, atoms, nuclei, nucleons, quarks and gluons. Each level can be approximately described by use of the related degrees-of-freedom and a corresponding theoretical description, that is an effective theory. The quantities revealing this possibility are energies or length scales ordered in classes according to size. The small parameters are assumed to be zero and the larger parameters are infinitely large. The adjective “field” refers to the formulation as a field theory.

The present level of applications is interacting nucleons in bound or low-energy continuum nuclear states [28]. The length and energy scales are about 1 fm and 140 MeV, corresponding respectively to the nucleon size and the pion mass, m_π , in energy units. Thus the theory aims at describing corresponding properties larger than the nucleon radius and of lower energies, E , where the pion cannot be produced. The theory then order interactions in powers of energy divided by pion mass, $(E/(m_\pi c^2))^n$, where c is the velocity of light. The leading order, LO , corresponds to $n = 0$, next to leading order, NLO , has $n = 1$, next to next to leading order, N^2LO has $n = 2$, etc. as $N^n LO$.

The leading order results already give indications, but is far from sufficient for present days applications where accuracy demands require at least $n = 2$. One more order, $n = 3$, seems to provide converged results although indications are that $n = 4$

also gives significant contribution in accuracy calculations. Each order introduces a number of new terms where all strengths, except one, are fully determined by preceding orders. The strength of this new term has a free parameter left for phenomenological determination. Each order also introduces a higher order multi-body interaction which for higher than (or equal to) three-body character are neglected under the expectation that it is insignificant.

The advantages are that the correct symmetries from QCD are maintained, and the method is systematic and in principle controllable to any order required. Clearly, practical and precise formulations must be preceded by selection of the level in the hierarchy and the corresponding active degrees-of-freedom. It is in principle possible to include more than four orders in a more complete theory, but this may be unnecessary and certainly more difficult. Once the form and strengths of the interactions are derived and determined, the applications still need to decide on a method to solve the many-body problem of interest. We shall sketch possibilities in the next subsections. Practical complications involving spin and angular momenta are present as always in nuclear physics. The applications are limited to few particles and therefore to light nuclei.

2.2. The shell model concept

The analogs to the atomic electrons in their orbits around the nucleus are that the nucleons also can be envisaged to move in single-particle orbits [29, 30, 31]. Since an analogous attractive center is non-existent, a potential created by the other nucleons must be responsible for these orbits. With the related single-particle states and given two-, three-, and N -body interactions [32, 33, 34], a method to solve the nuclear many-body problem is easily formulated.

First choose a complete basis for the single-particle states, which not necessarily are derived from the above hypothetical single-particle orbits. Then construct a complete basis for the N -body nuclear system, and compute and diagonalize the corresponding hamiltonian matrix. This is easily expressed but in practice usually impossible because the necessary matrix size is insurmountably huge. A variety of approximations have been employed over the years.

2.2.1. Non-interacting shell model. The simplest and first attempts are to avoid calculations while guessing the average potential responsible for the single-particle motion [35]. The temptation here is obviously to use analytically solvable models, where the square well and harmonic oscillator are traditional choices. The square well is of finite range extending to its radius and therefore zero at large distances as known for the short-range nuclear forces. It is most appropriate for medium and heavier nuclei. The harmonic oscillator never decreases to zero at large distances, but for bound states it is remarkably successful for lighter nuclei due to rather accurate reproduction of the potential at the decisive intermediate distances.

Modifications of the oscillator to allow broader applications on heavy and deformed

nuclei were also extremely successful [2, 36]. As soon as computers were available, the more realistic Woods-Saxon potential resembling the square well with smooth edges was, and still is, abundantly used. These non-interacting shell models are clearly only as good as the guesses. Nevertheless, essentially all stable nuclear structures were discovered with such phenomenological models. However, surprises or unexpected tendencies can not be correctly predicted as desired for unknown and unstable nuclei. The Pauli principle is in all these cases accounted for by allowing only single occupancy of levels by identical neutrons and protons.

2.2.2. Self-consistent mean-field models. One major step beyond guessing forms of the potential is to assume an interaction, usually of two-body character, and a product of neutron and proton Slater determinants. Minimizing the energy by varying the single-particle wave functions produce the non-linear Hartree-Fock equations with solutions of both average potential and corresponding single-particle wave functions [37]. The solutions are self-consistent in the sense that the particles move in orbits from a potential created by themselves. The predictive power of this procedure is far better than from the potentials found by guesses based on properties of known stable nuclei.

The product wave function has by definition no correlations and consequently is only directly able to provide meaningful average values of observables. The all too obviously missing pair correlations are therefore on top included in the BCS approximation or better by self-consistent calculations of the pair field in the Hartree-Fock-Bogoliubov scheme [38]. The crucial interactions are left as phenomenological input adjusted to reproduce a number of essential observables for example of selected (often spherical double magic) nuclei.

The product character of the single-particle wave functions expresses that the particle states only are related through the average potential. These models are therefore denoted independent particle models. Now-a-days the same type of calculations are instead denoted density functional theory [39, 40], where the only difference is the procedure to choose the interactions. The same form of the interactions are parameterized to reproduce properties much closer to the basic nucleon-nucleon interaction, but the philosophy remains unchanged. This implies that the mean-field, if allowed, may turn out to be deformed with the usual problem of violation of angular momentum conservation. The remedy is variation before or preferentially after projection of angular momentum.

To keep the perspective it is worth emphasizing that the bulk properties of nuclei are described by the continuous liquid drop, or rather the droplet models. The quantum features of the independent particle models are modifications on top of this classical model. The effects in absolute terms are often relatively small but all decisive for the applications, let alone the understanding. However, this suggests that the underlying independent particle model interactions are constrained by bulk (nuclear matter) properties like saturation energy and density, compressibility, asymmetry energy, surface tension. The semi-classical model, with extended Thomas-Fermi approximations for the

kinetic energy operator, utilizes these properties, where the quantum shell effects can be calculated and added as in the independent particle model.

These mean field models are numerically easy to apply, and simultaneous calculations of all nuclei in the nuclear chart are feasible. Then any choice of interaction can be confronted with statistics of how well binding energies and other observables are reproduced [39].

2.2.3. Interacting shell models. One conceptual improvement is to allow correlations in the wave function and interactions between single-particle states [33]. The insurmountable obstacle is the huge basis necessary to obtain convergent numerical results. The cure is to cut down on the Hilbert space in the basis where three different restrictions can be made. First, only the active particles in the valence shell(s) are treated, while an inert central core is assumed. Second, the shell model basis are constructed from the single-particle states in the partly occupied valence shell(s) above the inert core. Third, the expansion in terms of for example an oscillator basis is restricted to a few oscillator excitations and the lowest angular momenta.

Unfortunately, each of these restrictions are very delicately related to convergence. The cure, as almost always, in nuclear physics is to use a phenomenological interaction adjusted to reproduce specific observables. The concept of effective interactions designed to be used in a non-complete subspace is then of greatest importance [41, 42, 43]. The numerous calculations over the years have provided detailed understanding of nucleonic correlations in nuclei but of course subject to the restrictions by the allocated Hilbert space. It quickly turned out that rather large oscillator quanta are needed even when the length in an oscillator basis is optimized. Also, one valence shell is inadequate for more than very few valence particles. Nevertheless, the accumulated experience are invaluable now where larger computers allow substantial extension of the Hilbert space.

One major development is to remove the core all-together, resulting in the no-core shell model [31, 44]. After curing initially appearing problems, first of all related to the monopole properties of the interactions, applications to light nuclei have been very successful. Clearly the prize for full treatment of the core is that even medium heavy nuclei cannot be studied. Also, the combination of accurate dealings with both small and large distances remain a problem. The shell-model is designed to do well at small distances whereas a complete basis, also including a fair treatment of larger distance, quickly becomes much too expensive due to demands in the number of basis states. The tail or large-distance properties influence the energy minimization much less than short-distance properties, and incorporating both are not practically possible.

The light nuclei are the targets for the no-core shell-model. Unfortunately, this immediately implies that dealing with the huge variation in structure of the individual nuclear states becomes difficult. The general concept of the shell model is very appealing but allowing descriptions of both single-particle and cluster structures is complicated in practice. Extensions to include shell-model alien cluster-components in the basis has recently been attempted [31]. This means that at least two types of non-orthogonal

Hilbert spaces are active. This may very well be necessary until both structures can be described in the same no-core shell-model. At present these models become more and more like the genuine few-body models.

2.3. Few-body descriptions

Instead of brute force methods, where approximations are necessary at later stages of the computations, it can be advantageous to select and treat the anticipated most important degrees-of-freedom. Such a restricted problem can be solved exactly by analytical or numerical techniques. This can serve as the definition of few-body physics. The only inaccuracy is therefore the uncertainties in the input assumptions and the parameters. Every detail in the chosen Hilbert space are then available but only features describable in this space. If the solutions are missing desired quantitative agreement or specific features, more degrees-of-freedom can be included either fully or perturbatively.

The starting point is the two-body problem which is trivial in the present context. The much more complicated three-body problem has on the other hand received overwhelming attention over many years. Central in these treatments is the formulation in terms of the Faddeev equations [45], which formally is extended to Faddeev-Yakubowsky equations [46] applicable for more than three particles. However, in the practical numerical context the difficulties increase enormously with the number of particles. We shall sketch some of the diverse variations in few-body methods where different strategies are employed.

2.3.1. Cluster models. The conceptually simplest is a system of a finite small number of point-like particles, that is either without intrinsic structure or with frozen (non-active) intrinsic degrees-of-freedom. With nucleons as point-like particles the systems are all the light nuclei with nucleon number less than about 12, e.g. deuteron, ^3H , ^3He , alpha-particle, etc. More complicated structures are mixtures of alpha-particles and nucleons in for example ^8Be , ^6He , ^6Li , ^6Be , ^9Be , ^9B , ^{12}C . Also more complicated clusters may be constituents as found for example in ^{15}B , ^{17}B , ^{11}Be , ^{11}Li , ^{12}Be , ^{20}C , ^{21}C , ^{22}C .

The procedure is then to decide on the important degrees-of-freedom as exemplified by ^6He with an alpha-particle surrounded by two neutrons. The alpha-core is frozen and the neutron-neutron and the neutron-alpha interactions must be parameterized with all the necessary spin-dependences. The three-body structure problem is then well-defined and with many present techniques also relatively easily solved. It is worth emphasizing that the effect of the Pauli principle is that the effective interactions in the limited space easily differ wildly from those in vacuum. For the neutron- ^4He interaction in ^6He calculations, the *s*-wave is repulsive for that reason, since the α -core already has two *s*-neutrons.

The structure of *s* and *p* domination is the prototype of two- and three-body nuclear halos where the spatial extension is unusually large and the binding energy relatively weak [47, 48]. A number of other such nuclear halo states with the same characteristics

of large radii and small binding are established. Their properties are rather difficult to reproduce with shell model approximations. Thus the cluster models are not only technically simple to use, they are also able to describe structures inaccessible by more complicated models.

This conclusion becomes much more profound when continuum structures, reactions and decay are required. Even in cluster models these properties are not trivially obtained but still they are within reach due to the few decisive degrees-of-freedom. Use of these models therefore seems to be a logical first step in investigations of complicated systems which exhibit cluster features. Let us emphasize that some features or states may have cluster properties while others don't and consequently they would be inaccessible by cluster models.

The actual calculations using cluster models can be carried out in many ways, including solving the few-body Schrödinger equation numerically, performing variational calculations on the chosen degrees-of-freedom, or expansion on a convenient basis. Each method has been refined over the years, where subtle details often have been implemented into practical numerical procedures. We shall not here go into any such details but stop with the present qualitative overall descriptions.

2.3.2. Zero-range models. The Faddeev equations apply for three point-like particles (or clusters) without any intrinsic structure. Their interactions may still be of finite range. If only large-distance properties are of interest, an assumption can be made of interaction radii much smaller than the radius of the solution. This is appropriately called zero-range interaction models, which by definition then neglect all information carried by finite-range interactions. On the other hand, these models exhibit universal features defined by properties independent of any details of the interactions.

An immediate technical problem is that an unlimited Hilbert space leads to divergent three-body wave functions, since it is advantageous to be in the same point of space. This small-distance or large momentum divergence has to be removed. In coordinate space by applying a short-distance cut-off adjusted conveniently to a known measured quantity like the energy. Examples are the zero-range effective field models. In momentum space the same relevant regularization can be achieved by subtraction of the unphysical large-momentum dependence. The prominent example is the zero-range momentum space formulations of the Faddeev equations [49, 50].

These models can only describe universal properties, simply because the wave function always is located completely outside the zero-range potential. This implies a tendency to exaggerate occurrence of universality, since all structures are universal in these models. An analogy can be found in the most abundant halos of two-body structure, which over the years have been “seen” in different shell models, although a more precise description would have been single-particle states.

The advantage of zero-range interactions is the simplicity and the relatively moderate computing time. The results depend only on the relative masses and the bound or virtual state energies of the three two-body subsystems. Important results

are the universal curves obtained as dimensionless relations between two and three-body properties. These unique model relations are interaction independent and they are therefore by definition revealing universal properties of systems where observables are on such curves [15].

2.3.3. Resonating group and generator coordinate method. The degrees-of-freedom are first chosen and typically divided into a few slow and many fast changing coordinates [51, 52]. This is very similar to the Born-Oppenheimer approximation [53, 54]. In general this division could be between intrinsic and relative cluster coordinates [55]. First, define clusters and corresponding parameters, then place them geometrically in space by choosing suitable relative coordinates like relative center-of-mass coordinates [56, 57, 58], and finally quantize the slow coordinates and solve the corresponding equations of motion. More specific examples are the fission process described by the slow collective deformation parameters and the fast intrinsic nucleonic coordinates.

These procedures are inevitably violating basic conservation of the total angular momentum which one way or another has to be restored afterwards. This is done either by projection of the solution onto angular momentum eigenstates, or by minimizing the energy of the projected state.

2.4. Variational methods

The variational principle is almost always underlying all the methods to solve the many-body problem. However, in some cases it is used very directly as variation of parameterized wave functions which may be either functionals, or parameter dependent functions, or a combination of both. The starting point could be the shell model [33] or Green's function Monte Carlo [59] formulation with the huge basis, but built up by random selecting and trying the importance of new basis states [60]. In the end, only the most important contributions to the energy are then left, which inevitably leaves all exotic minor components inaccurately determined. This problem of determination of minor, but interesting components, remains in all variational calculations where the energy is used as measure of convergence.

2.4.1. Gaussian stochastic variation. The basic ingredients are conveniently chosen as a number of gaussian functions where their centers, widths, and strengths are the variational parameters. The gaussian structures allow analytical calculation of matrix elements provided the interactions are analytical and sufficiently simple or parameterized in terms of simple functions. The number of gaussians are increased using various dedicated strategies depending on the problem until the energy is converged. Again only significant basis states are then picked up, and also too similar gaussians give numerical problems as the basis then is close to overcomplete. In any case the basis is by construction non-orthogonal and should be handled accordingly.

The technique is very flexible but most directly efficient for ground states and the

first few excited states. Total angular momentum conservation is as always a problem in nuclear physics calculations. Similar practical difficulties are also present for identical particles with corresponding (anti)symmetrizations.

2.4.2. Molecular dynamics model. Antisymmetrized molecular dynamics (AMD) [61, 62] and fermionic molecular dynamics (FMD) [63] are two very similar techniques for treating nuclear systems. FMD and AMD can be viewed as improvements of the theory of quantum molecular dynamics [64], where the antisymmetrization of the many-body wave function is treated more explicitly.

In principle, FMD and AMD are created as quantum analogies to the classical picture of point particles interacting by two-body interactions. As such these methods were initially constructed to study nuclear collisions and fragmentation reactions [65]. Nucleons are viewed as very localized wave packets to avoid violating the Heisenberg uncertainty principle, and the many-body wave function must be antisymmetrized according to the Pauli principle [66]. The fundamental procedure of AMD and FMD is relatively traditional. An antisymmetric many-body wave function is used as a trial state in conjunction with an appropriate Hamiltonian for the system, and the relevant equations of motion are derived using the time-dependent variational principle [66].

The differences between AMD and FMD are mostly technical, where the main difference is that FMD contains more parameters. In particular, the width of the wave packets is a complex variational parameter in FMD which can be different for individual waves, while in AMD it is the same for all wave packets. Also the spin orientation is treated as a variational parameter in FMD [67].

Both FMD and AMD are very versatile methods, which are able to describe nuclear collisions as well as nuclear structures [65]. When describing mean-field type structures FMD and AMD are somewhat similar to ordinary Hartree-Fock methods, only including correlations, but when describing cluster type structures FMD and AMD are able to handle deformed or distorted cluster structures. It is also possible to describe both stable and unstable nuclei as well as excited states using FMD and AMD, and it is not necessary to assume inert cores or restrictions like axial symmetry [68].

All of this makes AMD and FMD very useful approaches, capable of describing many very different aspects of nuclear systems. However, one type of system that both methods struggle with is spatially extended and lightly bound systems, the so-called halo systems. The wave functions in AMD and FMD represented by Gaussians wave packets have difficulties in properly describing the extended tail of the halo structures [69], which makes these systems inaccessible to AMD and FMD. As always, there is also computational limitations to consider, which, although not as significant as in shell model calculations, still prevents the treatment of heavier nuclear systems [69]. The use Gaussian two-body wave packets implies that even three-body correlations must be described by combining individual two-body structures. This is a severe shortcoming compared to few-body models.

2.5. Renormalized *ab-initio* methods

The increased availability of high-performance supercomputers has allowed adaptation of various *ab-initio* methods [70]. They provide in principle a full description of the many-body system, and allow systematic improvements at the expense of computation time. These methods have some subtle differences, but the main principles are very similar. First the fundamental interaction(s) must be chosen or rather adjusted to reproduce the experimentally well established detailed nucleon-nucleon scattering data. The problem is that due to the strong interaction, the potentials which reproduce these phase shifts include strong short-range repulsion as well as strong short-range tensor forces. This causes couplings to high-momentum modes that cannot be ignored, which in turn leads to non-perturbative correlations.

There are basically only two practical possibilities for dealing with this problem; either the high momentum modes must be removed, or a transformation to decouple the high- and low-momentum modes must be employed. In either cases the Hilbert space is changed to be less complete. The interaction can then be adjusted to reproduce observables within this reduced space, preferentially maintaining basic QCD symmetries but allowing systematic improvements. The prominent examples are effective field theories applied to deal with the appropriate degrees-of-freedom like subnucleonic, relative nucleon motion in nuclei, or maybe halo degrees-of-freedom. However, the most popular method is to employ some kind of transformation. This requires renormalization of the interaction to match the restricted Hilbert space, but consistency simultaneously demands use of multi-nucleon effective interactions, which in turn necessitate truncation.

This is in stark contrast to quantum chemistry, where the weak electromagnetic force leads to much simpler perturbative correlations, which is why *ab-initio* calculations within that field have been in use for decades [13, 14].

2.5.1. Coupled cluster models. The coupled cluster method is an *ab-initio* or first principle method that was originally presented more than fifty years ago [71, 72], The use of cluster in the title is a little deceiving because the clusters here mean particle-hole numbers of excitation, that is N -body correlated structures within the many-body system. This method started receiving widespread use within nuclear physics rather recently, and after various difficulties with the necessary renormalization were removed [73], and while computing power also increased dramatically.

The starting point is an approximate solution given in terms of a set of single-particle states with ground state energy and a corresponding hamiltonian. A so-called similarity transformation is applied to the hamiltonian. The purpose is to decouple unwanted parts of the Hilbert space from those of interest. The transformation is expanded in particle-hole numbers of excitations and the transformed non-hermitian hamiltonian is diagonalized. The cluster (correlation) amplitudes are the solutions, and the wave function has minimum energy with respect to one and two particle-hole excitations of the transformed hamiltonian.

The interactions are not predetermined by the method, on the contrary it is possible to implement a number of different interactions, depending on the specific purpose. However, many of the more popular interactions are either derived from one-boson exchange models [74, 75] or from chiral effective field theory [76, 77]. The truncation eliminating higher order particle-hole excitations implies that three- and higher-body interactions are explicitly excluded, but possible to be circumvented partly by use of density dependent two-body interactions [78].

When including singles and doubles (CCSD), the computational cost for solving the coupled cluster equations in the m -scheme is A^2n^4 , where n is the number of single-particle valence states, which naturally will be much larger than the number of particles, A (see [79] for details). This results in a method that is computationally very expensive, although it is still cheaper than for instance a full no-core shell model calculation. The number of coupled equations are still huge but clearly sometimes affordable. Weakly bound and open quantum systems are difficult to incorporate in coupled cluster methods [80], unless they are in the proximity of sub-shell closure [81, 82].

2.5.2. Similarity renormalization group. A similarity transformation has also the purpose of decoupling unwanted parts of the Hilbert space from those of interest. The similarity renormalization group and the in-medium similarity renormalization group (IM-SRG) approaches [83, 84, 85] are very close cousins of coupled cluster models. The same overall strategy of transforming the Hamiltonian to decouple the perturbative and non-perturbative aspects of the interaction. The idea is to obtain a block-diagonalization of the initial Hamiltonian, by employing a continuous, unitary transformation [86].

For IM-SRG the central idea is to formulate and solve the intrinsically non-perturbative Heisenberg-like equation which is equivalent to diagonalizing the many-body Hamiltonian. In practice, the transformation is chosen to produce a normal-ordered Hamiltonian, expressed in terms of second quantization, which can then be truncated to only include interactions of a certain order. Usually, only up to second order interactions are included, resulting in an approximate evaluation of the eigenvalues of the equations. As in CC the main point is that the transformation allows for such a truncation at an appropriate level of complexity.

The main differences between coupled clusters and IM-SRG lie in the exact transformation employed (the transformed Hamiltonian is Hermitian in IM-SRG and non-Hermitian for coupled clusters), and how the resulting equations are solved. Given that these differences are mainly technical, while the general procedure and underlying philosophy is identical, the methods have many of the same advantages and limitations. For instance, the truncation again results in only an approximate factorization into an intrinsic and a center-of-mass wave function. As a result the same issues with translational invariance as in coupled clusters appears here in IM-SRG.

When truncated to normal-ordered two-body operators, IM-SRG(2) scheme, the computational effort for solving the flow equations is dominated by the two-body flow equation, which scales polynomially like $\mathcal{O}(N^6)$, where N is the single-particle basis size

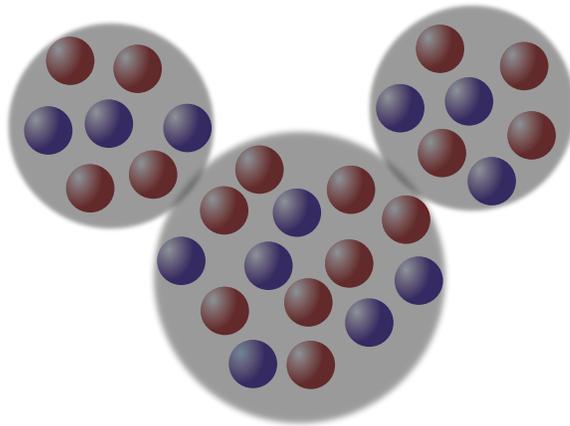


Figure 1. A schematic illustration of the many-body system viewed as a three-body cluster configuration with underlying structure. It should be noted that the constituent particles are considered as point particles throughout this work, and the effect of their internal structure is included through three-body interactions.

[86]. This means that the IM-SRG(2) has a sizable scaling factor with model space size like the CCSD.

3. Theoretical formulation

We shall in this report present a new method for treating many-body nuclear systems, which complements the existing methods by focusing on areas currently difficult to treat with these methods. Among them, two areas are particularly interesting: very extended, weakly bound systems and heavier, more complicated structures. The issue is fundamentally a computational or technical one, as both very extended systems and complicated systems with many constituents require a very large basis to be evaluated properly.

The primary goal here is to present a method which consistently connects extended, clusterized structures with the underlying many-body structure, whereas simultaneously being so efficient that it can be applied to very complicated many-body systems.

In Sec. 3.1 the theoretical framework will be presented with as few assumptions as possible, giving an intuitive overview of the approach and showing the general nature of the method. Afterwards, in Sec. 3.2, a number of assumptions, necessary to perform specific calculations, are made, and the details of the formulation are derived.

3.1. General formulation

Our fundamental idea is to view a many-body system as a structure consisting of few clusters, while still maintaining the full set of degrees of freedom in the description. This is illustrated in Fig. 1. Unless the particles in the clusters are fundamental, they will have some internal structure, and their substructure combined with two-body interactions

with many particles will invariantly lead to some form of effective three-body or higher-order interactions. Here the constituent particles are considered to be point particles, but three-body interactions are included, in addition to the two-body interactions, to account for their internal structure.

A general Hamiltonian for a many-body system consisting of A particles interacting with two- and three-body interactions (V_{ij} and V_{ijk}), in the center-of-mass frame of the system, can be written as

$$H_{gen} = \sum_{i=1}^A T_i - T^{(cm)} + \frac{1}{2} \sum_{i,j} V_{ij} + \frac{1}{6} \sum_{i,j,k} V_{ijk}, \quad (1)$$

where T_i is the kinetic energy operator of the i 'th particle, and $T^{(cm)}$ is the center-of-mass kinetic energy operator. It will be assumed that the system consists of three clusters, c_1 , c_2 , and c_3 with A_1 , A_2 , and A_3 particles respectively, but the generalization to n clusters is straightforward. The general Hamiltonian from Eq. (1) can then be rewritten as

$$H_{gen} = H_{c_1} + H_{c_2} + H_{c_3} + H_{fb}, \quad (2)$$

$$H_{c_l} = \sum_{i \in c_l} T_i - T_{c_l}^{(cm)} + \frac{1}{2} \sum_{i,j \in c_l} V_{ij} + \frac{1}{6} \sum_{i,j,k \in c_l} V_{ijk}, \quad (3)$$

$$H_{fb} = \sum_{l=1}^3 T_{c_l}^{(cm)} - T^{(cm)} + \frac{1}{2} \sum_{n \neq m=1}^3 \sum_{i \in c_n} \sum_{j \in c_m} V_{ij} + \frac{1}{6} \sum_{n \neq m=1}^3 \sum_{i,j \in c_n} \sum_{k \in c_m} V_{ijk} + \frac{1}{6} \sum_{l \neq n \neq m=1}^3 \sum_{i \in c_n} \sum_{j \in c_m} \sum_{k \in c_l} V_{ijk}, \quad (4)$$

where $T_{c_l}^{(cm)}$ is the center-of-mass kinetic energy operator for the l 'th cluster. For the two-body interaction in Eq. (4) both particles are never in the same cluster, and for the three-body interaction in Eq. (4) at least one particle is not in the same cluster as the others. The factors are to avoid double counting.

From Eqs. (2) to (4) it is clear that the cluster Hamiltonians, H_{c_l} , are just many-body Hamiltonians like Eq. (1) for a system of A_l particles. Also, the few-body Hamiltonian, H_{fb} , includes all the interactions that connect more than one cluster. If the clusters were considered as point particles, Eq. (2) would reduce to a regular three-body Hamiltonian.

Having settled on a conceptual approach, the following steps are in principle very simple; we have to choose a wave function, choose an interaction, and do a variation. From Eq. (2) the natural choice of the general wave function is an antisymmetric product of the cluster wave functions, Ψ_{c_i} , and the few-body wave function, Ψ_{fb} ,

$$\Psi_{gen} = \mathcal{A} [\Psi_{c_1}(\{\mathbf{r}_{c_1}\}) \Psi_{c_2}(\{\mathbf{r}_{c_2}\}) \Psi_{c_3}(\{\mathbf{r}_{c_3}\}) \Psi_{fb}(\mathbf{r}_{R_1}, \mathbf{r}_{R_2})], \quad (5)$$

where \mathcal{A} is the anti-symmetrization operator, \mathbf{r}_{R_1} and \mathbf{r}_{R_2} are the relative coordinates between the center-of-mass of the clusters, and $\{\mathbf{r}_{c_i}\}$ are the A_i (spin and space) coordinates for the particles in the i 'th cluster.

With the Hamiltonian from Eq. (2) and the wave function from Eq. (5) the total energy becomes

$$\begin{aligned} E &= \langle \Psi_{gen} | H_{gen} | \Psi_{gen} \rangle \\ &= \sum_{i=1}^3 \langle \mathcal{A}[\Psi_{c_i} \Psi_{fb}] | H_{c_i} | \mathcal{A}[\Psi_{c_i} \Psi_{fb}] \rangle + \langle \Psi_{gen} | H_{fb} | \Psi_{gen} \rangle. \end{aligned} \quad (6)$$

In connection with the variation of the energy, the Lagrange multipliers E_{c_1} , E_{c_2} , E_{c_3} , and E_{fb} are introduced as

$$\begin{aligned} \langle \Psi_{gen} | H'_{gen} | \Psi_{gen} \rangle &= \langle \Psi_{gen} | H_{gen} | \Psi_{gen} \rangle - \sum_{i=1}^3 E_{c_i} \int |\Psi_{c_i}(\{\mathbf{r}_{c_i}\})|^2 d\{\mathbf{r}_{c_i}\} \\ &\quad - E_{fb} \int |\Psi_{fb}(\mathbf{r}_{R_1}, \mathbf{r}_{R_2})|^2 d\mathbf{r}_{R_1} d\mathbf{r}_{R_2} \end{aligned} \quad (7)$$

To minimize the energy both, cluster and few-body wave functions, are varied individually

$$0 = \frac{\delta}{\delta \Psi_{c_i}^*} \langle \Psi_{gen} | H'_{gen} | \Psi_{gen} \rangle, \quad (8)$$

$$0 = \frac{\delta}{\delta \Psi_{fb}^*} \langle \Psi_{gen} | H'_{gen} | \Psi_{gen} \rangle, \quad (9)$$

for $i \in \{1, 2, 3\}$.

This results in a series of coupled equations for the cluster structures and the relative structure given by

$$\begin{aligned} E_{c_i} \Psi_{c_i}(\{\mathbf{r}_{c_i}\}) &= \langle \Psi_{fb} | H_{c_i} \Psi_{c_i} | \Psi_{fb} \rangle + \langle \Psi_{fb} | H_{fb} \Psi_{c_i} | \Psi_{fb} \rangle \\ &\quad + \left\langle \mathcal{A}[\Psi_{c_j} \Psi_{c_k} \Psi_{fb}] \left| \Psi_{c_i}^* \frac{\delta H_{gen}}{\delta \Psi_{c_i}^*} \Psi_{c_i} \right| \mathcal{A}[\Psi_{c_j} \Psi_{c_k} \Psi_{fb}] \right\rangle, \end{aligned} \quad (10)$$

$$\begin{aligned} E_{fb} \Psi_{fb}(\mathbf{r}_{R_1}, \mathbf{r}_{R_2}) &= \langle \mathcal{A}[\Psi_{c_1} \Psi_{c_2} \Psi_{c_3}] | H_{fb} \Psi_{fb} | \mathcal{A}[\Psi_{c_1} \Psi_{c_2} \Psi_{c_3}] \rangle \\ &\quad + \sum_{i=1}^3 \langle \Psi_{c_i} | H_{c_i} \Psi_{fb} | \Psi_{c_i} \rangle \\ &\quad + \left\langle \mathcal{A}[\Psi_{c_1} \Psi_{c_2} \Psi_{c_3}] \left| \Psi_{fb}^* \frac{\delta H_{gen}}{\delta \Psi_{fb}^*} \Psi_{fb} \right| \mathcal{A}[\Psi_{c_1} \Psi_{c_2} \Psi_{c_3}] \right\rangle, \end{aligned} \quad (11)$$

for $i, j, k \in \{1, 2, 3\}$, and $i \neq j \neq k$. The last terms in both equations are due to the fact that the interactions might be density dependent. Otherwise, these terms are zero. It is clear that the cluster interactions will depend on the three-body wave function and vice versa [87].

3.2. Specific formulation

So far the derivations have been very general. No specific type of system has been chosen, no specific many-body formalism has been chosen, and no specific few-body formalism has been chosen. The method outlined above could be implemented with almost any choice of few- and many-body formalisms.

Here a number of specific choices will be made. As the focus is on nuclear systems, and to keep the initial investigation simple, it is assumed that the system consists of one fairly heavy cluster with A nucleons surrounded by two valence nucleons, which are also assumed to be identical.

One main point of the method is then the core description, where almost any description could be employed. As an effort is made to make the method very computationally efficient, a self-consistent Hartree-Fock mean-field method is used to describe the core.

To only content with one core description it is assumed that the remaining two clusters consist of single, identical nucleons. As the present application focuses on weakly bound systems, two identical nucleons is in any case the most obvious choice. The separation of the neutron and proton driplines makes systems with simultaneously weakly bound neutrons and protons uncommon and exotic.

Finally, the three-body formalism employed is the hyperspherical adiabatic expansion of the three-body Faddeev equations in coordinate space [88]. Again, any few-body formalism could be chosen, but the hyperspherical adiabatic expansion is a powerful, flexible, and accurate method, particularly well suited for describing low-energy scattering and predicting both bound states and resonances.

Applying these choices, the Hamiltonian from Eqs. (2) to (4) initially simplifies to:

$$H = H_c + H_3 , \quad (12)$$

$$H_c = \sum_{i=1}^A T_i - T_c^{(cm)} + \frac{1}{2} \sum_{i,j=1}^A V_{ij} + \frac{1}{6} \sum_{i,j,k=1}^A V_{ijk} , \quad (13)$$

$$\begin{aligned} H_3 = & T_c^{(cm)} + T_{v_1} + T_{v_2} - T_{cm} + V_{v_1 v_2} + \sum_{i=1}^A (V_{iv_1} + V_{iv_2}) \\ & + \sum_{i,j=1}^A (V_{ijv_1} + V_{ijv_2}) + \sum_{i=1}^A V_{iv_1 v_2} , \end{aligned} \quad (14)$$

where v_1 and v_2 refers to the two valence nucleons.

3.2.1. Skyrme interaction. Being more specific, density dependent Skyrme forces [37] will be used in the self-consistent Hartree-Fock mean-field calculation of the core. This has the advantage of both extremely high computational efficiency, combined with generally very accurate predictive power, and a high degree of flexibility. In addition, it is assumed that the core is spherical and even-even with respect to neutron and proton number, as this greatly simplifies many of the equations for the initial investigation. The various generalizations are well-known and straightforward, albeit cumbersome [89, 90, 91], and their implementation is discussed in Sec. 8.

With a density dependent Skyrme force, the three-body interaction is parameterized as a density dependent two-body interaction. After introducing this parameterization, V_{ijk} in Eq. (13) is then included into V_{ij} . Likewise, in Eq. (14) V_{ijv_1} and V_{ijv_2} are included into V_{iv_1} and V_{iv_2} , respectively. For the moment, $\sum_i V_{iv_1 v_2}$ is kept as a regular

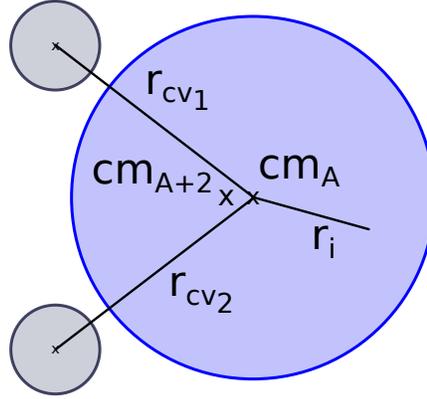


Figure 2. Schematic illustration of the spatial coordinates for the wave functions in Eq. (17). The center of mass for the core is indicated by cm_A , while the total center of mass is indicated by cm_{A+2} . The A core particles have a corresponding coordinate \mathbf{r}_i , while the valence nucleons are distinguished by \mathbf{r}_{cv1} and \mathbf{r}_{cv2} , respectively.

three-body interaction, V_3 . This interaction is discussed in greater detail in Sect. 4.4.1. The Hamiltonians H_c and H_3 then reduce to

$$H_c = \sum_{i=1}^A T_i - T_c^{(cm)} + \frac{1}{2} \sum_{i,j=1}^A V_{ij}, \quad (15)$$

$$H_3 = T_c^{(cm)} + T_{v1} + T_{v2} - T_{cm} + V_{v1v2} + \sum_{i=1}^A (V_{iv1} + V_{iv2}) + V_3. \quad (16)$$

For the simplified system the wave function (5) reduces to

$$\Psi = \mathcal{A}[\psi_c(\mathbf{r}_1, \dots, \mathbf{r}_A)\psi_{3b}(\mathbf{r}_{cv1}, \mathbf{r}_{cv2})], \quad (17)$$

where the core wave function is a Slater determinant of single-particle wave functions, i.e., $\psi_c = \det(\{\psi_i\})$ where i runs over all the core nucleons, and ψ_{3b} is the three-body wave function. As Skyrme interactions have been adjusted to Slater determinants, this is the natural choice of the core wave function, unless the Skyrme interaction is reparameterized. The coordinates are illustrated in Fig. 2. As mean-field calculations break translational invariance, this problem is inherited here. However, the discrepancy decreases with core mass, and it does not have a significant effect on the present calculations.

As indicated by Eq. (6) the simplest expression for the energy is

$$E = \langle \Psi | H | \Psi \rangle = \langle \Psi | H_c | \Psi \rangle + \langle \Psi | H_3 | \Psi \rangle. \quad (18)$$

As a result the Lagrange multipliers ϵ_i and E_3 can be introduced by

$$\langle \Psi | H' | \Psi \rangle = E - \sum_{i=1}^A \epsilon_i \int |\psi_i(\mathbf{r})|^2 d\mathbf{r} - E_3 \int |\psi_{3b}(\mathbf{r}_{cv1}, \mathbf{r}_{cv2})|^2 d\mathbf{r}_{cv1} d\mathbf{r}_{cv2} \quad (19)$$

To minimize the energy both, core and three-body wave functions, are again varied individually as

$$0 = \frac{\delta}{\delta\psi_i^*} \langle \Psi | H' | \Psi \rangle, 0 = \frac{\delta}{\delta\psi_{3b}^*} \langle \Psi | H' | \Psi \rangle. \quad (20)$$

The Skyrme force used has the form

$$\begin{aligned} V_{jk} = & t_0 (1 + x_0 P_\sigma) \delta(\mathbf{r}_j - \mathbf{r}_k) \\ & + \frac{t_1}{2} (1 + x_1 P_\sigma) (\mathbf{k}'^2 \delta(\mathbf{r}_j - \mathbf{r}_k) + \delta(\mathbf{r}_j - \mathbf{r}_k) \mathbf{k}^2) \\ & + t_2 (1 + x_2 P_\sigma) \mathbf{k}' \delta(\mathbf{r}_j - \mathbf{r}_k) \mathbf{k} + \frac{1}{6} t_3 (1 + x_3 P_\sigma) (n_c + n_3)^\alpha \delta(\mathbf{r}_j - \mathbf{r}_k) \\ & + iW_0 (\boldsymbol{\sigma}_j + \boldsymbol{\sigma}_k) \cdot (\mathbf{k}' \times \delta(\mathbf{r}_j - \mathbf{r}_k) \mathbf{k}), \end{aligned} \quad (21)$$

where $P_\sigma = \frac{1}{2}(1 + \boldsymbol{\sigma}_j \cdot \boldsymbol{\sigma}_k)$, $\boldsymbol{\sigma}_{1,2,3}$ are the Pauli matrices, and $\mathbf{k} = \frac{1}{2i}(\boldsymbol{\nabla}_j - \boldsymbol{\nabla}_k)$ acting on the right and $\mathbf{k}' = -\frac{1}{2i}(\boldsymbol{\nabla}_j - \boldsymbol{\nabla}_k)$ acting on the left. The density in the t_3 term is the total single-particle density including both core, n_c , and valence, n_3 , nucleon densities, calculated in the center-of-mass of the two particles in question. It is the t_3 term which necessitates the variation of the interaction with respect to the wave functions (or densities). The t_i , x_i , W_0 , and α are parameters of the Skyrme interaction. To this Skyrme interaction the Coulomb interaction (see Eq. (A.54) or for instance Ref. [92]) must be added for interactions between protons.

The variation itself, Eq. (20), is rather lengthy, but conceptually simple. As the variations are with respect to ψ_i and ψ_{3b} they will lead to a core and a three-body equation, where the effective interactions in both will be coupled by ψ_i and ψ_{3b} . The details are presented in Appendix A, and lead to Eqs. (A.44) and (A.50), which are the following coupled three-body and core equations:

$$\begin{aligned} E_3 \psi_{3b}(\mathbf{r}_{cv1}, \mathbf{r}_{cv2}) = & [T_x + T_y + V_{cv}(\mathbf{r}_{cv1}) + V_{cv}(\mathbf{r}_{cv2}) + V_{v_1 v_2}(\mathbf{r}_{cv1}, \mathbf{r}_{cv2}) \\ & + V_3(\mathbf{r}_{cv1}, \mathbf{r}_{cv2})] \psi_{3b}(\mathbf{r}_{cv1}, \mathbf{r}_{cv2}), \quad (22) \\ \epsilon_{iq} \psi_{iq}(\mathbf{r}) = & \left[-\boldsymbol{\nabla} \cdot \frac{\hbar^2}{2m_q^*(\mathbf{r})} \boldsymbol{\nabla} + U_q(\mathbf{r}) - i\mathbf{W}_q(\mathbf{r}) \cdot (\boldsymbol{\nabla} \times \boldsymbol{\sigma}) \right. \\ & \left. - \boldsymbol{\nabla} \cdot \frac{1}{m_q'^*(\mathbf{r})} \boldsymbol{\nabla} + U_q'(\mathbf{r}) - i\mathbf{W}_q'(\mathbf{r}) \cdot (\boldsymbol{\nabla} \times \boldsymbol{\sigma}) \right] \psi_{iq}(\mathbf{r}) \quad (23) \end{aligned}$$

The details regarding the three-body equation are found following Eq. (A.44), and will be discussed in Sec. 4.2. In short, T_x and T_y are the three-body kinetic energy operators, V_{cv} is the core-valence nucleon interaction given in Eq. (A.45) and the equations below, $V_{v_1 v_2}$ is the valence nucleon-nucleon interaction, and V_3 is the three-body interaction. The full derivation of V_{cv} is included in Appendix A, whereas $V_{v_1 v_2}$ and V_3 are discussed in Sects. 4.4.1 and 4.4.2, respectively. It should be noted, that V_{cv} contains effective mass terms, resulting from the gradients in the Skyrme interaction, in addition to regular central- and spin-orbit terms.

The details regarding the core equation are found following Eq. (A.50), and will be discussed in Sec. 4.1. The three first terms, without primes, are the terms found in a

regular Skyrme-Hartree-Fock Schrödinger equation [37], while the prime indicates the contribution from the valence nucleons, and q stands for either neutrons or protons.

The technical implementation along with the practical methods for solving these equations are discussed in Sec. 4.1, including the proper inclusion of the Pauli principle in Sec. 4.3.

4. Technical implementation

In practice Eqs. (22) and (23) are solved iteratively. First, Eq. (23) is solved for the core in isolation, without including the new contributions from the valence nucleons. The details of the solution to Eq. (23) are included in Sec. 4.1. This calculation gives rise to the density functions (A.49), and therefore to the effective potential $V_{cv}(\mathbf{r})$ in Eq. (A.45), which is used to solve the three-body equation (22). The details of the modifications to the traditional hyperspherical expansion of the Faddeev equations are presented in Sec. 4.2.

The valence nucleon densities (A.2), (A.4) and (A.6), produced in the three-body calculation, are then used in a new core calculation, which provides the potentials for a new three-body calculation. The process is repeated until convergence in energy is reached. Unless otherwise stated, convergence is here in the numerical calculations defined as the three-body energy of two consecutive iterations differing by less than 0.02 MeV. This criterion can of course be changed to fit the purpose, but in any case the structure must also converge.

The new terms in Eqs. (22) and (23) do not add much computational complexity, yet this process is still more computationally demanding than both regular Skyrme-Hartree-Fock calculations and regular hyperspherical adiabatic Faddeev calculations because of the iterations. However, convergence usually happens within 3 to 5 iterations, so the added computation time is roughly a factor of 3 to 5 on the solution of the adiabatic expansion, which is the bottleneck of the calculation. As a result, the computation time is only on the order of a few days on a single, regular processor core.

4.1. The mean-field core equation

As seen from Eq. (23), the core Schrödinger equation is very similar to the traditional Skyrme-Hartree-Fock Schrödinger equation [37, 89, 93, 94]. There are kinetic, effective mass, central, spin-orbit terms, and nothing else. In fact, the traditional Skyrme-Hartree-Fock equation is given by Eq. (23) if all "primed" potentials are omitted, and using the expressions from Eq. (A.51), only with $n_3 = 0$. The influence of the valence nucleons amounts to including the primed potentials and n_3 , and also using the expressions from either Eq. (A.52) or Eq. (A.53), depending on whether or not the valence nucleons are of the same type as the core nucleon in question. As only the expressions change, and no fundamentally new terms are included in the interaction, the method for solving Eq. (23) is identical to the solution method known from traditional

Skyrme-Hartree-Fock [37, 93].

The new three-body densities, n_3 , τ_3 , and \mathbf{J}_3 from Eqs. (A.2), (A.4), and (A.6), respectively, are produced by the three-body calculation, Eq. (22), as functions of distance, and they enter directly into the calculations. The core densities, n_c , τ_c , and \mathbf{J}_c from Eqs. (A.1), (A.3), and (A.5), respectively, are produced in the traditional self-consistent manner, as the Hartree-Fock equations are always solved iteratively (not to be confused with the iteration between our core and three-body equations).

For a spherical, even-even nucleus the single-particle wave function can be separated into spherical coordinates as

$$\psi_i(\mathbf{r}, \sigma) = \rho_\alpha(r) y_\beta(\hat{r}, \sigma), \quad (24)$$

where ρ contains the radial part, whereas y contains the angular (and spin) part. In α the relevant quantum numbers are contained, i.e. the nucleon type, q , the principal quantum number, n , the orbital angular momentum, l , and the total angular momentum, j , of the state, while β contains the l , j , and q quantum numbers, as well as the magnetic quantum number m .

Due to the spherical symmetry of the core, the core densities can be expressed in terms of $R_\alpha(r)$, where $\rho_\alpha(r) = R_\alpha(r)/r$, as

$$n(r) = \frac{1}{4\pi r^2} \sum_{\alpha} (2j_{\alpha} + 1) R_{\alpha}^2(r), \quad (25)$$

$$\tau(r) = \frac{1}{4\pi} \sum_{\alpha} (2j_{\alpha} + 1) \left(\left(\frac{d\rho_{\alpha}}{dr} \right)^2 + \frac{l_{\alpha}(l_{\alpha} + 1)}{r^2} \rho_{\alpha}^2 \right), \quad (26)$$

$$\mathbf{J}(r) = \frac{\hat{r}}{4\pi r^2} \sum_{\alpha} (2j_{\alpha} + 1) \left(j_{\alpha}(j_{\alpha} + 1) - l_{\alpha}(l_{\alpha} + 1) - \frac{3}{4} \right) R_{\alpha}^2(r). \quad (27)$$

Initially, a first approximation to the unknown radial part of the wave function, R_α , is produced using harmonic oscillator wave functions. Using the expressions above, first approximations of the core densities are produced, which again is used to calculate the potentials and effective masses in Eq. (23). This is used to produce a new radial wave function R_α , and the process continues until convergence in single-particle energies is reached.

As the parameters of the Skyrme forces used here are fitted using the Hartree-Fock equations where the spin density in the spin-orbit part of the potential has been omitted, the spin densities are also here omitted from the spin-orbit parts of Eq. (23). They could be included at the expense of a reparameterization, but they are in any case of very minor importance.

4.2. The three-body equation

As mentioned in Sect. 3.2 our chosen three-body formalism is the hyperspherical adiabatic expansion of the Faddeev equations in coordinate space [88, 95]. However, unlike the core equation, the three-body equation contains terms not usually found

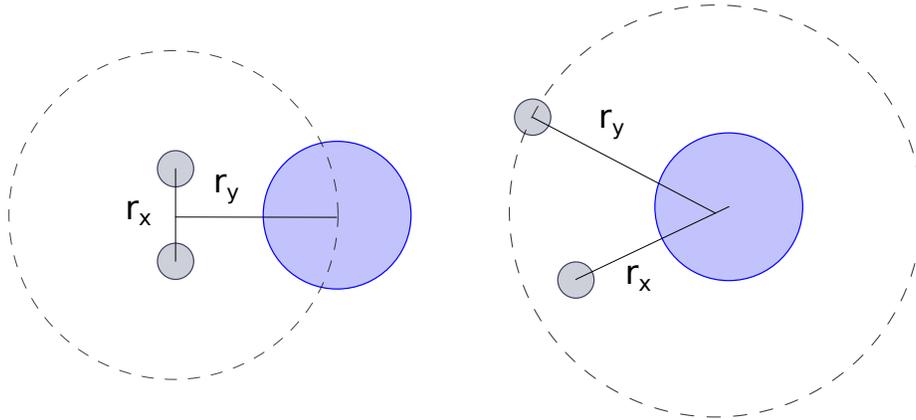


Figure 3. The two relative set of coordinates for a three-body system with a large, heavy core surrounded by two identical particles, with coordinate set 1 on the left and coordinate set 2 on the right. Also illustrated is the rotational symmetry of the two coordinate sets.

within this formalism, and more attention will be devoted to this. Specifically, the almost-local derivatives in the effective mass terms require special attention.

First, the well known three-body Jacobi coordinates are introduced as

$$\mathbf{x}_i = \sqrt{\frac{\mu_{jk}}{m}} (\mathbf{r}_j - \mathbf{r}_k) = \sqrt{\frac{\mu_{jk}}{m}} \mathbf{r}_x, \quad (28)$$

$$\mathbf{y}_i = \sqrt{\frac{\mu_{jk,i}}{m}} \left(\mathbf{r}_i - \frac{m_j \mathbf{r}_j + m_k \mathbf{r}_k}{m_j + m_k} \right) = \sqrt{\frac{\mu_{jk,i}}{m}} \mathbf{r}_y, \quad (29)$$

$$\mu_{jk} = \frac{m_j m_k}{m_j + m_k}, \quad (30)$$

$$\mu_{jk,i} = \frac{m_i (m_j + m_k)}{m_i + m_j + m_k}, \quad (31)$$

where \mathbf{r}_i , \mathbf{r}_j , and \mathbf{r}_k are the center-of-mass coordinates of the three clusters, with associated masses m_i , m_j , and m_k , while m is an arbitrary normalization mass. In a three-body system with two identical particles there are two possible sets of relative coordinates, as illustrated in Fig. 3.

The Jacobi coordinates are used to define the hyperspherical coordinates, which consist of two pairs of directional angles, $(\Omega_{x_i}, \Omega_{y_i})$, for \mathbf{x}_i and \mathbf{y}_i , as well as the hyperangle, α_i , and the hyperradius, ρ , coordinates defined by

$$\alpha_i = \arctan \frac{x_i}{y_i}, \quad \text{and} \quad \rho = \sqrt{x_i^2 + y_i^2}, \quad (32)$$

from which one can easily get that $x_i = \rho \sin \alpha_i$ and $y_i = \rho \cos \alpha_i$.

When introducing these five angular and one radial coordinates the three-body

kinetic energy operator separates into a hyperradial and a hyperangular part

$$T = T_x + T_y = T_\rho + \frac{\hbar^2}{2m\rho^2}\Lambda^2, \quad (33)$$

$$T_\rho = -\frac{\hbar^2}{2m} \left(\frac{\partial^2}{\partial \rho^2} + \frac{5}{\rho} \frac{\partial}{\partial \rho} \right), \quad (34)$$

$$\hat{\Lambda}^2 = -\frac{\partial^2}{\partial \alpha_i^2} - 4 \cot(2\alpha_i) \frac{\partial}{\partial \alpha_i} + \frac{\hat{l}_{x_i}^2}{\sin^2 \alpha_i} + \frac{\hat{l}_{y_i}^2}{\cos^2 \alpha_i}, \quad (35)$$

where \hat{l}_{x_i} and \hat{l}_{y_i} are the angular momentum operators related to \mathbf{x}_i and \mathbf{y}_i , and $\hat{\Lambda}^2$ is the hyperangular momentum operator whose eigenfunctions are the hyperspherical harmonics [88].

The fundamental idea behind the hyperspherical adiabatic expansion is to introduce a set of ρ -dependent angular wave functions, $\phi_n(\rho, \alpha)$, on which the three-body wave function can be expanded. The angular part of the Schrödinger (or Faddeev) equation is then solved for all values of ρ , and the solution is used to solve the radial part of the equation. The expanded wave function is

$$\psi_{3b}(\mathbf{x}, \mathbf{y}) = \frac{1}{\rho^{5/2}} \sum_n f_n(\rho) \phi_n(\rho, \alpha), \quad (36)$$

and the Schrödinger equation is

$$\left[T_\rho + \frac{\hbar^2}{2m\rho^2}\Lambda^2 + V_{cv_1} + V_{cv_2} + V_{v_1v_2} + V_3 \right] \psi_{3b}(\mathbf{x}, \mathbf{y}) = E_3 \psi_{3b}(\mathbf{x}, \mathbf{y}). \quad (37)$$

First introduced in 1968 by J. H. Macek [95], the hyperspherical adiabatic representation has a unique position in the theory of multiparticle fragmentation reactions, namely, it is the only representation that maps complex, multiparticle, fragmentation theory onto a set of coupled-channel differential equations identical to those familiar from the theory of two-body reactions [96]. In addition, pure three-body continuum channels are asymptotically completely separated from bound state channels, and, at the same time, all the channels are asymptotically correct [96]. These calculations converge very quickly, and usually only the few lowest angular wave functions in the expansion (36) are needed to produce an accurate calculation, as the coupling to higher wave functions is very modest. This is in particular important for weakly bound or very extended states, where the adiabatic expansion method is both very efficient and accurate.

Combining the adiabatic expansion with the Faddeev formalism has the added benefit of treating all Jacobi coordinate sets identically. For systems with more than one internal two-body bound or low-lying resonance state, all are treated in their natural coordinate system. When solving a regular Schrödinger equation the necessary rotation between coordinate systems reduces the accuracy.

We choose the angular functions ϕ_n to be the eigenfunctions of the angular part of the Faddeev equations, where, as mentioned, the two-body interactions include almost-local gradient terms (see Eqs. (A.45) and (A.48)). In Appendix B it is shown how these gradient terms can be separated into radial and angular parts. Letting \tilde{V} contain the

usual central and spin-orbit terms as well as the angular part of the new gradient terms, the angular Faddeev equation becomes, Eq. (B.10),

$$\left(\hat{\Lambda}^2 + \frac{2m\rho^2}{\hbar^2} (\tilde{V}_{cv_1} + \tilde{V}_{cv_2} + \tilde{V}_{v_1v_2}) \right) \phi_n(\rho, \Omega) = \lambda_n(\rho) \phi_n(\rho, \Omega), \quad (38)$$

where λ_n is the (ρ -dependent) angular eigenvalues. Multiplying Eq. (37), or more precisely (B.9), from the left by $\phi_m^*(\rho, \Omega)$ and integrating over $\Omega = (\Omega_{x_i}, \Omega_{y_i})$ we get the set of coupled hyperradial equations

$$\begin{aligned} 0 = & (1 - C_{nm}) \frac{\partial^2 f_n}{\partial \rho^2} - \frac{\lambda_n + \frac{15}{4}}{\rho^2} f_n + \frac{2m(E - V_3)}{\hbar^2} f_n \\ & + 2 \sum_m (P_{nm} + P'_{nm}) \frac{\partial f_m}{\partial \rho} + \sum_m (Q_{nm} + Q'_{nm}) f_m, \end{aligned} \quad (39)$$

where

$$P_{nm}(\rho) = \langle \phi_n(\rho, \Omega) | \frac{\partial}{\partial \rho} | \phi_m(\rho, \Omega) \rangle_{\Omega} \quad (40)$$

and

$$Q_{nm}(\rho) = \langle \phi_n(\rho, \Omega) | \frac{\partial^2}{\partial \rho^2} | \phi_m(\rho, \Omega) \rangle_{\Omega} \quad (41)$$

are the usual coupling terms arising from the standard adiabatic expansion method [88] ($\langle | \rangle_{\Omega}$ indicates integration over the hyperangles only). The remaining coupling terms, C_{nm} , P'_{nm} and Q'_{nm} are new couplings coming from the hyperangular part of the gradient terms in Eq. (22). They are defined in Eq. (B.13) and (B.15).

Solving first Eq. (38) and then Eq. (39) provides the full solution for the three-body system. From there anything that could be calculated with ordinary three-body formalism, can also be calculated here. The two main differences between the traditional adiabatic expansion, and the method presented are the origin of the potentials in Eq. (38) and the new couplings in Eq. (39).

Traditionally, the two-body potentials in Eq. (38) are completely phenomenological in nature [97]. The solution to the Faddeev equations involves a partial wave expansion, where the two-body interactions for the individual partial waves can differ. It is known that the couplings to higher partial angular momentum in each Faddeev component is of second order in the potentials [88], but a number of different partial angular momentum values are often still needed for medium heavy systems. In addition, each two-body interaction would include central and spin-orbit parts, at the very least, and possible spin-spin or tensor parts as well. Even with a simple interaction like a double Gaussian, there are easily between 30 and 50 free parameters, depending on the system. As a result, more or less any result could be obtained with a traditional hyperspherical expansion of the three-body Faddeev equations, unless heavily restrained by experimental information.

For the method presented here, a crucial aspect is that the two-body interactions are completely determined by the core description. Specifically, the Skyrme

parameterization dictates the produced core potential, which translates into the two-body interactions in the three-body equation. The only important, remaining degrees of freedom lie in the choice of Skyrme parameterization and possibly in the three-body interaction to be discussed in Sec. 4.4.2.

The new couplings in Eq. (39) are caused by the gradient terms in the Skyrme interaction in Eq. (A.48), and it is therefore a result of the specific core description chosen, and not a unavoidable necessity of the method. However, as shown in Appendix B they are neither particularly problematic nor time consuming to include. On the contrary, they represent an interesting new development within three-body Faddeev formalism in their own right.

4.3. The Pauli principle

Implementation of the Pauli principle has the two sides when facing either the core or the three-body calculations. The Slater determinant in the mean-field formulation guaranties orthogonality between occupied orbits, and the exchange terms in the corresponding Schrödinger equation only allow interaction contributions from identical fermions in different states.

The core only requires information about the valence nucleons through ordinary and kinetic energy densities, and terms of minor importance also depending on currents. The Hartree-Fock iteration procedure usually applied to reach self-consistency then only has information about the states occupied by the valence nucleons from these densities, which enter in Eq. (23) through Eqs.(A.51), (A.52), and (A.53). The choice of occupied states is usually the lowest possible consistent with one for each indistinguishable nucleon.

In principle, another choice of occupied states could be made where two of these core-occupied states are left unoccupied for the valence nucleons while two higher-lying instead are occupied. The Hartree-Fock solution obtained with the fixed valence densities must in a chosen approximation span a space orthogonal to the space of the two valence nucleons. To which extent this is correct can be tested by calculation of the overlap integrals,

$$\int \psi_i^*(\mathbf{r}_{cv_1})\psi_k^*(\mathbf{r}_{cv_2})\psi_{3b}(\mathbf{r}_{cv_1}, \mathbf{r}_{cv_2}) d\mathbf{r}_{cv_1} d\mathbf{r}_{cv_2}, \quad (42)$$

for any pair, (i, k) , of mean-field occupied states. Even independent of r there should be vanishing overlap for each of the occupied states, ψ_i ,

$$\int \psi_i^*(\mathbf{r}_{cv_1})\psi_{3b}(\mathbf{r}_{cv_1}, \mathbf{r}) d\mathbf{r}_{cv_1}. \quad (43)$$

However, for weakly bound systems, valence nucleons occupying states above the core occupied states are the most natural assumption, and it is the assumption made here.

The three-body calculation receives input from the Hartree-Fock solution in the form of various effective potentials, Eqs. (A.46), (A.47) and (A.48), which by definition

are the potentials acting on one nucleon from all core-nucleons. These are deep potentials, and the solution to such a nucleon-core problem would produce a number of bound states corresponding to at least the number of occupied mean-field states. This follows from the fact that these potentials are precisely those entering the Hartree-Fock calculation with a bound core. In other words, the already occupied single-particle states in the core must be excluded from the space employed in the three-body calculation. This problem has been solved by three rather different methods added to the fundamental three-body approach [88].

The first method is to adjust the two-body potential parameters to allow only the desired number of core-valence nucleon bound states, and at the same time reproduce the low-energy scattering data through a correct scattering length. In effect, the deep potentials are replaced with shallow potentials only supporting the Pauli allowed (highest lying) states [98]. The main problem with this is that, since the potential is provided by the mean-field calculation, there is not the necessary freedom in the potential in order to produce the desired effect.

The second method redefines the two-body potential such that the initial and the new potential have precisely the same scattering properties for all energies. The only difference is that the number of bound two-body states is reduced by precisely the number of Hartree-Fock occupied single-particle states. The new potential is called a phase equivalent potential [99]. Any bound state, and not necessarily the lowest lying, could be removed using such phase equivalent potentials, without affecting the other states above or below.

A third method of dealing with the Pauli principle is to go through the hyperspherical adiabatic expansion procedure, and in the calculations of the radial wave functions, Eq. (39), explicitly omitting the lowest adiabatic potentials corresponding to the core occupied states. The remaining adiabatic potentials are fully exploited with their complete angular wave functions. This is a unique feature of the adiabatic method, where bound states asymptotically correspond to a distinct λ -function. However, this is only asymptotically, and excluded and included adiabatic potentials are not always completely decoupled at small and intermediate distances, which in turn translates to the subsequent radial calculations. It is therefore not always strictly correct directly to exclude states by dividing the space in this way.

The Pauli principle is accounted for with the first or second construction, since the deeper lying states are excluded as bound two-body states in the new potentials. The emerging solutions then appear as ground states in the new potential, and consequently with no nodes in the wave functions even at small distances. The orthogonality is not achieved through a larger number of nodes inside the core as for the ideal structure in ideal calculations. However, the resulting observables obtained by use of this type of averaging can be very accurate if either the three-body wave function is located outside the nodal region or the observable averaging eliminate the influence of the nodal structure.

With the third construction this is not an issue, as the wave functions are not

reconstructions made to reproduce the asymptotic behavior. Instead, the allowed wave functions are represented within the unoccupied space considered as separate from the occupied space. The Pauli principle is then obeyed provided the mixing is negligibly small between these two spaces in a full calculation. Some of the defining features of the adiabatic expansion is the separation of bound and continuum states, and the tendency to asymptotic decoupling between the angular wave functions. Most of the occupied core states should decouple completely, while only the highest-lying core states could couple to the unoccupied, valence allowed states at intermediate distances, making the assumed separation of spaces exact in many cases.

In practice, the most efficient and accurate method to account for the Pauli principle is a combination of the second and the third method. All the completely decoupled states are eliminated as described in the third method, but if any of the highest lying core states couple to the unoccupied states, these are removed using phase equivalent potentials. This implementation of the Pauli principle is both unusually simple and very close to being completely exact, and therefore this is the method used in this work.

4.4. *Finer points of the three-body equation*

The fact that the Hilbert space is intrinsically connected to the choice of the interaction is often not considered explicitly. Unless the Hilbert space is infinite, the interaction must be adjusted to the truncated space. Naturally, this is also true for the method presented here, where the Hilbert space for a many-body core is expanded to encompass the additional valence nucleons. This is particularly important for the interaction between valence nucleons, which is considered in the following.

It is known that a three-body system with zero-range two-body interactions produces an infinite number of strongly bound states, an effect often referred to as the Thomas effect [100]. This is closely related to the Efimov effect [101], and is in fact given by the same limit $|a/r_0| \rightarrow \infty$, where a is the s -wave scattering length and r_0 is the range of the potential. Irrespective of the s -wave scattering length the contact interaction in the Skyrme force will lead to a Thomas effect in the three-body system, which makes it a delicate process to include properly.

4.4.1. The valence nucleon-nucleon interaction. When it comes to the interaction between the valence nucleons there are three possibilities. The first and probably most obvious choice is to use exactly the same interaction between the valence nucleons as between all other nucleons. The main advantage from an aesthetic point of view is that this is very consistent, but this is also the most problematic. As all kinds of effective Hartree-Fock interactions are in-medium interactions, they are not directly applicable to free nucleons without some kind of renormalization. In particular, a Skyrme interaction would produce a bound two-body system when applied to two free nucleons, where the density of the core nucleons is (approaching) zero. As one of the main reasons for developing this combination of few- and many-body formalisms is to produce a wave

function with a consistent evolution from compact to extended configurations, having incorrect long range, asymptotic properties would be detrimental to our purpose.

The second and definitely most simple choice is to use an ordinary phenomenological nucleon-nucleon interaction [102] between the valence nucleons. This lacks the pleasant consistency of the first option, but as no new implementations are needed this has the advantage of being very simple. More importantly, the long-distance, asymptotic behavior is known to be correct by construction.

The third and initially most appealing choice is to use a combination of the two options above. More specifically, to use the same effective Hartree-Fock interaction between the valence nucleons as between all other nucleons, when the valence nucleons are close to the core, but then transition to a phenomenological interaction, with the correct asymptotics, as the valence nucleons move away from the core. The valence nucleons would then be treated consistently in compact configurations, but would regain the important correct asymptotic behavior with regards to scattering lengths and internal two-body energies for extended configurations and break-up reactions. The only slightly arbitrary choice would be the method of transitioning from one interaction to the other.

More specifically, the transition could be achieved by

$$V_{v_1 v_2} = W_{sk} V_{sk} + W_{ph} V_{ph}, \quad (44)$$

where V_{sk} is the Skyrme interaction, and V_{ph} is the phenomenological interaction, while W_i is the associated weight, with $W_{sk} + W_{ph} = 1$. A simple choice of weights would be a Woods-Saxon shape depending on the spatial extension of the system.

The transition is in the first Jacobi coordinate system where \mathbf{x} is between the two valence nucleons. If R_c is the radius of the core, then the limits for both valence nucleons being either inside or outside the core are given by

$$R_c \leq \left| \mathbf{r}_y \pm \frac{1}{2} \mathbf{r}_x \right| = \left| \frac{1}{\mu_y} \mathbf{y} \pm \frac{1}{2\mu_x} \mathbf{x} \right|, \quad (45)$$

$$R_c \geq \left| \mathbf{r}_y \pm \frac{1}{2} \mathbf{r}_x \right| = \left| \frac{1}{\mu_y} \mathbf{y} \pm \frac{1}{2\mu_x} \mathbf{x} \right|. \quad (46)$$

The transition point, where it changes from one interaction to the other being the most favored, is at $R_c = r_y$, and a sensible transition width would be half the corresponding r_x , see Fig. 3. As the extent of the core is not sharply defined a diffuseness parameter, d_c , could be added to the transition width. Using that $x = \rho \sin \alpha$ and $y = \rho \cos \alpha$, the weights become

$$\begin{aligned} W_{sk}(r_x, r_y) &= \left(1 + \exp \left(\frac{r_y - R_c}{\frac{1}{2} r_x + d_c} \right) \right)^{-1} \\ &= \left(1 + \exp \left(\frac{\sqrt{\frac{m}{\mu_{jk,i}}} \rho \cos \alpha - R_c}{\frac{1}{2} \sqrt{\frac{m}{\mu_{jk}}} \rho \sin \alpha + d_c} \right) \right)^{-1}, \quad (47) \\ W_{ph}(r_x, r_y) &= 1 - W_{sk} = \left(1 + \exp \left(\frac{R_c - r_y}{\frac{1}{2} r_x + d_c} \right) \right)^{-1} \end{aligned}$$

$$= \left(1 + \exp \left(\frac{R_c - \sqrt{\frac{m}{\mu_{jk,i}}} \rho \cos \alpha}{\frac{1}{2} \sqrt{\frac{m}{\mu_{jk}}} \rho \sin \alpha + d_c} \right) \right)^{-1}. \quad (48)$$

This transition description only involves α in the first Jacobi set with \mathbf{x} between valence nucleons, and it treats the limits appropriately. For $\rho \rightarrow 0$, $W_{sk} \rightarrow (1 + \exp(-R_c/d_c))^{-1} \rightarrow 1$ for $R_c/d_c \rightarrow \infty$. Likewise, for $\rho \rightarrow \infty$, $W_{sk} \rightarrow (1 + \exp(2\mu_x \cos \alpha / (\mu_y \sin \alpha)))^{-1} \rightarrow 0$ for $\alpha \rightarrow 0$ as would be the case for a contact valence nucleon-nucleon interaction.

The implementation of the potential in Eq. (44) within the hyperspherical adiabatic expansion, and in particular the solution of the angular eigenvalue problem (38), requires calculation of the matrix elements of the potential within the hyperspherical harmonics. The calculation of such matrix elements for a contact Skyrme interaction, although not complicated from the conceptual point of view, is rather lengthy and cumbersome. For this reason, and specially as a result of the discussion below, we skip here the details and focus just on the final result.

In particular, we show in Fig. 4 the λ_n spectrum obtained after solving Eq. (38) with potential (44) and using the transition described in Eqs. (47) and (48), with $d_c = 0.5$ fm and $R_c = 3.0$ fm. The Skyrme potential V_{sk} has been taken to be the SLy4 Skyrme force [92], whereas the phenomenological nucleon-nucleon potential V_{ph} has been taken from Ref. [102]. The result shown in the figure by the dashed curves corresponds to ^{26}O , viewed as $^{24}\text{O} + n + n$, after the first iteration. Also included for comparison in Fig. 4 is the λ_n spectrum obtained from an identical calculation, where the valence neutron-neutron interaction is just the traditional phenomenological interaction [102] (solid curves). The spectra are seen to be identical except for a single unphysical λ tending towards $-\infty$ as $\rho \rightarrow 0$ for a Skyrme interaction between the valence neutrons.

The infinitely deep λ is an example of the Thomas effect caused by the contact interactions in the Skyrme force. Even though these infinitely many bound states are here clearly supported by the lowest λ , they are difficult to exclude systematically. The lowest λ crosses all other λ 's at intermediate distances, which makes it impossible to simply remove that specific λ outright. The second option would be to use a phase equivalent potential, as discussed in Sec 4.3. However, as this λ is not tied to a specific state this is not feasible either.

For these reasons, for the moment the best option is therefore to forget the transition in Eq. (44) and simply use a phenomenological interaction instead. Fortunately, as seen in Fig. 4, this will have no effect on the relevant λ spectrum. Given that the λ spectrum dictates every other consecutive three-body calculation, using a phenomenological interaction will have no measurable effect on any of the results.

In the future this could be remedied by replacing the Skyrme force with a finite-range force such as the Gogny force [103]. Without a contact interaction there would be no Thomas effect, and the transition in Eq. (44) could be implemented without problems. Another benefit is that Gogny forces are based on Gaussians, which would make the transition to a (Gaussian) phenomenological interaction much less drastic. Then all

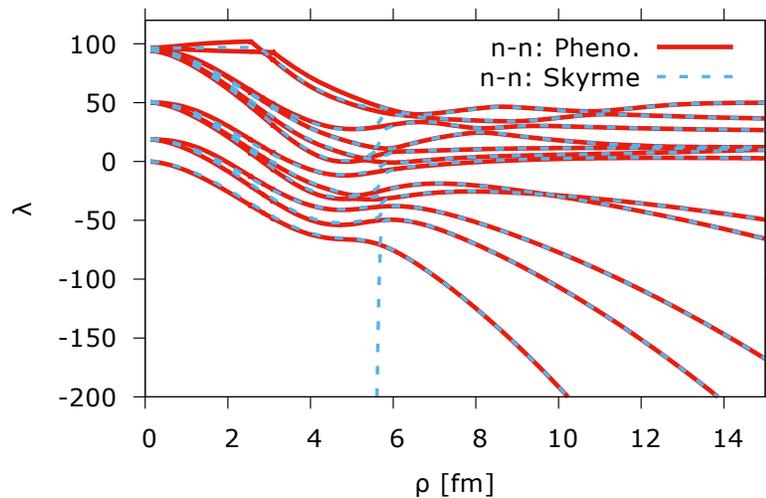


Figure 4. Comparison between the raw λ spectrum after the first iteration for a phenomenological valence neutron-neutron interaction (solid) and a more consistent interaction which transitions from Skyrme to phenomenological as described in Eq. (44) (dashed). The system in question is ^{26}O viewed as $^{24}\text{O} + n + n$.

nucleon-nucleon interactions in both valence and core space would be the same.

4.4.2. The three-body interaction. The final component to be discussed is the three-body interaction, V_3 , from Eq. (22). One option is to proceed as with the three-body interaction in the core, i.e. parameterize it as a density dependent two-body interaction and include it in $V_{v_1 v_2}$. In fact, if a Skyrme interaction were used between the valence nucleons, the density dependent t_3 term would be derived from a three-body interaction between the two valence nucleons and a sum over the core nucleons. Historically, it has been found that the density dependence was needed in the Skyrme interaction to counteract the massive and divergence causing t_0 term. As such it would not be sensible to parameterize V_3 as a density dependent two-body interaction without also using a Skyrme interaction between the valence nucleons.

It should be noted that if a finite-ranged Gogny type interaction were used for the core, it would, as mentioned, be possible to implement this interaction between the valence nucleons. In that case, the three-body interaction between the two valence nucleons and the core nucleons should be reparameterized as a density dependent two-body interaction and included in the t_3 term between the two valence nucleons. That would result in a method where the only freedom of any kind was in the choice of Gogny force.

Instead, at present we use a phenomenological three-body interaction of the form

$$V_3(\rho) = V_0 \exp\left(-\left(\frac{\rho}{r_0}\right)^2\right). \quad (49)$$

This form of the three-body interaction was originally added to the three-body Faddeev formalism to better account for three-body effects related to the Pauli principle and

Table 1. The results of choosing the three-body interaction strength V_0 before and after the iterations for $^{24}\text{O} + n + n$. Included is the three-body energy E_3 , the rms size of the system $\langle \rho^2 \rangle^{1/2}$, the weights of the three lowest λ_n 's in the radial solution, and the weights partial wave contributions. In both cases $r_0 = 6.0$ fm and $V_0 = -6.45$ MeV. The energies are in MeV, the sizes in fm, and the weights and contribution in percent.

			Weights			Contribution						
	E_3	$\langle \rho^2 \rangle^{1/2}$	λ_1	λ_2	λ_3	$s_{\frac{1}{2}}$	$p_{\frac{1}{2}}$	$p_{\frac{3}{2}}$	$d_{\frac{3}{2}}$	$d_{\frac{5}{2}}$	$f_{\frac{5}{2}}$	$f_{\frac{7}{2}}$
Before	-0.28	6.50	86	14	0	1	1	2	90	3	0	3
After	-0.27	6.53	86	14	0	1	1	2	90	3	0	3

polarization effects [104, 105]. As the Skyrme force is a global force, which is mainly fitted to nuclei near stability, it cannot reasonably be expected to provide predictions with an accuracy on the keV scale. This is in particular true for systems very far from stability at the dripline. The three-body interaction is then a useful free parameter, which can be used for fine-tuning the energy at the keV scale, whereas the structure and long-range behavior is kept completely unchanged.

The preservation of the long-range behavior is a given as the Gaussian is short-ranged. The preservation of the structure can be seen by considering the application of the three-body interaction before and after the iterations described in the beginning of Sec. 4. This is illustrated in Table 1, where the result of adjusting the three-body interaction before and after the iterations is seen for $^{24}\text{O} + n + n$. It should be noted, that the three-body energy has not been adjusted to anything in particular, the intent is only to illustrate the effect of applying the three-body interaction. The table includes the three-body energy, the root-mean-squared (rms) size of the system, the weights of the lowest three λ_n 's, and the partial wave contributions in the core - valence neutron system. All the weights are identical both for the three λ 's and the partial wave composition. Given that convergence is here defined as consecutive iterations differing by less than 0.02 MeV, a difference in energy of 0.01 MeV is within the uncertainty. The difference on the second decimal of the rms size is then also to be expected.

5. Experimental verification: $^{24}\text{O} + n + n$

To test the method derived in the previous sections a suitable system must be identified. This should to a good approximation be a three-body system, which means it should be possible to impose an assumed clusterization. Ideally, the clusters should be weakly bound to make the three-body formalism more viable. As stated in Sec. 3.2 it is assumed that two of the clusters are single, identical nucleons, and that the core is much heavier than the nucleon. It is also assumed that the core is spherical, and consisting of an even number of neutrons and protons.

Our system of choice is ^{26}O viewed as a ^{24}O core and two valence neutrons, which is

well suited for several reasons. First of all, ^{24}O is widely believed to be doubly magical and spherical, and also at the very edge of the neutron dripline [17]. Even though ^{26}O is ever so slightly on the unbound side, it has recently come within experimental reach [18, 19, 20]. This provides a few key observables to compare with calculations, while many questions remain unanswered.

5.1. Fundamental considerations: Iterations and potentials

At the heart of the hyperspheric, adiabatic expansion of the Faddeev equations lies the hyperangular eigenvalues, λ_n , from Eq. (39). They are the main connection between the hyperangular and the hyperradial equations, which are the crucial part of the adiabatic expansion. The various coupling terms (C_{nm} , P_{nm} , P'_{nm} , Q_{nm} , and Q'_{nm} in Eq. (39)) also connect the two, but should more be considered as corrections to the main quantities determined by λ_n .

One of the interesting aspects about the method presented here is how the iterative process allows the mean-field structure to affect the three-body calculation, and vice versa. This is seen in Fig. 5, where the spectrum of hyperangular eigenvalues is presented as a function of hyperradius for the first and last iteration. The calculation is for $^{24}\text{O} + n + n$ using the Skyrme parameterization known as SkM* [106]. The interpretation of the λ spectrum is the same as for a regular three-body calculation, namely that λ 's which tend to $-\infty$ as $-\rho^2$ correspond to bound states in the two-body systems. The energy of the bound states is given by the large distance asymptotic behavior of λ by

$$E_{2b} = \frac{\hbar^2}{2m} \frac{\mu_{jk}}{m} \frac{\lambda}{\rho^2} \quad (50)$$

where m is the normalizing mass, and μ_{ij} is the reduced mass.

The 16 lowest neutron levels, corresponding to the $1s_{1/2}$, $1p_{3/2}$, $1p_{1/2}$, $1d_{5/2}$, and $2s_{1/2}$ states, are occupied by the core neutrons and therefore Pauli forbidden. The change in the λ 's corresponding to these five states in Fig. 5 reflects the change in core structure due to the valence neutrons. As discussed in Sec. 4.3 the Pauli forbidden states are removed either by use of phase equivalent potentials or by simply eliminating the corresponding decoupled λ 's. As the core-occupied states clearly are decoupled, the simplest solution is here to eliminate the corresponding λ 's.

The effect of the iterative process is also seen in the changes of the three-body energy. In Table 2 the three-body energy for each iteration in a $^{24}\text{O} + n + n$ calculation is seen for three different parameterizations of the Skyrme forces known as SkM* [106], SLy4 [92], and Sk3 [107]. The calculations are done with the three-body interaction from Eq. (49) using $V_0 = -8$ MeV and $r_0 = 6$ fm in all three instances. Unless otherwise stated convergence is defined as when the three-body energies of two consecutive iterations differ by less than 0.02 MeV, but other criteria could be chosen, depending on the focus of the investigation. Here, the energy was chosen because it is a fairly direct representation of the change between the iterations.

In Table 2 it should first of all be noted how fast the convergence is, which means

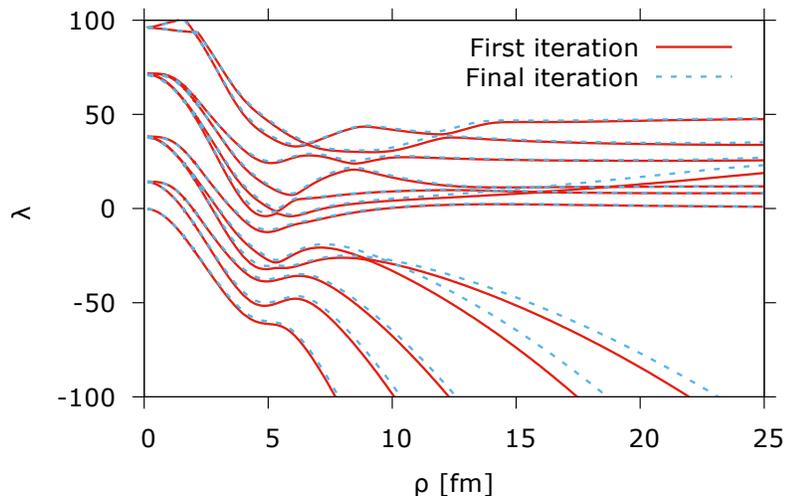


Figure 5. The λ spectrum for $^{24}\text{O} + n + n$ after the first (red, solid) and last (blue, dashed) iteration using the Skyrme parameterization SkM* [106]. The lowest five λ s correspond to core occupied states, and are therefore Pauli forbidden. Note how the iterative process changes the λ spectrum for the occupied states, indicating a change in core structure.

Table 2. The changes in three-body energy, E_3 , in MeV between iterations for the three Skyrme forces SkM*, SLy4, and Sk3. The energy is said to have converged when the difference in three-body energy between consecutive iterations is less than 0.02 MeV. The three-body interaction strength (V_0) has not been adjusted to anything in particular. It is -8 MeV for all forces and iterations, with $r_0 = 6$ fm.

	E_{3B}			
	1	2	3	4
SkM*	-1.75	-1.06	-1.12	-1.14
Sk3	-0.31	-0.07	-0.10	-0.11
SLy4	-0.93	-0.85	-0.87	

the added computation time from the iterations is rather limited. Secondly, there is a relatively large difference between the first and the second, compared to the later, iterations. This is because the mean-field in the first iteration by choice cannot include the effect of the valence neutrons. In the second iteration the effect of the nucleons are felt, and a significant change in energy is seen to occur.

Skyrme forces have over the years been shown to be very successful effective two-body interactions in mean-field calculations of ground state properties of nuclei. The parameters are usually fitted to reproduce nuclear matter properties, as well as binding energies and root-mean-square charge radii of doubly magic nuclei. However, different parameterizations can satisfy these requirements, and as a result, multiple Skyrme forces are found in the literature. It is therefore not surprising that the final energies in Table 2 vary by slightly more than 1 MeV for the three Skyrme parameterizations used here.

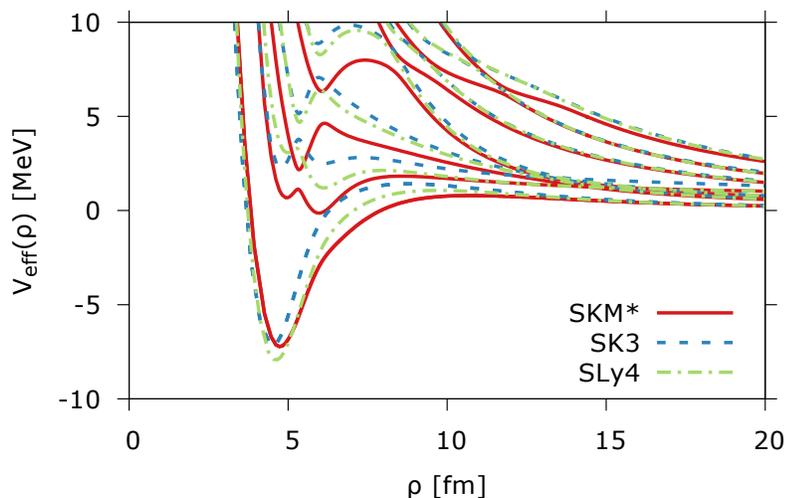


Figure 6. The effective potentials for $^{24}\text{O} + n + n$ using the Skyrme parameterizations known as SkM* [106] (solid, red), Sk3 [107] (dashed, blue), and SLy4 [92] (dashed-dotted, green). The core occupied, Pauli forbidden states have been removed by excluding the corresponding effective potentials. This does not include three-body potentials and couplings such as Q_{nn} . Note the overall similarity between the potentials, where the main difference is at the second effective potential at intermediate distances. The results for SLy4 are taken from Fig.1 of Ref. [21].

The Sk3 parameterization is an example of one of the earliest and most simple, but also very successful parameterizations. It contains a linear dependence on the density ($\alpha = 1$) and $x_0 = 1$ as the only x_i parameter. The SkM* parameterization is more elaborate, and originally constructed to improve $E0$ and $E1$ giant resonances, as well as fission barriers. Finally, the SLy4 parameterization is a more recent example of Skyrme forces being revisited with the aim of improving the isospin properties of nuclei away from the valley of stability. As such, it should be well-suited as a starting point for many of our investigations along the nucleon driplines.

However, the apparent differences between the results of the various Skyrme parameterizations are mainly an overall displacement and not a structural difference. This is seen in Fig. 6, where the effective potentials based on the Skyrme parameterizations from Table 2 are shown for $^{24}\text{O} + n + n$. Neglecting coupling terms and the three-body interaction to better compare the parameterizations directly, the effective diagonal potentials can be seen from Eq. (39) to be

$$V_{eff}(\rho) = \frac{\hbar^2}{2m} \frac{\lambda_n(\rho) + 15/4}{\rho^2}, \quad (51)$$

where m is the normalization mass.

The λ 's corresponding to core occupied, Pauli forbidden states are not included in Fig. 6. It is seen that all three parameterizations form a pocket at roughly the same distance and depth, capable of sustaining a three-body state. The differences in shape and width of this pocket is responsible for the variations in energies seen in Table 2. The higher-lying effective potentials have the same qualitative structure, but differ slightly

in their exact placements. Importantly, the asymptotic behavior of the potentials are basically identical, which ensures very similar long-range structures and dynamics.

5.2. Reproducing experimental values

Given that ^{25}O and ^{26}O have recently come within experimental reach a quantitative examination and comparison can be performed. The lowest-lying resonance in ^{25}O has been measured to be a $d_{3/2}$ resonance at 0.749(10) MeV with a width of 88(6) keV [20]. Likewise, the ground-state of ^{26}O is measured to be a 0^+ state at 0.018(3) MeV [20]. In the same study the half-life was deduced to be $T_{1/2} \sim 0.01 - 1$ fs.

The observed ground-state of ^{26}O can be used to fix the three-body interaction, which is the only freedom remaining within this method, after a specific Skyrme parameterization has been chosen. Every other calculation and observable are completely determined by these choices. This is in contrast to most phenomenological models, where the two-body resonance state would also be used as an input parameter [108]. In Table 3 the predicted energy of the $d_{3/2}$ resonance in ^{25}O is shown for the three Skyrme parameterizations, along with the energy predicted using regular mean-field Hartree-Fock (HF) calculations with the same parameterizations. In addition, the half-lives resulting from the calculated $d_{3/2}$ energies have also been included. Finally, as the various Skyrme parameterizations produce different energies, it is necessary to use different three-body interaction strengths, to achieve total three-body energy of 0.018 MeV. These strengths are also included in Table 3.

All four rows in Table 3 deserve attention. First of all, it is interesting to note that the three-body interaction strengths for SLy4 and SkM* are almost identical despite the final energies in Table 2 differing by almost 0.3 MeV. The different response to the three-body interaction is caused by the slight difference in potential shape, as seen in Fig. 6. Despite this, the produced $d_{3/2}$ resonance energies are basically identical for the SLy4 and the SkM* parameterization. Not only that, but they are within 0.1 MeV of the experimental value. It is not so surprising that the Sk3 prediction is slightly further off, given that it is one of the simpler, earlier parameterizations, fitted to a much more limited data set, close to stability. It should also be noted that the fine-tuning with the three-body interaction just shifts the three-body energy slightly. It does not affect the structure or the two-body interaction, as discussed in Sec. 4.4.2. The very accurate reproduction of the $d_{3/2}$ energy level is therefore not a result of the three-body interaction. It is a direct consequence of the method, with no remaining freedom after the Skyrme parameterization has been chosen.

It is then very interesting to see, that regular mean-field Skyrme calculations with the same parameterizations yield predictions that are not only far from the experimental value, but also clearly bound. Mean-field calculations are known to become inaccurate, when approaching the driplines, so an erroneous result is to be expected. What is interesting is that the two-body potential, which produces the $d_{3/2}$ resonance energy in our method, is provided by the core calculation. This indicates that the combination

Table 3. This table is divided according to the three different Skyrme forces used. The three-body energy has been adjusted to the experimental value of 0.018 MeV using the three-body interaction strength V_0 , but keeping the range constant at $r_0 = 6$ fm. All presented results are after the final iteration. Included is the energy of the first $d_{3/2}$ resonance state in ^{25}O computed using our method and compared to the result of traditional HF calculations. This should be compared with the experimental value of 0.749(10) MeV [20]. The half-life $T_{1/2}$ is calculated using a WKB approximation for the tunneling probability, and harmonic oscillator approximation for the knocking rate. The experimental value from Ref. [20] is $\sim 0.01 - 1$ fs. All energies are in MeV and all lengths are in fm.

	SLy4	Sk3	SkM*
V_0	-5.71	-7.71	-5.72
$E_{d_{3/2}}(Our)$	0.85	1.23	0.83
$E_{d_{3/2}}(HF)$	-0.96	-0.53	-1.15
$T_{1/2} [fs]$	0.4	0.6	0.2

of the three-body approach with the self-consistent mean-field calculation provides a small, but crucial change to the effective potential.

The fourth and final row in Table 3 is the half-life of ^{26}O calculated using a simple WKB approximation for the tunneling probability, and a harmonic oscillator approximation for the knocking rate. Despite the simple approximations, the calculated half-life is right in the middle of the experimental interval. Given that the half-life depends exponentially on the barrier height and thickness this is a remarkably good agreement.

The predicted energy for the $d_{3/2}$ state is derived from the invariant mass spectrum seen in Fig. 7. For the core-neutron system the invariant mass, E_{core-n} , can be interpreted as the kinetic energy of this system in the final state (after removal of a neutron), where $\mathbf{p}_{core} + \mathbf{p}_n = 0$, with \mathbf{p}_{core} and \mathbf{p}_n being the core and neutron three-momentum, respectively [98]. The resonance energy is then defined as the energy, where this spectrum has a maximum.

The invariant mass spectrum is particularly useful for two reasons. First, it is a direct calculation of the resonance energies, which can otherwise be difficult to calculate when there is no barrier to enable bound-state approximations. And second, it is a physical observable allowing for direct comparison between theory and experiment [109]. In Fig. 7 the experimental data from Ref. [20] is seen alongside the three Skyrme parameterizations. Unfortunately, the experimental beam profile is not available (and therefore not taken into account), which makes the calculated width slightly more narrow than the experimental one [98]. Also included is the neutron-neutron invariant mass spectrum, which is structureless as there are no neutron-neutron resonances.

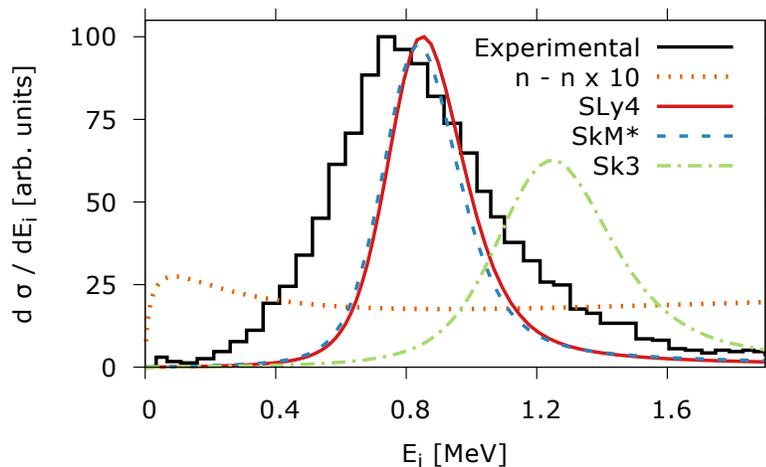


Figure 7. The invariant mass spectrum of the core-neutron two-body system for $^{24}\text{O} + n + n$ with the SLy4 (solid, red), SkM* (dashed, blue), and Sk3 (dashed-dotted, green) Skyrme parameterizations as a function of the two-body energy. The SLy4 neutron-neutron (dotted, orange) invariant mass spectrum is also included, scaled by a factor of 10 to make it visible. The black curve is the measurements from Ref. [20]. The SLy4 and SkM* curves are taken from Fig.4 of Ref. [21].

5.3. Further predictions

Technically, the core-nucleon invariant mass spectrum is calculated from the core-nucleon phase-shifts through the cross section under the so-called sudden approximation [98, 110, 111, 112]. The sudden approximation is the assumption that a high-energy beam hits a target such that one constituent particle is removed instantaneously from the three-body system. Instantaneous here means that the reaction times are much shorter than the time for motion of the particles in the three-body system. As the focus here is on systems with very weakly bound valence nucleons this requirement is fulfilled even for moderate beam-energies.

Given that there is a final state interaction between the two remaining particles after the sudden removal of the third, the two-body wave function will be distorted. In keeping with the convention for three-body Jacobi coordinate systems the relative and total momentum of the two-body system with respect to the center-of-mass of the three-body system is \mathbf{k}_x and \mathbf{k}_y , respectively. The probability, P , of finding the remaining two particles with momentum $(\mathbf{k}_x, \mathbf{k}_y)$ is proportional to the transition matrix element

$$P_{s_x \sigma_x}^{JM}(\mathbf{k}_x, \mathbf{k}_y) \propto \langle e^{i\mathbf{k}_y \cdot \mathbf{y}} w_{s_x \sigma_x}(\mathbf{k}_x, \mathbf{x}) | \psi^{JM}(\mathbf{x}, \mathbf{y}) \rangle, \quad (52)$$

where J and M are the total spin and projection of the halo nucleus, while s_x and σ_x are the spin and projection of the two-body final state, and w is the distorted two-body wave function [110]. The cross section (or momentum distribution) is then proportional to the square of the transition matrix element, averaged over initial states (M), and

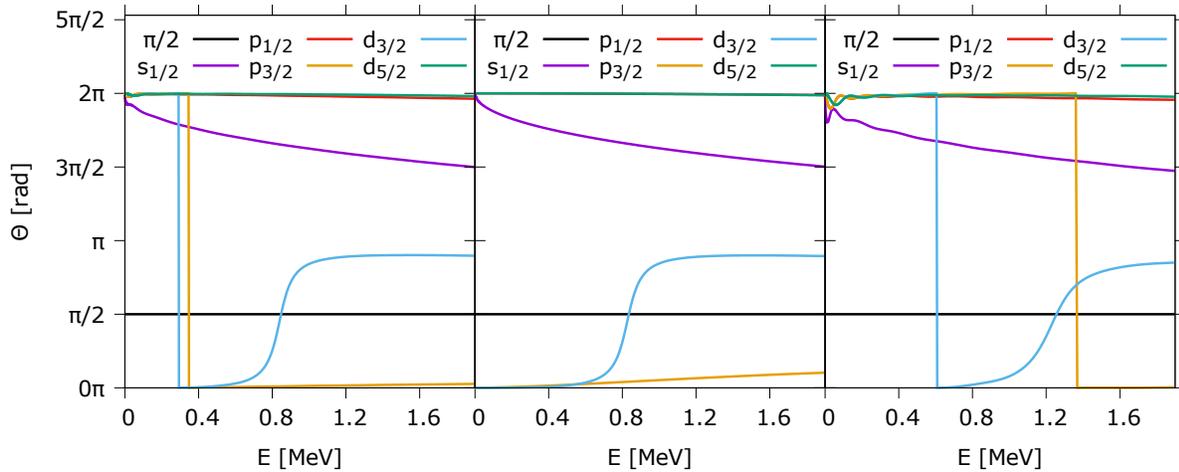


Figure 8. The phase shifts for the core-neutron two-body system in $^{24}\text{O} + n + n$ for the s -, p -, and d -states for SLy4 (left), SkM* (middle), and Sk3 (right). The horizontal black line at $\pi/2$ is included to guide the eye. The vertical transitions do not indicate a resonance, but are a result of the phase shifts being calculated in the range 0 to 2π .

summed over final states (s_x, σ_x)

$$\frac{d^6\sigma}{d\mathbf{k}_x d\mathbf{k}_y} \propto \sum_M \sum_{s_x, \sigma_x} |P_{s_x \sigma_x}^{JM}(\mathbf{k}_x, \mathbf{k}_y)|^2. \quad (53)$$

The earlier interpretation of the invariant mass as the kinetic energy in the final two-body system can be expressed more explicitly as

$$E_{\text{core-n}} = ((E_{\text{core}} + E_n)^2 + c^2(\mathbf{p}_{\text{core}} + \mathbf{p}_n)^2)^{1/2} - (M_{\text{core}} + M_n)c^2, \quad (54)$$

where E_i is the energy, \mathbf{p}_i the momentum, and M_i the rest mass of the individual particles. Based on this, it can be shown [98] that the invariant mass spectrum, defined as $d\sigma/dE_{\text{core-n}}$, is related to the cross section as

$$\frac{d\sigma}{dE_{\text{core-n}}} = \frac{m(M_{\text{core}} + M_n)}{M_{\text{core}}M_n} \frac{E_{\text{core}} + E_n}{E_{\text{core}}E_n} \frac{1}{k_x} \frac{d\sigma}{dk_x}, \quad (55)$$

where the cross section from Eq. (53), integrated over unobserved parameters, results in $d\sigma/dk_x$.

The invariant mass spectrum therefore depends on this cross section, which is determined by the distorted wave function. As the distorted wave function depends crucially on the phase shifts, the energy structure seen in Fig. 7 could also be deduced from the phase shifts themselves. These are seen in Fig. 8, where the crossing of $\pi/2$ indicates a resonance state. The phase shifts are here calculated modulo 2π , which means the vertical lines are not resonance states. The decomposition into individual partial waves clearly shows that there are no other possible resonances in the low energy region, and it also shows the state to be a $d_{3/2}$ state in accordance with the experimental observations.

Various other interesting observables can be extracted from the cross section in Eq. (53). The momentum distribution of the fragments after a breakup reaction is

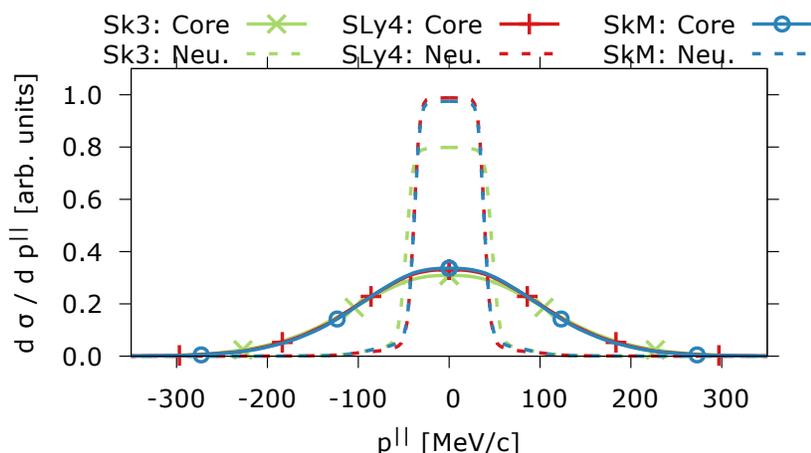


Figure 9. The longitudinal momentum distributions of the ^{24}O core (solid) and neutron (dashed) after knockout of one neutron calculated using the SLy4 (red), Sk3 (green), and SkM (blue) Skyrme parameterizations.

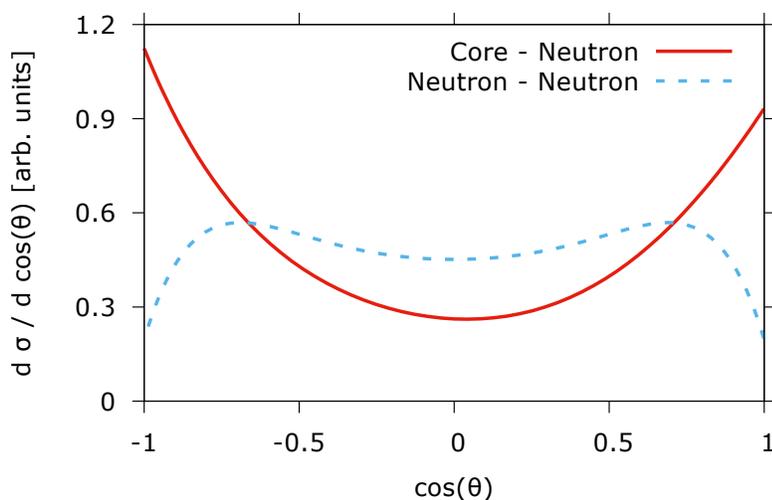


Figure 10. The angular distribution of $^{24}\text{O} + n + n$ between directions of neutron and core-neutron, and core and neutron-neutron momenta, respectively. The results are for the SLy4 Skyrme force.

experimentally a very direct look into the structure of the system. The main difficulty in interpreting such measurements is that there is often a mixture of effects stemming from both the original structure of the system and the reaction mechanism itself, and it is not easy to disentangle these contributions. However, if the third particle is removed suddenly, the structure of the remaining two particles is unaffected by the reaction mechanism. Under the sudden approximation, the remaining particles are released with momentum distributions equal to the distribution in the initial wave function.

The longitudinal momentum distribution for both the ^{24}O core and the remaining neutron in $^{24}\text{O} + n + n$ are shown in Fig. 9 after removal of one of the neutrons. The full width at half maximum (FWHM) for the core distribution is about 200 MeV/c. In

contrast, the FWHM for the neutron distribution is only about 100 MeV/c, which reveals the moderate neutron halo structure allowed in d -waves. The relatively restrained spatial configuration leads to a more extended configuration in momentum space. The almost identical distributions resulting from the various Skyrme parameterizations once again demonstrate how independent of the specific parameterization the results presented here are.

Further structural insights are provided by the angular distribution seen in Fig. 10, where both the angular distribution after removal of a neutron (core-neutron system) and the angular distribution after removal of the core (neutron-neutron system), are shown. These angular distributions are again derived from Eq. (53) by integrating over unobserved parameters. In the angular distribution for the core-neutron system the angle is between the ^{25}O momentum and the relative momentum between neutron and core after fragmentation, while the angle is between the center-of-mass momentum and the relative momentum of the two neutrons after fragmentation. Angular distributions are very sensitive to the mixing of various partial waves, and can therefore be used to probe the structure of the system [113]. In Fig. 10 the asymmetric parabola is again an indication of the dominating d -wave in the state. Neither the momentum distribution, nor the angular distribution has been measured in ^{26}O so far, but both Figs. 9 and 10 are predictions for the observables of a state that lives sufficiently long for a knockout process to be initiated.

6. Clusters and Efimov: $^{70}\text{Ca} + n + n$

The specific parameters in the Skyrme forces are fitted to experimental data on stable nuclei. Naturally, this makes any prediction based on such forces more reliable closer to stability and in areas where changes from nuclei to nuclei is more gradual [114]. This is very clearly reflected in the uncertainty of the predicted positions of the dripline based on various parameterizations. This uncertainty is inherent in any mean-field prediction reaching outside the experimentally known region. Considering for instance the calcium isotope chain, the neutron dripline is usually thought to be in the range $A = 68 - 76$ [115, 116]. With the SLy4 parameterization [92] ^{70}Ca is the last bound isotope, while ^{72}Ca ($^{70}\text{Ca} + n + n$) can be bound in the following three-body calculation with three unbound subsystems, depending on the three-body interaction.

The main point of interest in this section is the neutron dripline for calcium isotopes studied from a new and systematic perspective with the method presented here [117]. Given that Skyrme parameters are fitted to observable quantities of experimentally well-known nuclei, existing parameterizations cannot be expected to present accurate predictions well into experimentally unknown regions without alterations. This fact will here be exploited to examine how nuclear configurations evolve as the dripline is approached. Specifically, it will be examined how halo structures and possibly even Efimov states could appear close to the dripline, and whether this would be reflected in observable long-distance structures.

With the traditional ordering of the single-particle levels ${}^{70}\text{Ca} + n + n$ is an ideal choice to study halo and possible Efimov states. The 50 neutrons in ${}^{70}\text{Ca}$ would traditionally exactly fill the $g_{9/2}$ state, making it a very strong magic number, and leaving $s_{1/2}$ and $d_{5/2}$ as the nearest unoccupied states for the two valence neutrons. In particular, the available $s_{1/2}$ is interesting as sufficiently low binding in this state should lead to the formation of halos [47, 118, 119, 120]. It is also a necessary requirement for the formation of Efimov states, along with an extremely large s -wave scattering length [101, 121, 122, 123, 124, 125, 126, 127].

To allow for systematic continuous variation, a specific Skyrme parameterization—the SLy4—is chosen and the overall t_i parameters are scaled as $t_i \rightarrow S t_i$, while the x_i and W_0 parameters are left unchanged. Scaling identically the t_i parameters amounts roughly to an overall scaling of the potential itself, approaching the dripline as needed, while the structure dictated by x_i and W_0 is left unchanged. The SLy4 parameterization is chosen as a baseline as it was originally designed to improve predictions for nuclei far from stability.

Far from stability the magic numbers are less sharply defined, they could change slightly, or there could be inversion of the ordering in gds shell [22, 128]. However, an inversion, placing the $g_{9/2}$ state above the $s_{1/2}$ state and making ${}^{60}\text{Ca}$ the last bound calcium isotope, as suggested by some recent coupled-cluster calculations [22], would have a very minor effect on any conclusion drawn here. This would change only the neutron-core potential by the contribution from the $g_{9/2}$ state. As this is fully occupied in the ${}^{70}\text{Ca}$ calculation, it does not affect strongly the valence nucleons. The essential part in both cases is the unoccupied $s_{1/2}$ state.

6.1. Short-distance structure

Scaling the Skyrme parameters in a ${}^{70}\text{Ca} + n + n$ calculation as $t_i \rightarrow S t_i$ for the SLy4 parameterization with the factor $S = 1.17$ and 1.20 , in addition to $S = 1.00$, yields the core-valence neutron central and spin-orbit potential shown in Fig. 11. These specific scaling values are chosen for the interesting properties of the resulting potentials in relation to halo formations and Efimov physics, which will be discussed later. The important point is that for $S = 1.17$ there is a near degeneracy between the relevant two-body energies $E_{s_{1/2}} = 0.017$ MeV and $E_{d_{5/2}} = -0.026$ MeV, but for $S = 1.20$ the relevant two-body energies are $E_{s_{1/2}} = 2.4 \cdot 10^{-4}$ and $E_{d_{5/2}} = -0.32$, all in MeV. For values of S below 1.17 the ordering is opposite, and $s_{1/2}$ is above $d_{5/2}$.

An interesting complication to be studied here is therefore how the value of S affects the energy of the $d_{5/2}$ state relative to the $s_{1/2}$ state. The inversion between the s - and d -level with S makes it possible to study the conditions for halo structures. It is suspected that there might be a near degeneracy among the s -, d -, and possibly even g -orbitals around the very neutron-heavy end of the calcium isotope chain [22, 128]. Any realistic investigation of these isotopes must therefore be able to account for such a degeneracy, in particular with respect to halos and Efimov states as these depend so

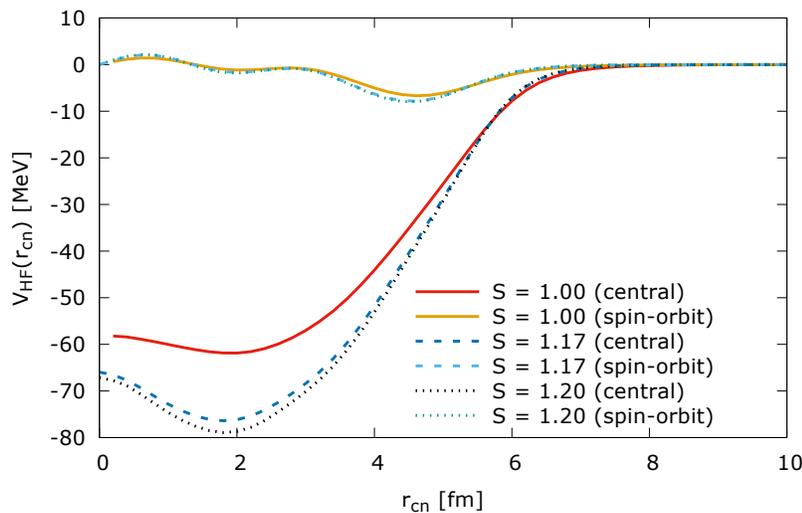


Figure 11. The central and spin-orbit part of the self-consistent mean-field core-neutron potential for $^{70}\text{Ca} + n + n$ calculated for three different scalings of the Skyrme parameters ($t_i \rightarrow St_i$) using the SLy4 parameterization as a baseline.

crucially on the characteristics of the s -orbital.

A clear difference is seen in Fig. 11 for the central part, which becomes more attractive as the potential initially is attractive, and the factor is larger than one. However the spin-orbit potential is basically unchanged indicating the structure of energy levels is mostly unchanged, they are only shifted down.

The structure of a three-body system is fundamentally determined by two aspects: the two-body and the three-body interactions. Assuming a given valence neutron-neutron interaction, here the phenomenological interaction from Ref. [102], the crucial quantities for the formation of cluster structures are the core-valence neutron interaction and the overall binding of the three-body system. The core-valence neutron interaction is the SLy4 parameterization of the Skyrme force, scaled as specified. However, the binding of the three-body system is not completely determined by that interaction alone, as there remains a degree of freedom in the three-body interaction.

As previously a Gaussian three-body interaction is used of the type specified in Eq. (49), where the range is kept constant at $\rho_0 = 8$ fm, and the strength V_0 is used to adjust the three-body energy. Changing the three-body energy without changing the underlying two-body interactions makes it possible to see how and under which circumstances halo structures and possibly Efimov states appear for a given two-body interaction.

To gain an initial understanding of the nature of the system from these potentials the probability distribution of the three-body wave function can be considered in traditional relative coordinates as in Fig. 3. The detailed spatial structure can be seen by integrating the probability distribution of the three-body wave function over

the directional angles, i.e

$$P(r_x, r_y) = \int r_x^2 r_y^2 |\psi_{3b}(\mathbf{r}_x, \mathbf{r}_y)|^2 d\Omega_x d\Omega_y, \quad (56)$$

where Ω_x and Ω_y are the directional angles from Sec. 4.2. Using the coordinates from Fig. 3 results in two different visual representations of Eq. (56). In addition, a specific value of S and a specific three-body energy must be chosen. Figure 12 contains 8 sub-figures showing the probability distribution for the ground state of $^{70}\text{Ca} + n + n$ for $S = 1.10$ and 1.17 as well as for $E_3 = -1.5$ MeV and 0.00 MeV in both relative coordinate sets.

In Fig. 12 it is therefore possible to directly see the effect both of changing three-body energy and of scaling the two-body interaction. Unsurprisingly the most unambiguous configuration is seen in Fig. 12 (f), where the two-body interaction is most attractive and the three-body system is most bound. Here three clear peaks are observed. Although three-body configurations in general are complicated superpositions of many possible particle placements, it is common to try and reduce them qualitatively to more intuitively understandable configurations. For Fig. 12 (f) the three peaks correspond roughly to three very distinct and understandable configurations. The first peak at $r_{n,c} \simeq 2$ fm and $r_{n,cn} \simeq 6$ fm can be interpreted as a configuration where one valence neutron is very close to the core and the other is further away. The second peak at $(r_{n,c}, r_{n,cn}) \simeq (6, 2)$ (both in fm) can be interpreted as the opposite, where the other neutron is close to the core. Finally, the central peak can be interpreted as a more separated structure where both neutrons are away from the core.

However, the configurations are not as sharply defined as the discussion above leads to believe. As illustrated in Fig. 3 the direction of the orientation is not specified, so a rotation is possible for each configuration. This is demonstrated by Fig. 12 (e), which specifies exactly the same wave function as Fig. 12 (f), but it is much more smeared out. There are five less sharply defined peaks, which roughly correspond to range from both neutrons being closely together on the same side of the core, to the neutrons being far apart on opposite sides of the core. In effect, a more exact specification of the configuration would be to say that for each of the probable configurations in Fig. 12 (f), each of the probable configurations in Fig. 12 (e) are allowed.

Fortunately, the evolution is generally as one would expect. Given an initial configuration in the second coordinate system, as for instance the one seen in Fig. 12 (f) or Fig. 12 (b), the probability distribution tends towards a more diluted structure when the three-body binding is weakened, but maintains the underlying configuration. When increasing the strength of the two-body interaction with S the tendency is the same, only less pronounced. The same is true for the first relative coordinate set, only the structure is more muddled.

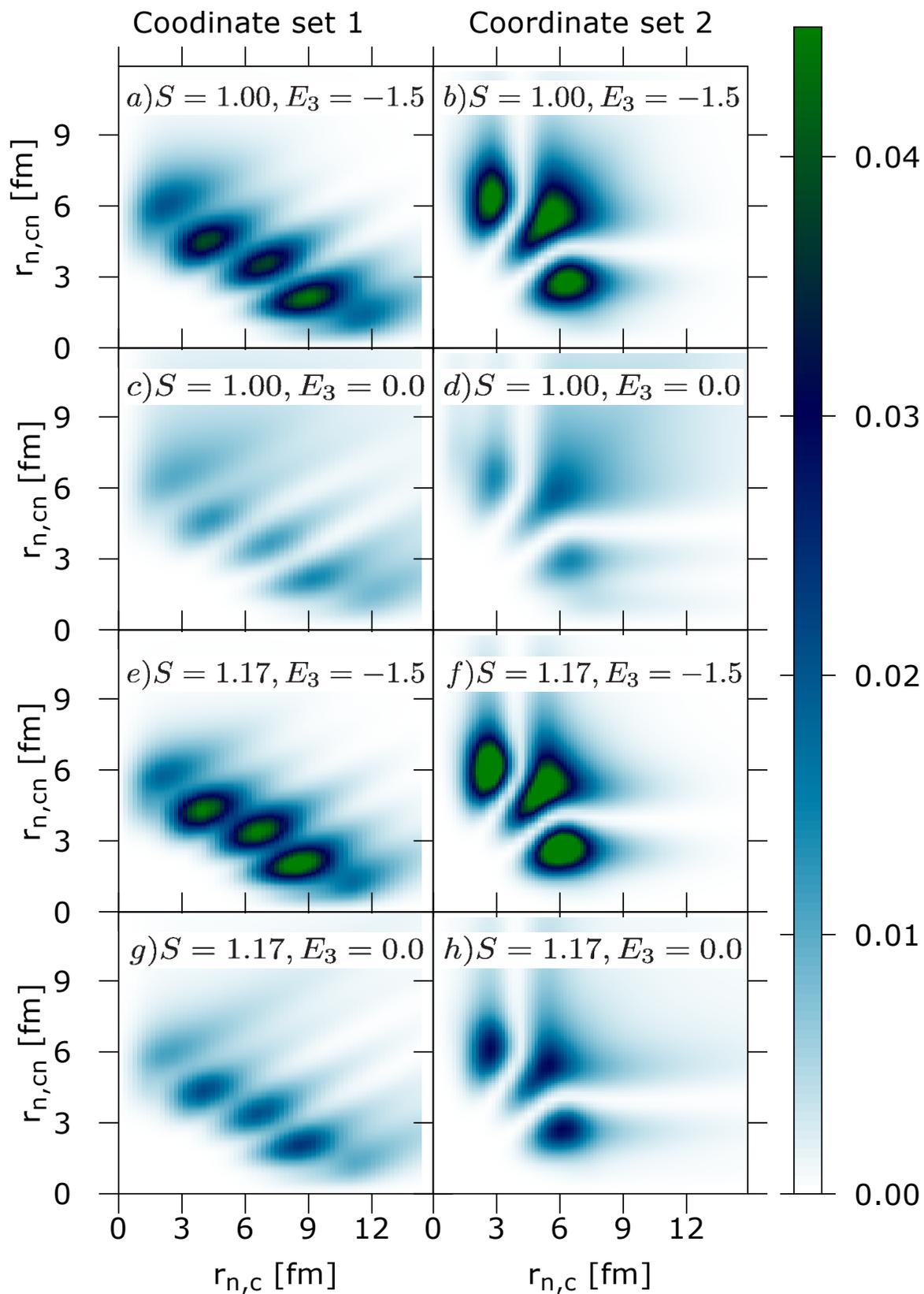


Figure 12. The probability distribution from Eq. (56) for the ground state $^{70}\text{Ca}+n+n$ for both relative coordinate systems, with $S = 1.00$ and 1.17 for both $E_3 = 0.00$ MeV and $E_3 = -1.5$ MeV.

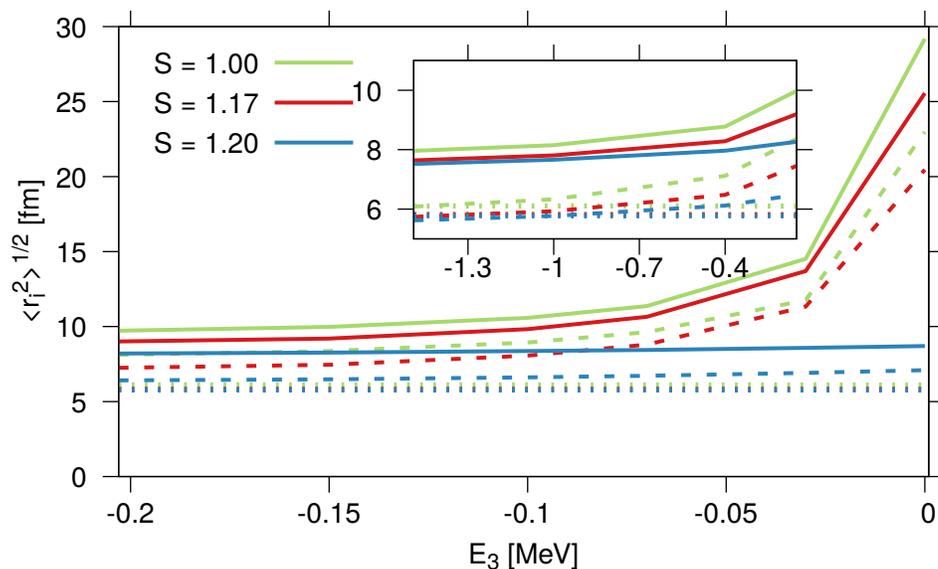


Figure 13. Root-mean-square distances as functions of the three-body energy, E_3 , for the ground state of $^{70}\text{Ca} + n + n$. The two-body systems distances are valence neutron-neutron $\langle r_{n,n}^2 \rangle^{1/2}$ (solid), valence neutron-core $\langle r_{c,n}^2 \rangle^{1/2}$ (dashed), and core neutron-neutron $\langle r_{c,c}^2 \rangle^{1/2}$ (dotted) radius for $S = 1.00$ (red curves), $S = 1.17$ (blue curves), and $S = 1.20$ (green curves). The insert shows the behavior for larger binding. (Update of Fig.2 in Ref. [117]).

6.2. Long distance structure

Halo structures are defined by their very large spatial extension, which necessitates s -wave (or possibly p -wave) structures, with very small binding, and no long-range Coulomb interactions [47, 118]. As seen from Fig. 12 very weakly bound extended structures are difficult to interpret directly from the three-body wave function. Instead, simplest properties reflecting the structure for very extended systems are the various average nucleon-nucleon distances. At least three different distances are of interest: the valence neutron-neutron average distance, $\langle r_{n,n}^2 \rangle^{1/2}$, the valence neutron-core center of mass average distance, $\langle r_{c,n}^2 \rangle^{1/2}$, and neutron-neutron average distance inside the core, $\langle r_{c,c}^2 \rangle^{1/2}$. These are seen in Fig. 13 as functions of three-body energy, E_3 , for $S = 1.00$, 1.17, and 1.20.

Much information about the structure is gained from Fig. 13. First of all, for a large binding the valence neutron-core distance (dashed lines) approaches the core neutron-neutron distance (dotted lines), because the system becomes more tightly bound. However, the valence neutron-core distance remains larger reflecting the fact that the valence neutrons are located at the surface of the core. As the threshold is approached the valence neutrons move away from both the core and each other (solid lines), while the core neutron-neutron distance remains unchanged, indicating the core is not changing, and the three-body structure is preserved in the calculation.

This behavior is identical for $S = 1.00$ and $S = 1.17$, only slightly more slowly for

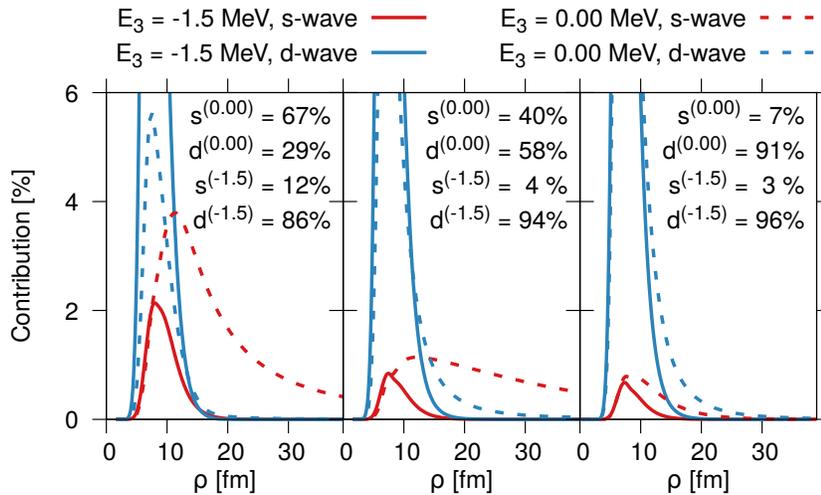


Figure 14. The partial wave contributions from s - (red) and d -waves (blue) for the neutron-core subsystem in $^{70}\text{Ca} + n + n$ as functions of hyper-radius, ρ , for $S = 1.0$ (left), $S = 1.17$ (center), and $S = 1.20$ (right). Full and dashed lines indicate a three-body energy of -1.5 MeV and 0.00 MeV, respectively. The total partial wave contribution after integration over ρ is also given for both energies. (Update of Fig.3 in Ref. [117]).

$S = 1.17$ due to the more attractive potentials, demonstrating how the mere availability of the $d_{5/2}$ state does not affect the emergence of halos. However, for $S = 1.20$ a clearly bound $d_{5/2}$ state is produced, as mentioned above, and the corresponding adiabatic potential will by definition asymptotically approach the energy of this state. Decreasing the three-body binding energy towards this threshold will populate the d -wave, which will prevent an increase in spatial extension, leaving the average distances unchanged as seen in Fig. 13. The appearance of halo structures is therefore not an inherent characteristic of the method when approaching the dripline, but requires some particular conditions accounted for by the method itself.

To further explore how the two-body structure affects the formation of halos one can study the partial wave composition as function of three-body energy, S , and ρ . This is seen in Fig. 14, where the three panels from left to right correspond to $S = 1.00$, 1.17 , and 1.20 . For large binding the wave function is dominated by d -waves, but as the energy is increased the wave function is extending further out with an s -wave tail that becomes more favorable for $S = 1.00$ and $S = 1.17$. For $S = 1.20$ the d -wave dominates so heavily that the s -wave tail is completely suppressed. This is also reflected in the relative weights of the s - and d -wave included in the figure, where for $S = 1.20$ the overall s -wave contribution is insignificant even at $E_3 = 0.00$ MeV.

The partial wave composition is determined by the contributing adiabatic potentials, the structure of which is determined by the underlying valence neutron-core interaction. As a result the large distance nature of the tail of the wave function is affected by the fine-tuning of the Skyrme interaction. The characteristics of the wave function tail will later be seen to have profound effect on calculated observables.

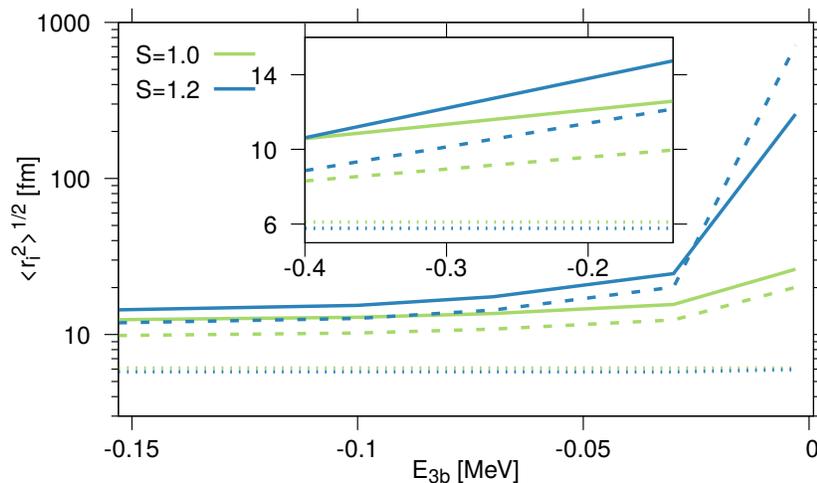


Figure 15. Root-mean-square distances as functions of the three-body energy, E_{3b} , for the first excited state of ${}^{70}\text{Ca} + n + n$. The two-body systems distances are valence neutron-neutron $\langle r_{n,n}^2 \rangle^{1/2}$ (solid), valence neutron-core $\langle r_{c,n}^2 \rangle^{1/2}$ (dashed), and core neutron-neutron $\langle r_{c,c}^2 \rangle^{1/2}$ (dotted) radius for $S = 1.00$ (green curves) and $S = 1.20$ (blue curves). (Update of Fig.4 in Ref. [117]).

It is equally possible for halo structures to form in excited states, it is again only dependent on the energy and partial wave structure of the state. However, these states will naturally be more unstable and are often very delicate. In Fig. 15 the same average distances are shown with the same line coloring and type as in Fig. 13, only for the first excited state in ${}^{70}\text{Ca} + n + n$. Again a halo structure is seen for $S = 1.00$ at small energies, but unlike in Fig. 13, halo structure also appears for $S = 1.20$.

This is best explained by considering the partial wave composition shown in Fig. 16, analogous to Fig. 14. For $S = 1.00$ (left panel) some d -wave contribution is seen irrespective of energy, while for $S = 1.20$ (right panel) almost no d -wave contribution is seen. Actually, for $S = 1.20$ the composition is almost the reverse of what was seen in Fig. 14, which means there is no barrier to confine the wave function spatially.

The formation of halo structures is sometimes superficially quoted as the natural consequence of two requirements: the very small binding energy, and the lack of the barrier associated with s -wave. However, based on Figs. 13 to 16, the second requirement is seen to be more complicated than that. Fractional halo structures are possible even in a state dominated by d -waves, given only a relatively small s -wave tail in the wave function.

Even though the wave function is not an observable, it can still be used to calculate useful observables, that have unambiguous interpretations. One of the most accessible non-trivial observables is the final state single-particle energy distribution. The scattering length is known to greatly affect the energy distribution [123], therefore different outcomes are to be expected based on the value of S .

As the method provides a consistent connection between the short-distance bulk properties and the large-distance observable, it is even possible to speculate which path

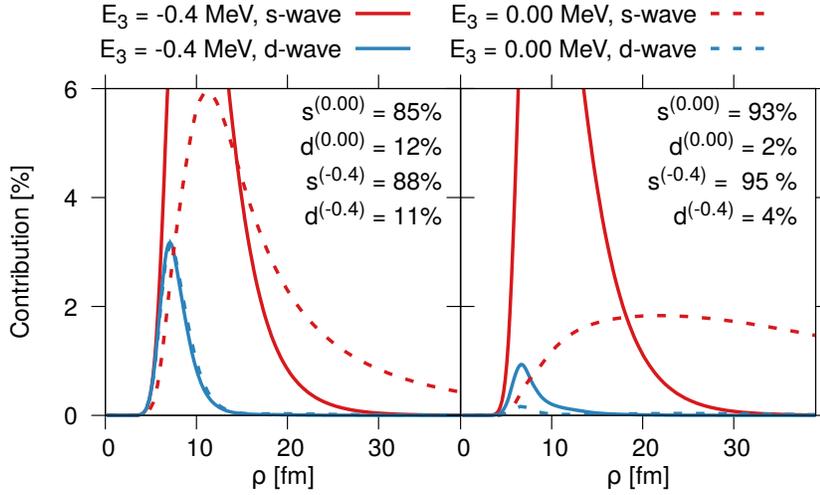


Figure 16. The partial wave contributions, similar to Fig. 14, with $S = 1.00$ (left) and $S = 1.20$ (right), for the excited states shown in Fig. 15.

the particle is likely to take before observation. As quantum mechanics only treat initial and final states, a more accurate statement would be that it is possible to deduce the initial state related to the observed final state. In turn this can be used to infer the general structure of the original system before decay.

It can be shown that the kinetic energy distribution of the fragments in a three-body decay can be expressed by the square of the wave function in coordinate space, with the important difference that the hyper-angles are angles in momentum space [129, 130]. If \mathbf{k}_x and \mathbf{k}_y are the Jacobi momenta corresponding to the Jacobi coordinates \mathbf{x} and \mathbf{y} , then $k_y^2 \propto \cos^2 \alpha$. But k_y is the momentum of the third particle relative to the center of mass of the other two (with appropriate mass factors), which means $k_y^2 \propto \cos^2 \alpha$ is the energy of the particle relative to its maximum possible energy [129]. As a result the energy probability distribution can be expressed as

$$P(\rho, \cos^2 \alpha) \propto \sin(2\alpha) \int |\psi_{3b}(\rho, \alpha, \Omega_x, \Omega_y)|^2 d\Omega_x d\Omega_y. \quad (57)$$

The energy distribution for $^{70}\text{Ca} + n + n$ is shown in Fig. 17 for selected values of ρ for both $S = 1.00$ and $S = 1.17$. This is the "second" relative coordinate system where \mathbf{k}_y is the relative momentum of a valence neutron compared to the center of mass of the core-neutron system. It has been expressed directly in terms of $E_n/E_n^{(max)}$ instead of $\cos^2 \alpha$. Also included is a schematic illustration of the long-distance configuration.

The structure seen in Fig. 17 is almost identical for $S = 1.00$ and $S = 1.17$ at short distances. Three peaks are seen with maximums at around $E_n/E_n^{(max)} \simeq 1/6, 3/6,$ and $5/6$. However, the evolution to their respective large distance structure is remarkably different.

For $S = 1.00$ the oscillations disappear, and a single peak is seen at around $E_n/E_n^{(max)} \simeq 1/2$. Energetically, this can be interpreted as a situation where both valence neutrons are moving away from the core. This type of energy distribution

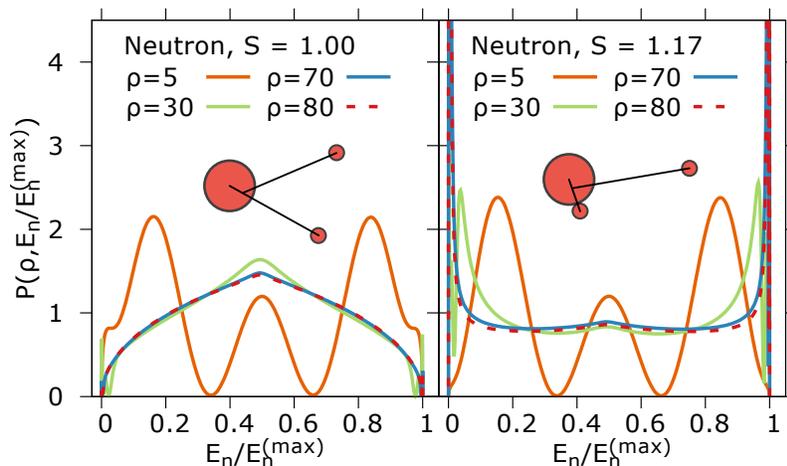


Figure 17. The single-particle energy distributions for the neutron after decay of $^{70}\text{Ca} + n + n$ at $\rho = 5, 30, 70,$ and 80 fm, for $S = 1.0$ (left) and $S = 1.17$ (right). Schematic illustrations of the large distance configurations are also included. (Fig.5 in Ref. [117]).

indicates a decay directly into the continuum without the involvement of any two-body resonance states.

For $S = 1.17$ the oscillations also disappear, but the final energy distribution is different. Two peaks are seen, instead of one, at $E_n/E_n^{(max)}$ approaching 0 and 1, corresponding to a situation, where either one of the neutrons are close to the core, while the other moves away. This is a clear indication of a sequential decay, where a two-body resonance is used to facilitate the decay. The most likely scenario is that the core-neutron d -state is being used.

This demonstrates how large-distance observables not only potentially differ substantially from the equivalent short-distance structures, but are also completely determined by potentially very subtle changes in these short-range characteristics. In other words, to explore the experimentally inaccessible short-distance nature of nuclear systems, it is necessary to rely on theoretical interpretations. Much then hinges on a proper connection between how the short- and long-ranged aspects of the systems are treated.

6.3. Possibility of Efimov behavior

The specific values of S were chosen due to their effect on the scattering length of the potential and the virtual energies of the first unoccupied states. The s -wave scattering length for the core-neutron potential is seen in Fig. 18 as a function of S . Also included in Fig. 18 is the virtual energy of the unoccupied $s_{1/2}$ state calculated as

$$\epsilon_v(s_{1/2}) = \frac{\hbar^2}{2\mu a^2}, \quad (58)$$

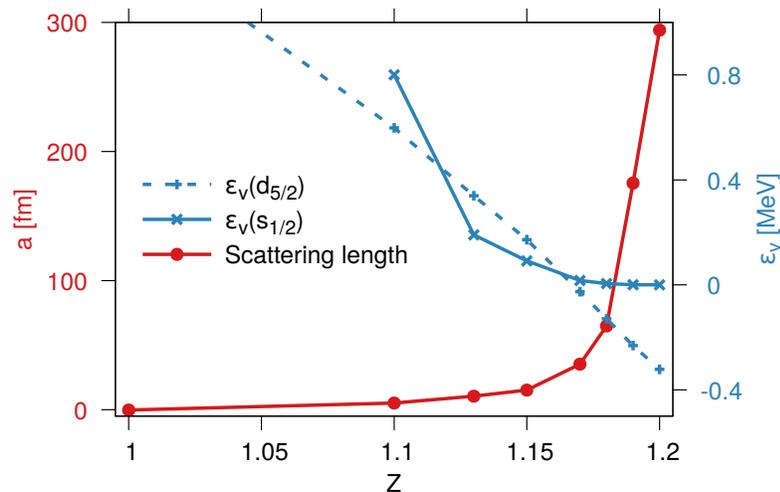


Figure 18. The s -wave neutron-core scattering length (red, solid) as function of the scaling of the Skyrme-parameters, S , for $^{70}\text{Ca} + n + n$. The virtual energy of $s_{1/2}$ (blue, solid) is calculated from Eq. (58), while the energy of the $d_{5/2}$ (blue, dashed) is obtained from the corresponding invariant mass spectrum, when it is unbound, and from a two-body calculation, when bound.

where μ is the reduced mass of the system, and a is the corresponding scattering length. Where the following sign convention is adopted

$$\lim_{k \rightarrow 0} k \cot \delta(k) = \frac{1}{a}, \quad (59)$$

with k being the wave number, and $\delta(k)$ the phase shift. Finally, the energy of the $d_{5/2}$ state, calculated from an invariant mass spectrum when unbound and from a straight forward two-body calculation when bound, is also shown in Fig. 18.

The results in Fig. 18 are shown for several values of S , and not just the three specific values from Fig. 11. The values of $S = 1.00$, 1.17 , and 1.20 are simply particularly interesting cases. For $S = 1.00$ the parameters correspond to regular, unaltered SLy4, which gives a sensible starting point for later comparisons. At $S = 1.17$ the $s_{1/2}$ and $d_{5/2}$ states are nearly degenerate. This will help illustrate how the wave function responds to the interplay between several allowed, and energetically equally favorable, states. Finally, for $S = 1.20$ the s -wave scattering length is starting to tend towards infinity. Already for $S = 1.201$ the s -state becomes bound with a scattering length of $a = -251$ fm.

As an extension of the halo structures discussed above, one could consider the possibility of Efimov states. It has been a long standing theoretical prediction that an infinite series of bound three-body states can be formed in a three-body systems where two or three of the two-body subsystems have a bound or virtual s -wave state very close to zero energy [101]. The energy and mean square radii of neighboring solutions in this series are related by the scaling s defined by

$$s^2 = \exp\left(\frac{2\pi}{\xi}\right), \quad (60)$$

where ξ is a constant related to both the underlying two-body interactions, the effective range of the potentials, and the scattering length of the two-body systems. The effective potential for three-body systems in hyper-spherical coordinates will maintain the value

$$V_{eff}(\rho) = -\frac{\hbar^2}{2m} \left(\frac{\xi^2 + 1/4}{\rho^2} \right), \quad (61)$$

(where m is the normalizing mass) for a large ρ -interval which is needed for the formation of Efimov states [122]. However, this convergence is very slow and an added requirement is that the effective range, r_0 , of the potential is several orders of magnitude smaller than ρ , which again must be several orders of magnitude smaller than the scattering length, i.e. $r_0 \ll \rho \ll a$. This necessitates a scattering length well above 10^4 fm, which generally is extremely unlikely in nuclei.

However, to go one step further before rejecting the idea of Efimov states in nuclei completely, one could assume a system with a sufficiently large core-neutron scattering length, and this should then be the foundation for a series of Efimov states. With identical masses and large scattering lengths ξ is determined by (see Ref. [122])

$$8 \sinh\left(\frac{\xi\pi}{6}\right) = \xi\sqrt{3} \cosh\left(\frac{\xi\pi}{2}\right). \quad (62)$$

This results in $\xi = 1.00624$, which in turn gives the famous scaling value $s = 22.7$. The expression becomes more complicated if there is mass differences between the particles along with the three large scattering lengths.

However, as the defining characteristic of an Efimov state is its relation to the other states in the series, a state cannot reasonably be called an Efimov state in isolation. The assumption of three simultaneously large scattering lengths (compared with the range of the potentials) includes the assumption that the neutron-neutron scattering length is not only much larger than r_0 [15, 16], but that it is also larger than the extend of second Efimov state (at s times the first state). With a neutron-neutron scattering length of around 20 fm, the assumption does not hold, and instead this must be treated as a system with only two large scattering lengths. This will always be the case for two nucleons connected to some core, due to the inherently modest neutron-neutron scattering length. For only two large scattering lengths, ξ is determined by (see again for instance Ref. [122])

$$\xi \cosh\left(\xi\frac{\pi}{2}\right) \sin(2\phi) = 2 \sinh\left(\xi\left(\frac{\pi}{2} - \phi\right)\right), \quad (63)$$

$$\phi = \arctan\left(\frac{\sqrt{(m_c(m_c + 2m_n))}}{m_n}\right), \quad (64)$$

where m_c and m_n is core and neutron mass respectively.

Using this in relation with ^{72}Ca , where $m_c \simeq 70m_n$, results in $\xi \simeq 0.01035$ and a scaling factor of $s \sim 10^{131}$, completely outside any realm of possibility. The possibility of Efimov states has been considered in many other nuclei over the years, such as ^{60}Ca [22] or ^{11}Li [122]. For ^{60}Ca the mass imbalance leads to $\xi \simeq 0.01205$ and $s \sim 10^{113}$ and for ^{11}Li the mass imbalance leads to $\xi \simeq 0.07382$ which results in a scaling of $s \sim 10^{18}$. This might be smaller, but is still many, many orders of magnitude too large to be realizable.

In nuclear physics systems of three identical particles are not realistic candidates for Efimov physics. Three neutrons do not form a bound system, and anything heavier would include Coulomb interactions whose long-range nature would prohibit formation of Efimov states. Furthermore, from Eq. (63) it is clear that no realistic scaling can ever be obtained with only two identical particles. To make this even clearer, one could look at a series expansion of Eq. (63)

$$|\xi| \approx \frac{4m_{\text{light}}}{\sqrt{3\pi}m_{\text{heavy}}}. \quad (65)$$

With an exponential dependence on the mass ratio, and the masses being discrete, there is no hope of having a second Efimov state in a nuclear system. However, in other areas of physics, such as cold atomic gases, where three identical particles can be used, it has become possible in recent years to actually detect Efimov states [131]. Another possibility, in other areas of physics, is to use two heavy and one light particle, which also produces more favorable scaling conditions, and very recently the emergence of Efimov physics has even been suggested in relation to strongly interacting photons [132].

7. Astrophysical applications

In previous sections, we have focused on applications of the formalism at the neutron dripline. Clearly, since the formalism is of a general nature, it is perfectly well-suited to also address the questions with protons as the valence nucleons. In this section, we therefore discuss the case of proton valence particles and examine an important example along the proton dripline. In particular, we will adapt the case of the nuclear astrophysical rapid proton capture (rp) process [133] and cases where the process can have important contributions from three-body dynamics. The rp-process involves the rapid capture of protons by a nucleus in a stellar environment, forming a system further from the line of stability. At some point the proton dripline is reached, where additional proton capture would render the system unstable.

Although, neutron capture processes are more discussed and well-known [134, 135], the importance of the proton capture processes must not be underestimated. The formation of at least 40 stable and a large number of unstable nuclei is only possible due to various proton capture processes [136, 137, 138, 139]. Among them, the rp-process is thought to be most important in relatively high-temperature, hydrogen rich

environments [140]. The most likely environment is in the accretion of a close binary system containing a neutron star or white dwarf, which results in x-ray bursts [141, 142]. Other possibilities include inside supermassive stars or in nova and supernova bursts [133], but all scenarios include temperatures in the Giga-Kelvin range.

At the proton dripline, where the capture of single protons would lead to reemission, the system will initially wait for the comparably slow β^+ decay. Following a β^+ decay, the capture of one or more protons is usually possible, until the new position of the proton dripline is reached. This implies that there is an accumulation of matter at the nuclei with the longest β -decay lifetime, and these nuclei are therefore referred to as waiting points of the rp-process. Going beyond the light nuclei, the most important rp-process waiting points, the so-called critical waiting points, are ^{64}Ge , ^{68}Se , and ^{72}Kr [142, 143], which have a β -decay half-life of 64 [144], 36 [145], and 17 [146] seconds, respectively. Out of these critical waiting point nuclei, ^{68}Se is thought to be the most important [147, 148].

In this section we therefore focus on this particular nucleus as the prime example that demonstrates the applicability of the method to proton capture processes and the proton-rich parts of the nuclear chart. Different effects including nuclear pairing [114] make the driplines become quite rugged in structure. Here the three-body formalism that we discuss offers unique opportunities in relation to the critical waiting points, as it should be possible to bridge the mass gap in the dripline through a three-body reaction. Although the addition of one proton would form a particle unstable system, two protons could be added, forming a stable, Borromean system. Our focus is on the process $^{68}\text{Se} + p + p \rightarrow ^{70}\text{Kr} + \gamma$, and the rate for this two proton capture process would affect the effective lifetime of the waiting points in a stellar environment. Consequently, this would affect where, in a proton-rich nucleosynthesis process, matter is accumulated and in turn influences the evolution of the particular stellar system.

The rest of this section is devoted to a discussion of the cross sections and rates for the process calculated based on the three-body framework discussed in previous sections, as well as a discussion of the decay mechanism for which knowledge can also be accessed. Lastly, we include a section that discusses the technicalities of the potential terms that need to be included and in particular of the couplings between different hyperspherical effective potential channels in relation to the physical parameters that enter the setup.

7.1. Cross sections and reaction rates

The process in question is the capture of two protons on a core, c , forming a three-body system, A , which then γ -decays to the 0^+ ground state. The cross section, σ_{ppc} , for this process $c + p + p \rightarrow A + \gamma$, is related to the dissociation cross section, σ_γ , for the reverse process by [12]

$$\frac{\sigma_{ppc}(E)}{\sigma_\gamma(E_\gamma)} = \nu! \frac{2(2J_A + 1)}{(2J_{p_1} + 1)(2J_{p_2} + 1)(2J_c + 1)} \frac{32\pi}{\kappa^5} \left(\frac{E_\gamma}{\hbar c} \right)^2, \quad (66)$$

where J_i is the total angular momentum of the related particle, ν is the number of identical particles, and κ is the three-body momentum, which is defined as $\kappa = \sqrt{2mE/\hbar^2}$. The mass m is the normalization mass used to define the Jacobi coordinates in Eqs. (28) and (29), and the energies are related by $E_\gamma = E + |E_{gr}|$, where E_{gr} is the (0^+) ground-state energy, E is the three-body energy, and E_γ is the energy of the emitted photon.

The process can occur as a resonant reaction, going through a well-defined three-body resonance, or a non-resonant reaction, going through a continuum state. In either case the dissociation cross section is a sum over contributing electric and magnetic multipole transitions of order ℓ . Here we shall focus on the electric transitions, and the corresponding dissociation cross section is given by [149]

$$\sigma_\gamma^\ell(E_\gamma) = \frac{(2\pi)^3(\ell+1)}{\ell((2\ell+1)!!)^2} \left(\frac{E_\gamma}{\hbar c}\right)^{2\ell-1} \frac{d}{dE} \mathcal{B}(E\ell, 0 \rightarrow \ell), \quad (67)$$

where $E\ell$ represents the electric multipole transition of order ℓ whose strength function for the $0 \rightarrow \ell$ transition is

$$\frac{d}{dE} \mathcal{B}(E\ell, 0 \rightarrow \ell) = \sum_i \left| \langle \psi_\ell^{(i)} | \hat{\Theta}_\ell | \Psi_0 \rangle \right|^2 \delta(E - E_i), \quad (68)$$

where $\hat{\Theta}_\ell$ is the electric multipole operator, and $\psi_\lambda^{(i)}$ is the three-body wave function of energy E_i , for all bound and (discretized) three-body continuum states in the summation.

The reaction rate, R_{ppc} , can be expressed in terms of σ_γ^ℓ by [150, 151]

$$R_{ppc}(E) = \frac{8\pi}{(\mu_{cp}\mu_{cp,p})^{3/2} c^2} \left(\frac{E_\gamma}{E}\right)^2 \sigma_\gamma^\lambda(E_\gamma), \quad (69)$$

where μ_{cp} and $\mu_{cp,p}$ are the reduced masses of the proton-core system and the proton to proton-core system, respectively.

We want to address reactions in an astrophysical environment described as a gas of temperature T , hence the reaction rate must be averaged over the (energy normalized) Maxwell-Boltzmann distribution

$$B(E, T) = \frac{1}{2} \frac{E^2}{T^3} \exp(-E/T), \quad (70)$$

resulting in an energy average reaction rate given by

$$\langle R_{ppc}(E) \rangle = \int_0^\infty B(E, T) R_{ppc}(E) dE, \quad (71)$$

where the temperature is in units of energy (the Boltzmann constant is set to unity).

7.2. $^{68}\text{Se} + p + p$ cross sections

A potential problem with a traditional three-body investigation of the systems that we are considering is the phenomenological character of the approach, which makes it difficult to present concrete predictions [149, 152]. However, very little arbitrariness is left in the method we use here, and therefore the prediction capability increases.

For the particular case of the $^{68}\text{Se} + p + p \rightarrow ^{70}\text{Kr} + \gamma$ reaction, the SLy4 Skyrme parameterization is again used, as it is well suited for describing nuclei far from β stability. Importantly, as the reaction rate will depend exponentially on the barrier thickness at the resonance energies, accuracy in the keV range is needed. To achieve this, we recall the discussion in Sec. 6 and rescale the Skyrme parameters t_i as $t_i \rightarrow St_i$ to achieve this level of accuracy, leaving x_i and W_0 unchanged. Experimentally, the lowest lying resonance in ^{69}Br ($^{68}\text{Se} + p$) is known to be a $f_{5/2}$ state at 0.6 MeV [153]. Using an unaltered SLy4 parameterization the lowest allowed state also turns out to be an $f_{5/2}$ state [151], in accordance with experimental findings. To achieve the correct energy the SLy4 parameterization is scaled by a factor of $S = 0.9515$, which has been used in all the results presented in this section. With this scaling there are no 1^- resonance states, and the important states are therefore the 0^+ and 2^+ states. Notice that S is very close to unity, again attesting that only a small adjustment is needed to get the experimental data correct to the necessary keV accuracy.

Once the known $f_{5/2}$ resonance in ^{69}Br has been used to fine tune the Skyrme parameterization, the only remaining degree of freedom is the three-body interaction. The 0^+ ground state is predicted from systematics to be at -1.34 MeV [154], and the three-body interaction is used to reproduce this value. The form from Eq. (49) is used with a range of $r_0 = 6$ fm and a strength of $V_0 = -17.5$ MeV. To see the effect of the resonance energy the 2^+ state is varied from 0.5 up to 4.0 MeV using the same range, r_0 , but varying the strength from -35.05 to -26.22 MeV.

With a choice of Skyrme interaction and a choice of the three-body interaction the set of discretized 2^+ continuum states can be calculated by discretization with a box boundary condition. As the plane wave state for a free particle contains all possible angular momentum in a partial wave expansion, the continuum states are not characterized by one complete set of discrete quantum numbers [149]. However, the bound final states are clearly defined by a set of quantum numbers, and the transition is dictated by an appropriate multipole operator, as specified in Eq. (68). The transitions for the individual discretized continuum states are independent, and they can as such also be calculated and added individually. As the available single-particle levels all have odd angular momentum, it is not possible to produce negative parity final states such as 1^- . Likewise, there are no excited 0^+ states available, so the only relevant transition is the $E2$ transition.

Once we have calculated the discretized continuum spectrum, Eq. (68) produces the photodissociation cross section in combination with Eq. (67). This is directly related to the proton capture cross section through Eq. (66). The proton capture cross section is shown in Fig. 19 for a range of different 2^+ resonance energies and box sizes.

First of all, Fig. 19 illustrates that the box size used to discretize the continuum is sufficiently large. For a 2^+ resonance energy of 0.5 MeV the cross section is calculated using box sizes of 150 fm and 200 fm, and the results are identical, as they should be for large box sizes [155]. In addition, it is seen how the peaks at the cross section correspond to the resonance energies, while the non-resonant, background contribution between the

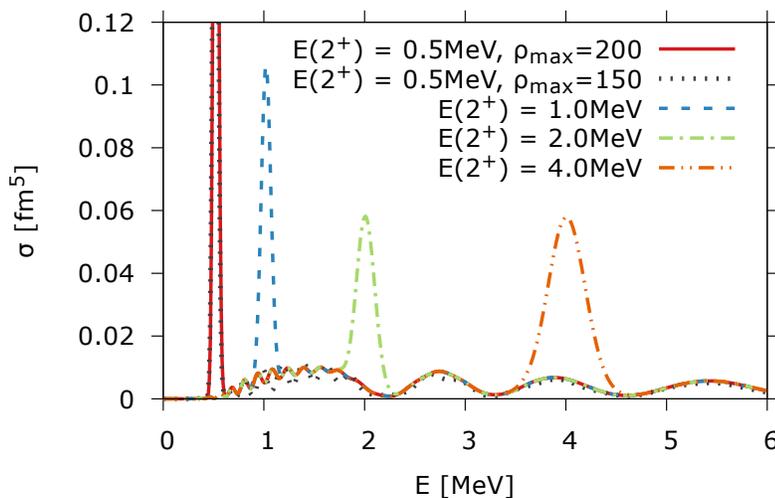


Figure 19. The electromagnetic $\mathcal{E}2$ proton capture cross section, $\sigma_{ppc}(E)$, for the process, ${}^{68}\text{Se} + p + p \rightarrow {}^{70}\text{Kr} + \gamma$, as a function of three-body energy. The 0^+ final state energy is -1.34 MeV and the 2^+ resonance energies are $E = 0.5, 1.0, 2.0,$ and 4.0 MeV, respectively. The discretized continuum states are obtained using box sizes of $\rho_{max} = 150, 200$ fm for $E = 0.5$ MeV, and only $\rho_{max} = 200$ fm for all other energies.

peaks is less important, although not insignificant. This follows from Eqs. (67) and (68) where the overlap between the ground state the continuum state is seen to dictate the cross section. This background contribution is also independent of the the 2^+ resonance energy.

7.3. ${}^{68}\text{Se} + p + p$ reaction rates

The proton capture cross section leads to the two-proton absorption rate through Eq. (66) and Eqs. (69) to (71), which is the central result in relation to astrophysical evaluations. The average rates from Eq. (71) are shown in Fig. 20. The four solid lines correspond to the four cross section calculations from Fig. 19, while the dashed line is the non-resonant, background contribution, common to all four calculations.

These average rates are smeared out due to the Maxwell-Boltzmann energy distribution, but the rates have their maximum at the Gamow peak [156] resulting from the compromise between the decreasing temperature distribution and the tunneling probability increasing with resonance energy. The non-resonant, background contribution is clearly smaller, but by less than a factor of 2 for temperatures above 4 GK (GigaKelvin). As the non-resonant contribution is independent of the resonance energy, this very firmly determines the scale of the reaction rate. For temperatures in the astrophysically relevant regime for the rp-process, i.e. 2–4 GK, the reaction rate for the two-proton capture process is of the order $\sim 4 \cdot 10^{-11} \text{cm}^6 \text{s}^{-1} \text{mol}^{-2} N_A^2$. This result depends on the specific shape of the potential barrier, which again depends on the charge, mass, and available single-particle states of the system.

It should be noted that given a specific choice of Skyrme parameterization, this is a

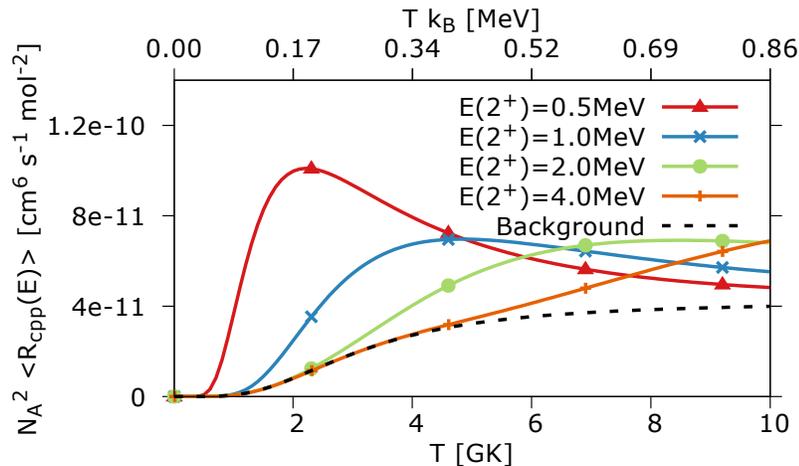


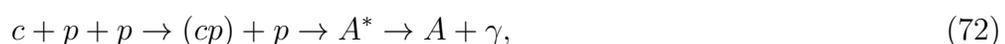
Figure 20. The reaction rate for the radiative capture process $^{68}\text{Se} + p + p \rightarrow ^{70}\text{Kr} + \gamma$, as function of temperature for the different 2^+ resonance energies in Fig. 19. The black dashed curve is the background contribution. The top axis shows the temperature multiplied by Boltzmann’s constant in MeV. (Fig.3 in Ref. [151]).

very comprehensive calculation. First of all, other types of transitions are very unlikely, as 1^- and 3^- resonance states are not possible due to the available single-particle states [157], while no excited 0^+ states are found – something also supported by the mirror nucleus [158]. Excited 2^+ states are fully included, as the full cross section spectrum is included in the rate calculation. Core excitations are also unlikely to be significant, as the first excited state of ^{68}Se is at 0.854 MeV above the ground state [159]. The probability of occupation at a temperature of 4 GK would then be $\exp(-E_{cl}/T) = 0.09$, which heavily suppresses any contribution from this state [149].

As a result the reaction rates presented here provide a very solid range for use in the calculations of evolutions of stellar environments. The upper limit is to a large extent given by the rate curve with a low-lying resonance, while the lower limit is given by the background contribution.

7.4. Reaction mechanisms

Another vital issue, which touches on the most fundamental aspects of the reaction, is to examine the reaction mechanism [149, 151]. The two-proton capture process can proceed through a well-defined three-body resonance, or as a non-resonant reaction through a continuum state, while after penetrating the Coulomb barrier the only transition to the 0^+ ground state is through γ -decay. However, both the resonant and the non-resonant penetration of the Coulomb barrier can be imagined as a direct, one-step process, where both protons are captured simultaneously, or a sequential, two-step process, where the protons are captured successively one at the time. In other words, the sequential process [160, 161] can occur as



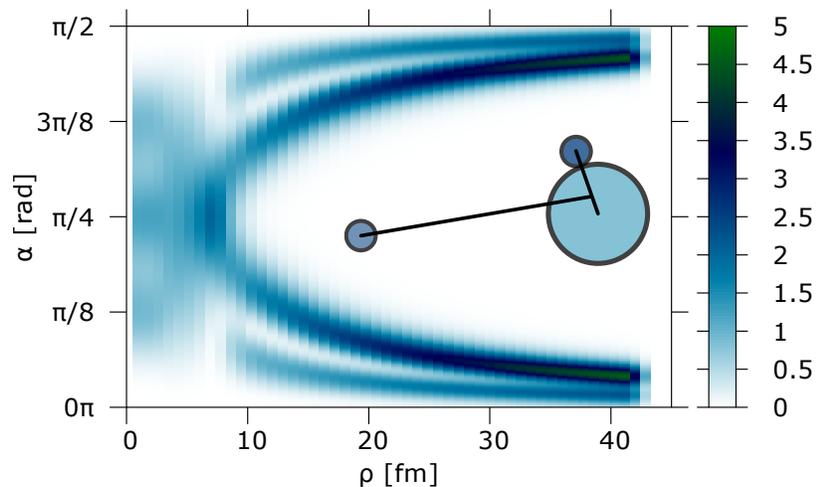


Figure 21. The probability distribution, as expressed by Eq. (76), of the three-body, $^{68}\text{Se} + p + p$, wave function for the lowest allowed potential in a 2^+ state. This is given as a function of hyperradius, ρ , and hyperangle, α , related to the Jacobi coordinate system where "x" is between core and proton. (Fig.4 in Ref. [151]).



where A^* is the well-defined resonance state. Likewise, the reaction mechanism usually referred to as direct [161, 162] can proceed as



These distinctions in practice mostly conceptual, as the actual reaction mechanism would be superpositions of all possibilities, all of which are accounted for in the present formulation. They are, nonetheless very important for understanding physical mechanisms. Moreover, extreme cases would be observable [163], as the resulting energy distribution would carry distinct signatures of the mechanism. This is similar to the discussion in Sec. 6.

In order to pin down specific reaction mechanisms, we turn to the angular wave function, integrated over directional angles as

$$P(\alpha, \rho) = \sin^2(\alpha) \cos^2(\alpha) \int |\phi_n(\alpha, \rho, \Omega_x, \Omega_y)|^2 d\Omega_x d\Omega_y, \quad (76)$$

where $\sin^2 \alpha$ and $\cos^2 \alpha$ are phase factors. This probability distribution is shown in Fig. 21 for the lowest allowed angular eigenfunction, shown in the second Jacobi coordinate system in Fig. 3. This shows the reaction clearly proceeding through a sequential reaction mechanism, with only two clear peaks in the spectrum beyond $\rho = 10$ fm. An angle of $\alpha = 0$ or $\alpha = \pi/2$ represent to a configuration where one proton is close to the core, while the other is located somewhere at a much larger distance. In other words, this corresponds very clearly to an extreme sequential reaction. We note that the next few, higher-lying allowed angular eigenfunctions show the same behavior.

This very unambiguous mechanism can be understood through some schematic potentials associated with the geometric configuration of the reaction [164]. If one proton is moving away from a core-proton resonance state with energy E_{pc} , and it has passed outside the strongly attractive region, it would experience a Coulomb potential given by [149]

$$V_{seq}(\rho) = \frac{e^2(Z_c + 1)}{\rho} + E_{pc}, \quad (77)$$

where Z_c is the charge of the core. Alternatively, if both protons are moving away from the core symmetrically, they would experience a potential given by

$$V_{dir}(\rho) = \frac{E^2 (2Z_c + \frac{1}{2}) \sqrt{2}}{\rho}. \quad (78)$$

These schematic potentials cross at a distance, ρ_{crit} , and at a potential energy, V_{crit} , given by

$$\rho_{crit} = \frac{e^2 ((2\sqrt{2} - 1)Z_c - 1 + 1/\sqrt{2})}{E_{pc}} \approx \frac{2.6Z_c}{E_{pc}}, \quad (79)$$

$$V_{crit} = E_{pc} \frac{(2Z_c + 1/2)\sqrt{2}}{(2\sqrt{2} - 1)Z_c - 1 + 1/\sqrt{2}} \approx 1.6E_{pc}, \quad (80)$$

for $Z_c \gg 1$. With $E_{pc} = 0.6$ MeV and $Z_c = 34$ this results in $V_{crit} \simeq 0.94$ MeV and $\rho_{crit} \simeq 147$ fm, far outside the decisive region of interest discussed here. Given the relatively low-lying resonance, the reaction is clearly sequential.

8. Improvements, generalizations and perspectives

The spotwise demonstration of applicability and flexibility of the method in the previous sections can now be supplemented by a number of possible improvements and appealing generalizations. In principle, improvements can be related independently to the core description or to the few-body treatment. However, the interconnectivity of the core and few-body descriptions means that modifications affect both structures. We shall not here implement any of the extensions but discuss them in various degrees of details depending on the subject of investigation and short- or long-term goals.

We divide this section into four categories, that is first the immediately desirable or necessary improvements where details are available, second choices of more complicated systems or other modifications of the technical method, third descriptions of applications beyond those of the previous sections, and fourth indications of how and where to transfer the present experience to other subfields of physics. As we go along with this agenda the amount of details are clearly decreasing with the time perspective for the implementations.

8.1. Short-range valence nucleon-nucleon interactions

Contact interactions somehow need regularization due to the divergence at short distance. This was realized long before the first Skyrme interactions were used in mean-

field treatments, where the Slater determinant automatically eliminates the divergence problem. However, using the complete Hilbert space for the two valence nucleons revives this problem as touched upon in Sec. 4.4.1. This inconsistency with the use of Skyrme interactions in valence space leads to an infinite number of spurious deep-lying bound states built on the lowest diverging adiabatic potential described by λ , while the relevant higher-lying λ_n 's are unaffected. Thus, in principle the problem disappears with removal of this λ . Unfortunately the many crossing λ 's in practice make this difficult although not impossible.

A better and more obvious option to rectify this divergence problem and eliminate the spurious bound states, would be to replace the contact interaction with a finite-range interaction. If simplicity is still desired, a natural choice would be the finite-range Gogny interaction [103], which completely would eliminate all spurious bound states. The original Gogny-proposal in mean-field calculations was to replace t_0 , t_1 , and t_2 terms in the Skyrme force with a sum of two Gaussians, in the style of Brink and Boeker [165], but keeping contact t_3 and spin-orbit terms. This resulted in a density dependent two-body interaction between particles j and k of the form [93]. The spin-orbit and t_3 -terms remain as in Eq. (21) while t_0 , t_1 and t_2 -terms in this equation are substituted by

$$V_{jk}^{Gogny} = \sum_{n=1}^2 \left[\exp \left(-\frac{(r_j - r_k)^2}{\mu_n^2} \right) (W_n + B_n P_\sigma - H_n P_\tau - M_n P_\sigma P_\tau) \right] \quad (81)$$

where $P_\tau = (1 + \boldsymbol{\tau}_j \cdot \boldsymbol{\tau}_k)/2$ is defined in analogy to P_σ in Sec. 3.2.1. They are operators exchanging spin and iso-spin coordinates, while μ_n , B_n , H_n , M_n , are parameters of the interaction.

A large number of different versions exist for the Skyrme force, while for the Gogny force the so-called "D1S" force [166] is the most common. Other parameterizations, such as the D1N [167] and the D1M [40] do exist, but even today the D1S force is still the prevailing parameterization. More recent forces tackle the contact interaction in the density dependent t_3 -term, and are usually designated with the prefix "D2" to mark the two finite-range parts. One recent example is shown in Ref. [168], which demonstrate that a finite-range density dependent term generally improves the accuracy of various predicted nuclear matter properties.

To completely eliminate contact interactions the spin-orbit interaction should also be replaced by a finite-range version. This can be done similarly to the other terms [93, 168], but the parameters would necessarily have to be refitted to the new form of the force. However, the importance of the spin-orbit term is largest at the surface, diminishing at both small- and large-distances. It is therefore not in itself supporting spurious bound states in our method, and a contact spin-orbit interaction could be maintained between the valence nucleons while still achieving full consistency.

The procedure for implementing the Gogny interaction between all nucleons in the core equation is identical to the procedure for implementing the Skyrme interaction. The main difference is, that the input functions in the Schrödinger equation would

contain an integral over the coordinate which previously was trivially eliminated by the δ -function. This would increase the numerical complexity slightly, but as the integrands are Gaussians, this would only be a very minor complication. For the three-body part the procedure would not change, as the Gogny force along with central and spin-orbit potentials also produces effective masses, which could be incorporated in the same process.

It should be emphasized that even if a finite-range interaction, as for instance the Gogny interaction, is implemented between all nucleons, a reparameterization is needed when the valence nucleons are outside the core. This is imperative, as global mean-field interactions are fitted to reproduce in-medium nuclear matter properties, while the correct asymptotic nucleon-nucleon scattering properties in vacuum must be obeyed. The need for reparameterization can be viewed as a consequence of the increased Hilbert space expanded to encompass the added valence nucleons. Such a reparameterization, in one form or another, is always needed when changing the Hilbert space, but especially in the present case when free-space properties are crucial.

8.2. Adiabatic treatment of mean-field from valence space

While the improvements in Sec. 8.1 dealt with implementing more sophisticated and consistent nucleon-nucleon interactions, and the extensions in Sec. 8.3 shall deal with more complicated core structures, a third improvement has to do with the procedure for solving the coupled equations in our method.

Currently, the core and three-body equations are solved separately in an iterative manner, which means the solutions for the two (core and valence) equations are viewed independently. At the moment this is done as explained in Sect. 4.2 with the core solution found in the “external” average field of a full three-body solution, including angular and radial parts. The resulting mean-field calculation returns the input potentials for the three-body calculation and the process is repeated until convergence is reached.

One interesting, and more correct, procedure is to extend the hyperspheric adiabatic expansion, used to solve the three-body part, to perform the mean-field calculation at each hyperradius, ρ . More precisely this means to calculate the input needed in the mean-field calculation from the angular three-body wave function for a given fixed ρ . The core solution in turn provides the input needed for the three-body calculation. The process is repeated until convergence is reached for each ρ .

After core and angular calculations are found the three-body radial equation is solved as usual, only the equation itself is slightly different now. Our original radial equation from Eq. (39) is obtained by inserting the ρ dependent three-body wave function, expanded on the angular wave functions, see Eq.(36), into the Schrödinger equation, and using the solution from the angular part. If the connection between mean-field and three-body calculation is established at each ρ , the core wave function would also depend on ρ , and the radial equation would be slightly modified. The radial

equation would be based on the full wave function expanded as usual

$$\Psi = \psi_{3b}(\rho, \Omega)\psi_c(\rho, r_1, \dots, r_A) = \frac{1}{\rho^{5/2}} \sum_n f_n(\rho)\phi_n(\rho, \Omega)\psi_c(\rho, r_1, \dots, r_A) \quad (82)$$

where this total many-body wave function should be fully anti-symmetrized.

If the iterative process is conducted for fixed ρ , there is only remaining free parameter in the space of r_x and r_y , since, $\rho^2 = |x|^2 + |y|^2$. This affects the three-body aspect of the calculation in that there would be one integral less. For example, the three-body density in terms of traditional three-body coordinates is

$$\begin{aligned} n_3(\mathbf{r}) &= \int |\psi_{3b}(\mathbf{r}_x = \mathbf{r}, \mathbf{r}_y)|^2 d^3r_y + \int |\psi_{3b}(\mathbf{r}_x, \mathbf{r}_y = \mathbf{r})|^2 d^3r_x \\ &= \int r_y^2 |\psi_{3b}(\mathbf{r}_x, \mathbf{r}_y)|^2 dr_y d\Omega_y + \int r_x^2 |\psi_{3b}(\mathbf{r}_x, \mathbf{r}_y)|^2 dr_x d\Omega_x, \end{aligned} \quad (83)$$

for an infinitely heavy core and identical valence nucleons in the Jacobi set where \mathbf{x} is between the core and a valence nucleon. If the iteration is carried out for a given ρ , one coordinate integral has to be omitted. However, the general procedure would be the same as described in Sec. 4.2.

The differences are related to the ρ variation. In the radial differential three-body equation we can collect the new terms simply by applying T_ρ on the wave function in Eq. (82). To distinguish the origin we denote the new coupling terms, \tilde{Q} and \tilde{P} . They necessarily all contain derivatives of ψ_c , which has to be added to the ordinary and effective mass Q and P -terms. We get

$$\tilde{Q}_{nm} = \delta_{nm} \langle \psi_c | \frac{\partial^2}{\partial \rho^2} | \psi_c \rangle + 2P_{nm} \langle \psi_c | \frac{\partial}{\partial \rho} | \psi_c \rangle \quad (84)$$

$$2\tilde{P}_{nm} = \delta_{nm} \langle \psi_c | \frac{\partial}{\partial \rho} | \psi_c \rangle, \quad (85)$$

where the explicit matrix elements are to be computed over the core coordinates. The second of these Q -terms has a factor equal to the ordinary P coupling term. These new terms constitute a very natural extension of the previous radial equations, where we only added P - and Q -like terms arising from ρ -derivatives of ψ_c .

Using this expanded adiabatic formulation would more accurately connect the short-distance with the large-distance structure. However, it is more time consuming, since angular solutions now have to be found for each hyperradius, and the reduction due to fixed ρ in the density calculations does not provide sufficient compensation. Clearly both concept and formalism remain unchanged. This improved method provides the correct large-distance structure, since the large ρ implies isolated core structure surrounded by far away non-interacting nucleons. This is in contrast to the present ρ -independent core structure arising from an average influence of the valence particles. This would open up for interesting possibilities to study the evolution of the wave function, between these extremes (small and large ρ), in ways not currently possible with existing few- or many-body theories.

8.3. Deformed and/or odd systems

Before or after the improvements described in the previous subsections, it is possible to extend the region of applicability in several ways. We shall here consider the two extensions of deformation and odd numbers of neutrons and/or protons in the core.

8.3.1. Deformed even-even core. Allowing axial deformations, for instance in the Skyrme parameterization, would provide a more general core description, which in turn would produce modified core-valence nucleon interactions. This is a straightforward extension of the core Skyrme-Hartree-Fock description, and it was also the first improvement of the original spherical Skyrme-Hartree-Fock method [89]. For systems with axially deformed core structures, which maintain an even-even configuration, the assumption of time-reversal symmetry still holds true. In the derivation contained in [Appendix A](#) no assumptions were made regarding the shape of the core, so the fundamental equations from Eqs. (A.44) and (A.50) are still valid. However, it will be necessary to express the various densities in appropriate cylindrical coordinates [89].

In the spherical case, as explained in [Sec. 4.1](#), the core Hartree-Fock equations were solved in two iterative steps (not to be confused with the iteration between our core and three-body equations). First an ansatz to a radial wave function was produced from harmonic oscillator potentials. This was used to produce first approximations to the needed densities, which could then be used to solve the Schrödinger equation and calculate the effective mass, and central and spin-orbit potentials. Using these interactions a new radial wave function was produced, and the process continued until convergence in total energy is reached. For spherical nuclei this was all done in coordinate space, but solving a deformed Schrödinger equation in coordinate space is more difficult. The deformed wave function can be expanded and solved on a deformed harmonic oscillator basis. The evaluation of the potentials and the construction of the densities subsequently done in coordinate space [89].

Incorporating an axially deformed core in the three-body part is potentially more difficult. This is not something that has received much attention in the community or been considered terribly important, and as such there is not a well-established framework to draw upon. Internal structure of the constituent particles is traditionally not considered in few-body physics; the particles are viewed as point-like. At best internal structure is simulated using the characteristics of the effective potentials. Usually, this is not a problem as the finer structure of the constituent particles is unimportant at larger distances, in particular for halos [119]. The validity of the few-body results is generally related to the accuracy of the large-distance asymptotic behavior. The short-range structure is neglected as irrelevant and in any case previously not included properly.

The method presented here consistently connects the long-distance behavior with the short-range structure. As such the nature of the constituent particle structures becomes much more important, and a possibly deformed core potential is therefore important for the coherence of the method. There are various possible procedures

to resolve this problem. The simplest and most obvious solution would be to use the deformed mean-field formalism for the core calculations, but averaging over angles when applying the potential in the three-body description. This is equivalent to projection on zero core-angular momentum. In this way, the freedom allowed by the deformed formalism is used by the core to assume the most favorable configuration and produce the most realistic potential, while the information lost at short-distances by averaging in the three-body part should be minor even for moderately strong deformations. For larger distances this should have no effect at all. For very strong deformations the loss might be more significant, but situations with very strong core deformations are unlikely in this scenario as the most tempting candidates for this method are systems where the most significant extension is at the valence level, not the core level.

Another option would be to use the deformed potential directly in the three-body calculation. Due to the direction associated with the deformation, angular momentum would no longer be a conserved quantity. This could be rectified by calculating a number of angular momentum states and coupling them appropriately. As long as all relevant states are calculated, there should be no loss of generality.

8.3.2. Odd nucleons in the core. Unlike the expansion to include deformed core structures, the expansion to include odd nucleon numbers in the core is relatively difficult to incorporate in the mean-field part, but very simple to incorporate in the three-body part. The main problem from a mean-field perspective, is that an unpaired nucleon will break the crucial time-reversal symmetry. Without this symmetry, many of the equalities from [Appendix A.1](#) no longer apply, and a number of new terms appear beyond the even-even formalism.

Various methods have been developed to treat unpaired nucleons in mean-field calculations. One method is by the so-called exact blocking of the odd state [\[90\]](#). The idea is to view the unpaired nucleon as a quasi-particle excitation on top of the even-even "vacuum" produced by the remaining even number of nucleons. Done fully this is in principle exact. However, the complications incurred by breaking time-reversal symmetry are so considerable that other alternatives are often used instead.

One of the more popular alternatives is the equal filling approximation [\[91\]](#), where the central idea is to consider the unpaired nucleon as being half in one state and half in the time-reversed state simultaneously. This conserves time-reversal symmetry, and thereby simplifies the situation greatly. The simplicity of the approximation has caused it to be widely adopted and it has been used to study a great variety of odd nuclear systems [\[169, 170, 171\]](#). The precision of the equal filling approximation, both in comparison with available experimental information and with the exact blocking method, is generally considered to be more than sufficient for most practical purposes [\[90, 169\]](#).

The most common justification for the approximation is found in a statistical interpretation of quantum mechanics [\[172\]](#). Another argument is found in the decomposition of the mean-field energy functional into time-even and time-odd parts. It

can be shown that the time-even part of the energy density matrices are identical for the equal filling approximation and the blocking method [90]. As such the average values of time-even observables are identical in the two methods, which means the average values of time-even observables such as radii and multipole moments are the same in the two methods, while time-odd observables such as spin alignments and magnetic moments will differ slightly [90].

For the three-body part there are no such complications, but the valence nucleons would be allowed to occupy non-time reversed orbits. There are no inherent assumptions about time-reversal symmetries or pairing of nucleons. The three constituent particles just enter as a mass and charge with a given two- and three-body potential acting between a number of possible relative partial waves but coupled to the given conserved total angular momentum. The potential produced by the core calculation, be it with exact blocking or with equal filling or any other approximation, is adopted directly as the effective two-body core-valence nucleon interaction.

8.4. Applications and generalizations

We shall first describe how to employ more elaborate many-body methods on the core and second how to extend to more complicated systems of valence particles. Then we shall suggest a number of immediate applications, and finally we indicate how to transfer the method from nuclei to other subfields of physics.

8.4.1. Improved descriptions and complicated valence structure. The core and valence parts can each be changed or improved independently although both structures would be affected through the coupling. The present choice of Skyrme Hartree-Fock mean-field treatment of the core structure can be modified in several ways. The conceptually smallest change is to employ a finite-range two-body interaction, while maintaining the self-consistent mean-field approximation. This is discussed in more details in Sec. 8.1 for the Gogny-interactions, but a Gogny type interaction is not the only possibility, and the discussion is valid for any other finite-range mean-field calculation.

The core treatment can be substantially further improved by implementing advanced methods from many-body physics either variants of interacting shell models or directly ab-initio techniques, see Sec. 2 for options. In general, any many-body description of the core, which yields a potential to be incorporated into the few-body equation could be used. Implementing a more sophisticated core description, such as for instance a (no-core) shell model description (see Sec. 8.3 and 8.4) is possible, but not necessarily worth the effort. As was seen in Sec. 5, as long as the core description is fairly decent, very accurate results can be obtained. So the increased complexity might not produce a significantly better result, but the computation time would drastically increase. As such, other improvements, such as the inclusion of deformed or non-even cores, might be more worth the effort.

The immediate technical advantage of finite-range interactions is that the

connection between in-medium and in-vacuum nucleon-nucleon interactions becomes much smoother. Furthermore, the transition is obviously easier to simulate correctly when the scattering length of the finite-range interaction is close to the free value. However, the more fundamental advantage is that the same interaction is applied to both core and valence spaces, that means no new parameter. The valence particle few-body calculation would no doubt be more complicated as consequence of an improved core treatment, but in most cases probably practically doable with the same variational formulation.

The valence part is at the moment formulated for two structureless particles, that is directly valid for the three different combinations of two nucleons. However, it is tempting to include intrinsic structure of the valence particles, that could be one or two alpha-particles as simple examples. Three larger nuclear clusters each with intrinsic structure would be more complicated due to the combination of intrinsic structure, the relative coordinates, and the necessary more complicated handling of the Pauli principle. Sec. 3.1 contains an overall general formulation.

To be practical, before the complicated extension to larger chunks of nuclear clusters, it is illuminating to start with only two clusters. Each can first be treated in the mean-field approximation, and subsequently coupled in the product wave function ansatz described by relative coordinates. For two clusters described in the intrinsic coordinate system this amounts to one relative distance coordinate. Such a formulation is compatible with the two-center (non-interacting) shell model [173], which first of all is aimed at describing the fission process and heavy-ion collisions [174, 175]. A version with a two-cluster structure is to allow both a ground and an excited state in one of the clusters, but this is effectively a three-body problem.

The next extension towards three clusters with intrinsic structure is to allow only two of these and one point-like valence particle. The final step could turn out to be rather complicated but at least by now qualitatively formulated, see Sec. 3.1. Division into more than three clusters would not uncover new features because more clusters do not have radial divergences at the threshold of zero binding [176, 177]. This implies that a tendency to form correlated structures with more than three centers would be met by coalescence into fewer centers [47].

8.4.2. Application to correlated wave functions. All the numerical examples in the present paper have been on weakly bound and simple dripline nuclei. However, it is also possible to study correlations in ordinary well bound nuclei. The binding between core and valence particles should then be comparable to the binding between all other nuclear substructures. The two-body correlation between deeper-lying single-particle orbits in ordinary well bound nuclei is then within reach. The correlations under investigation correspond to the chosen valence structure, which in practice so far has been structureless nucleons. This restriction could be lifted by extension to more complicated systems as described in the previous subsection.

Another unexplored question is the interplay between short and long-range

interactions. In the present model this is made explicit in the different treatments of the dense core and the spatially extended and weakly bound valence particles. Nevertheless, the related two parts of the wave function are connected through the quantum mechanical equation of motion. However, the path connecting short and long-distance properties is not an observable, and as such only indirectly open to experimental investigations. Crudely speaking we can say that large-distance probabilities are measurable but not uniquely related to short-distance properties of the wave function [178].

The goal of understanding the structure, from which the measured probability originates, is then left to theoretical interpretation. In extreme cases the connection may appear as (almost) unique. This would be the case when the wave function in the corresponding parameter space is confined to a narrow path similar to a classical deterministic orbit. On the other hand a smeared-out wave function can be very similar at small distances but evolving into completely different structures at large distances, see an example in Sec. 6, which mostly resembles chaos conditions. An understanding of possibly systematic relations and quantitative validity conditions are highly desirable, because measurements then can be interpreted directly or at least the underlying uncertainties extracted. The present method is an invitation to study how far the information from measurements can be extended through this dynamic evolution of the wave functions.

The static properties of a (not necessarily stationary) wave function should be supplemented by more explicit time dependent properties. The simplest is probably decay mechanisms of resonances [161] or maybe decay of continuum states in general [12, 179]. Reaction investigations transferring one structure into another are readily formulated but a lot more difficult to carry out [180, 181]. A non-stationary state describable by our method may be populated by decay of a complex many-body state, perhaps beta-decay. The subsequent time evolution carries information about both decay process and initial population. Again the short and long-distance interplay is important. In general, time evolution of a non-stationary initial state is a tempting application.

8.4.3. Transfer to other subfields of physics. The concepts of halos, Efimov states, and many-body structure are general physics topics. The most special is probably the inherent properties from the short-range nuclear interaction. When the Coulomb force is dominating the present method is therefore most likely not suitable. When both short and long-range forces are active the interplay of correlations between different length scales is delicate but essential. For many subfields of physics this issue is of great interest. The core-valence division seems in general able to deal with these issues. A direct application is on hypernuclei mixed with nucleons and perhaps pions or other mesons [182].

On the other hand many subfields of physics, most prominently condensed matter, molecular and cold atomic physics, exhibit features with dominating short-range

characteristics [88, 47, 183]. The connecting property is the existence of universal structures which by definition is independent of details of the supporting potentials. The meaning of this statement is understandable already from “classical” nuclear physics where low-energy nucleon-nucleus scattering could be explained by disparate potentials with the same s -wave scattering length. From this originated the notion of nuclear halos, that is weakly bound and spatially extended structures describable by the scattering length [184]. Also existence of the extreme Efimov states have been (indirectly) established within the fields of cold atomic and molecular physics [185]. Recently also direct evidence has been obtained [186].

These universal structures appear as correlated substructures within the hosting many-body system. It is therefore appropriate to ask how they materialize in analogy to the present investigation of emergence of halos and Efimov states from the background of an essentially uncorrelated many-body system. The first necessary ingredient is here to add a genuinely external field to confine spatially all (core and valence) particles. The core treatment is then simple with rather weak two-body interactions perhaps parameterized as a mean-field. The correlations producing the few-body universal structures are then described by the valence particles. The appearance of halos and Efimov states can be studied with the present method. The advantage is that choices of systems are much more flexible and suitable mass asymmetric systems can be studied. In other words applications to other subfields of physics is only a matter of changing interactions while keeping the methodology.

9. Summary and conclusions

In this work we present the detailed derivation of a new method for treating many-body nuclear systems with correlated substructures. The report describes the method and is applied to three different nuclear systems, each illustrating characteristic aspects of the method. In this final section we first briefly survey important pieces of the theoretical development, second we draw lessons learned from the applications, and third we conclude with a general perspective derived from the present work.

9.1. Development of the method

A survey of central details of existing models describing many-body nuclear systems is first presented in Sec. 2. The intend is to explain the underlying philosophy and the fundamental operating methods in an effort to highlight strengths and weaknesses specific to each approach. We conclude that shortcomings among established methods are treatments of weakly bound and spatially extended systems as well as the computational requirements when applied to systems heavier than the very lightest nuclei. This expresses the need for an efficient method which incorporates these correlations along with ordinary many-body features. We present a new method to remedy these shortcomings, that is both allow these structures in the wave function and

without loss of computational efficiency for applications on heavier nuclei.

The underlying philosophy and the theoretical derivations are described in Sec. 3.1, with assumptions added as they become necessary. We present the idea behind the combination of few- and many-body structures and derive the fundamental coupled equations of motion. At first, this formalism is independent of specific correlations and in particular valid for all choices of nucleon-nucleon interactions. The few- and many-body treatments are independently formulated although connected in the resulting coupled equations. Then we continue the derivation in Sec. 3.2 with specific choices of few-body and many-body formalisms and subsequently corresponding selection of the Skyrme nucleon-nucleon interaction.

The few-body formalism is chosen to be the hyperspherical adiabatic expansion of the Faddeev equations in coordinate space. This choice has several advantages of particular importance for practical implementation of the method. All Jacobi coordinate systems are treated equally, and the bound and continuum channels decouple completely, which makes it much easier to account for the Pauli exclusion principle between few- and many-body treated nucleons. Finally, this part of the program is then as computationally efficient as the same few-body problem.

The many-body formalism is here chosen to be the mean-field Skyrme-Hartree-Fock description. The corresponding many-body treatment is related to the bulk part (core) of the nucleus. The advantage is again simplicity and efficiency of the method which in particular makes it possible to treat heavy nuclear systems. Our present focus is on weakly bound systems, where most of the characteristic behavior is dictated by the few-body treated (valence) nucleons. Efficiency is therefore a higher priority than sophistication, as long as a decent core description is delivered.

It should be noted that despite the close connection between the core and valence aspects of the system, it is still possible to account very well for the Pauli principle, as described in Sec. 4.3. To achieve this goal several procedures are available within the framework of our hyperspherical adiabatic expansion method. Phase equivalent potentials can be constructed to exclude occupation of one specific state, while still retaining precisely the same scattering properties. Due to the decoupling of many solutions in the spectrum of hyperangular eigenvalues, direct removal of occupied states is also possible. By employing a combination of these methods the Pauli principle is very accurately accounted for.

At the heart of the method is how the core description provides a potential to be used between the clusters in the three-body calculations. Producing this potential self-consistently within the framework of the method eliminates one of the main weaknesses of traditional three-body approaches, as there is (almost) no freedom to use for phenomenological adjustments. The choice of a nucleon-nucleon interaction containing derivatives leads to effective mass terms in the three-body as well as in the core calculations. Such terms are unusual in traditional three-body calculations, but in principle they amount to additional couplings between the different subsystems, and are as such not unfamiliar.

Another central aspect of the method is how the structure of the core affects the behavior of the remaining valence nucleons through the iterative procedure of the calculations. These iterations intimately connect the short-distance bulk properties of the system with the long-range behavior of the weakly bound valence nucleons. This connection allows for more meaningful investigations of the spatial evolution and reaction mechanisms of nuclear systems.

9.2. Summarizing the applications

Having presented all the details of the derivations along with a discussion of the technical implementation, we first apply the method on ^{26}O ($^{24}\text{O} + n + n$) as described in Sec 5. This system is particularly interesting as located at the edge of an abrupt discontinuity in the neutron dripline following $Z = 8$. As such it has in recent years received an increasing amount of attention, both theoretically and experimentally. We demonstrate the procedure with the effect of the iterations and the speed of the convergence. Using three different, unaltered Skyrme parameterizations, both the experimentally known energy levels and the half-life is very accurately reproduced. This is particularly striking considering the inaccuracy of the predictions from traditional Skyrme-Hartree-Fock calculations. This illustrates how well the method can work even with a very simple core description.

To further demonstrate the flexibility and computational efficiency of the method we examine the heavier nucleus, ^{72}Ca ($^{70}\text{Ca} + n + n$). Although this system is currently outside experimental reach, it is still very interesting due to the possibilities it presents. It is on the edge of the neutron dripline, but more importantly one of the lowest allowed states for the valence nucleons is an $s_{1/2}$ state. Having neither a Coulomb nor a centrifugal barrier, very extended configurations are possible, which relates the system to the field of halo physics, and it could potentially also allow for the formation of Efimov states. All these issues are discussed in Sec. 6.

In the same section, Sec. 6, we also discuss how the method closely relates the short-distance, bulk properties with the long-distance physical observables. We show how the fingerprints of the bulk properties can be detected in physical observables such as the energy distribution. We further discuss when and under which conditions halo formations are possible, and we demonstrate that the mere availability of a spatially confined d -state is not enough to suppress the formation of extended s -wave halo configurations. Finally, we consider the possibility of detecting Efimov states in this system, maybe as excited states. Despite the fascinating avenues of physics that would be available by such a possibility, we conclude that a series of Efimov states is not possible in ^{72}Ca or in any other nuclear system.

We continue with an application on the proton dripline, ^{70}Kr ($^{68}\text{Se} + p + p$), with astrophysical consequences in mind. The nucleus, ^{68}Se , is considered to be one of the most important of the heavier critical waiting points in the rp-process. The understanding of the effective lifetime of this nucleus in a stellar environment is central

in determining the evolution of for instance close binary systems containing neutron stars or white dwarfs. This effective lifetime is affected significantly by the possibility of skipping the mass gap in the proton dripline through a three-body reaction and forming ^{70}Kr by capturing two protons.

With that in mind the primary focus of the analysis is here on the two-proton capture rate, and to that end the associated proton capture cross section is an essential intermediate step. The analysis is complicated by the fact that very little experimental information is available in this region of the nuclear chart, and some uncertainty remains as to the energy level of the three-body resonance. Despite these uncertainties, it is still possible to provide rather narrow limits for the reaction rate. We find that the continuum (off resonance) background contribution is significant, and thereby establishing a scale for the reaction rate.

In addition to these practical predictions, the ^{70}Kr nucleus is also used to examine the more subtle parts of the new coupling terms, as well as fundamental properties of the reaction mechanism. The behavior of the new coupling terms is understandable when comparing to the already existing coupling terms. The capture reaction is seen to be a very unambiguous sequential reaction, which can be understood as proceeding through a resonance state and the related specific geometric configurations of the system.

9.3. Summary and perspective

In evaluating these results a number of obvious strong points in the method is seen. First and foremost is the ease with which weakly bound and extended systems are treated. This is an area that is very difficult to treat properly with existing methods, making this application particularly valuable. In relation to this point is the fact that the method intimately and self-consistently connect long-distance observable structures and short-distance bulk properties. This makes it possible to extract reliable information about the properties of the nuclear systems from the observable behavior.

A final noteworthy aspect of the method is its simplicity and computational efficiency. While many of the more sophisticated, existing many-body methods need supercomputer clusters and extremely large memory arrays to complete a calculation within a realistic time frame, this method can be implemented on a single, regular computer core, with a runtime of several days. Due to the simplicity of the mean-field method this is even true for heavy and complicated systems.

These obvious strengths of the method have to be further enhanced by implementing two or three improvements on top of the present formulation and applications. The first lies in the interaction between pairs of valence nucleons. As discussed in Secs. 4.4.1 and 4.4.2, it is possible, in principle, to use the same interaction between the valence nucleons as between the core nucleons. However, due to the zero-range nature of the Skyrme force, this leads to spurious, unphysical solutions, which strongly couple to all physical solutions. This is not much of a problem, as minor variations in the valence nucleon-nucleon interaction only has an insignificant influence on the three-body wave

function, as long as this interaction is asymptotically correct.

The second improvement is related to the three-body potential in the three-body equation. The philosophy behind the Skyrme effective interaction suggests parameterization in terms of a density dependent two-body interaction. This is in principle straightforward, but complicated, using the nuclear core density folded with the nucleon-nucleon interaction. However, this is not meaningful at the moment, since all present global many-body calculations are unable to provide keV-level accuracy, as needed to calculate desired reliable few-body properties. This is a problematic issue for the simple Skyrme force and for all other interactions as well. To be practical, we use here a phenomenological three-body interaction between the core and the two valence nucleons. So far, we keep this potential for fine-tuning the energy without affecting the three-body structure. This is important in situations where the energy is decisive as for tunneling or close to break-up thresholds. This degree of flexibility is unavoidable for precision calculations.

The third improvement is related to the average treatment of the “external” potential acting on the core nucleons and arising from the valence particles. This treatment should be replaced by a detailed hyper-radial dependence such that each average distance produces its own potential. The asymptotic limit of three free particles would then be correctly reproduced.

One limitation discussed in Sec. 8 is the structure of the system, currently assumed to be a spherical, even-even core surrounded by two identical valence point-like nucleons. This could be improved in several directions. The valence nucleons could be replaced by more complicated clusters with intrinsic structure, where the simplest probably is α -particles but larger compact nuclei could also be considered. The simplest choice is obviously to add structure on one valence particle at a time, and in particular start with only two clusters simulating the asymmetric fission process. The core could also be allowed to deviate from spherical symmetry, be deformed and in addition possibly containing odd numbers of nucleons. This would open up for many new possibilities. Beside these mean-field generalizations, other improvements of the many-body treatment are tempting. In general this could be to replace the mean-field core description with a more sophisticated *ab-initio* method, but this would sacrifice much of the efficiency, while probably gaining very little accuracy.

In conclusion, we have presented a conceptually simple, but technically advanced new method, which has unique application possibilities within the areas of weakly bound and extended three-body systems, while at the same time apparently exhibiting rather impressive computational efficiency. These initial applications demonstrate the accuracy and viability of the method. But a number of future improvements and applications, also beyond nuclear physics, are both tempting and possible.

Acknowledgments

This work was funded by the Danish Council for Independent Research DFF Natural Science and the DFF Sapere Aude program. This work has been partially supported by the Spanish Ministerio de Economía y Competitividad under Project FIS2014-51971-P.

Appendix A. Skyrme interaction variation

This appendix contains details of the variations expressed in Eq. (20). The variation of Eq. (15) with respect to ψ_i^* is a completely standard Skyrme mean-field variation only with a slightly different t_3 term. The focus is therefore on terms involving the valence nucleons, i.e. variations of V_{iv_1} and V_{iv_2} in Eq. (16). This will be done explicitly for the variation with respect ψ_{3b}^* , while the variation with respect to ψ_i^* follows by symmetry. Initially, the derivation is divided into contributions from the various terms in the Skyrme force (t_0 , t_1 , t_2 , t_3 , and W_0), which are then combined.

The results are expressed in terms of the densities known from regular mean-field calculations [37], along with analog densities for the three-body part. Specifically, the interactions are expressed in terms of

$$n_q(\mathbf{r}) = \sum_{i\sigma} |\psi_{iq\sigma}(\mathbf{r})|^2 = n_{q\downarrow}(\mathbf{r}) + n_{q\uparrow}(\mathbf{r}), \quad (\text{A.1})$$

$$n_3(\mathbf{r}) = \int |\psi_{3b}(\mathbf{r}_{cv1}, \mathbf{r})|^2 d\mathbf{r}_{cv1} + \int |\psi_{3b}(\mathbf{r}, \mathbf{r}_{cv2})|^2 d\mathbf{r}_{cv2}, \quad (\text{A.2})$$

$$\tau_q(\mathbf{r}) = \sum_{i\sigma} |\nabla \psi_{iq\sigma}(\mathbf{r})|^2, \quad (\text{A.3})$$

$$\tau_3(\mathbf{r}) = \int |\nabla_r \psi_{3b}(\mathbf{r}_{cv1}, \mathbf{r})|^2 d\mathbf{r}_{cv1} + \int |\nabla_r \psi_{3b}(\mathbf{r}, \mathbf{r}_{cv2})|^2 d\mathbf{r}_{cv2}, \quad (\text{A.4})$$

$$\mathbf{J}_q(\mathbf{r}) = -i \sum_{i\sigma\sigma'} \psi_{iq\sigma}^*(\mathbf{r}) (\nabla \psi_{iq\sigma'}(\mathbf{r}) \times \langle \sigma | \boldsymbol{\sigma} | \sigma' \rangle), \quad (\text{A.5})$$

$$\begin{aligned} \mathbf{J}_3(\mathbf{r}) = & -i \sum_{\sigma\sigma'} \left(\int \psi_{3b,\sigma}^*(\mathbf{r}_{cv1}, \mathbf{r}) \nabla_r \psi_{3b,\sigma'}(\mathbf{r}_{cv1}, \mathbf{r}) d\mathbf{r}_{cv1} \right. \\ & \left. + \int \psi_{3b,\sigma}^*(\mathbf{r}, \mathbf{r}_{cv2}) \nabla_r \psi_{3b,\sigma'}(\mathbf{r}, \mathbf{r}_{cv2}) d\mathbf{r}_{cv2} \right) \times \langle \sigma | \boldsymbol{\sigma} | \sigma' \rangle, \end{aligned} \quad (\text{A.6})$$

where the sum over i is a sum over single particle states, and the sum over σ is over spin components (also indicated by \uparrow, \downarrow), while $\boldsymbol{\sigma}$ are the Pauli matrices, and q indicates the associated nucleon type. Here q can be either core neutrons (n), core protons (p), core neutrons and protons combined (c), core nucleons of the same type as the valence nucleons (s), or core nucleons of opposite type to the valence nucleons (d).

To further simplify the expressions the following shorthand notation is also introduced at the end

$$t_{i1} = t_i \left(1 + \frac{1}{2} x_i \right), t_{i2} = t_i \left(\frac{1}{2} + x_i \right), \quad (\text{A.7})$$

where t_i and x_i are the parameters from the Skyrme force, with $i = 0, 1, 2$, and 3.

Appendix A.1. Assumptions and equalities

Because of the spin-operators in the Skyrme force from Eq. (21), and to treat the exchange term explicitly, the wave functions are decomposed into their spin-components. It will be used, that

$$|S = 0\rangle = \frac{1}{\sqrt{2}} (|\uparrow\rangle_1 |\downarrow\rangle_2 - |\downarrow\rangle_1 |\uparrow\rangle_2), \quad (\text{A.8})$$

$$|S = 1, s_z = 0\rangle = \frac{1}{\sqrt{2}} (|\uparrow\rangle_1 |\downarrow\rangle_2 + |\downarrow\rangle_1 |\uparrow\rangle_2), \quad (\text{A.9})$$

$$|S = 1, s_z = 1\rangle = |\uparrow\rangle_1 |\uparrow\rangle_2, \quad (\text{A.10})$$

$$|S = 1, s_z = -1\rangle = |\downarrow\rangle_1 |\downarrow\rangle_2, \quad (\text{A.11})$$

where $|\uparrow\rangle_i$ and $|\downarrow\rangle_i$ indicates the spin-up and down components of the i 'th particle. It is also used that

$$P_\sigma |S = 0\rangle = -|S = 0\rangle \quad \text{and} \quad P_\sigma |S = 1\rangle = |S = 1\rangle. \quad (\text{A.12})$$

The product of ψ_i and ψ_{3b} is written out as

$$\begin{aligned} \psi_i(\mathbf{r})\psi_{3b}(\mathbf{r}_{cv1}, \mathbf{r}_{cv2}) &= (\psi_{i\uparrow}(\mathbf{r}) |\uparrow\rangle_r + \psi_{i\downarrow}(\mathbf{r}) |\downarrow\rangle_r) \\ &\quad \times (\psi_{3b,\uparrow}(\mathbf{r}_{cv1}, \mathbf{r}_{cv2}) |\uparrow\rangle_{r_1} + \psi_{3b,\downarrow}(\mathbf{r}_{cv1}, \mathbf{r}_{cv2}) |\downarrow\rangle_{r_1}) \\ &= \frac{|S = 0\rangle}{\sqrt{2}} (\psi_{i\uparrow}(\mathbf{r})\psi_{3b,\downarrow}(\mathbf{r}_{cv1}, \mathbf{r}_{cv2}) - \psi_{i\downarrow}(\mathbf{r})\psi_{3b,\uparrow}(\mathbf{r}_{cv1}, \mathbf{r}_{cv2})) \\ &\quad + \frac{|S = 1, s_z = 0\rangle}{\sqrt{2}} \\ &\quad \times (\psi_{i\uparrow}(\mathbf{r})\psi_{3b,\downarrow}(\mathbf{r}_{cv1}, \mathbf{r}_{cv2}) + \psi_{i\downarrow}(\mathbf{r})\psi_{3b,\uparrow}(\mathbf{r}_{cv1}, \mathbf{r}_{cv2})) \\ &\quad + |S = 1, s_z = -1\rangle \psi_{i\downarrow}(\mathbf{r})\psi_{3b,\downarrow}(\mathbf{r}_{cv1}, \mathbf{r}_{cv2}) \\ &\quad + |S = 1, s_z = 1\rangle \psi_{i\uparrow}(\mathbf{r})\psi_{3b,\uparrow}(\mathbf{r}_{cv1}, \mathbf{r}_{cv2}) \end{aligned} \quad (\text{A.13})$$

As we are focusing on cores with an even-even spherical structure, time-reversal symmetry is implied. This allows us to use many of the traditional equalities known from spherical mean-field Skyrme calculations, seen for instance in Ref. [37]. We therefore have the following equalities for the core wave function

$$\frac{1}{2}n_n = n_{n\uparrow} = n_{n\downarrow}, \quad (\text{A.14})$$

$$0 = \sum_{i \in N} \psi_{i\downarrow}^* \psi_{i\uparrow} + \psi_{i\uparrow}^* \psi_{i\downarrow}, \quad (\text{A.15})$$

$$\frac{1}{4}\nabla n_n = \sum_{i \in N} \psi_{i\downarrow}^* \psi'_{i\downarrow} = \sum_{i \in N} \psi_{i\uparrow}^* \psi'_{i\uparrow} = \sum_{i \in N} \psi_{i\downarrow}^* \psi'_{i\downarrow} = \sum_{i \in N} \psi_{i\uparrow}^* \psi'_{i\uparrow}, \quad (\text{A.16})$$

$$\nabla^2 n_n = 2\tau_n + 2 \sum_{i \in N} \psi_i^* \nabla^2 \psi_i, \quad (\text{A.17})$$

where a prime indicates a gradient. The same equalities hold true for core proton densities. For the three-body wave function it is only needed that

$$\frac{1}{2}\nabla |\psi_{3b}|^2 = \psi_{3b,\uparrow}^* \psi'_{3b,\uparrow} + \psi_{3b,\downarrow}^* \psi'_{3b,\downarrow} = \psi_{3b,\uparrow}^* \psi_{3b,\uparrow} + \psi_{3b,\uparrow}^* \psi'_{3b,\uparrow} \quad (\text{A.18})$$

$$\nabla^2 |\psi_{3b}|^2 = 2|\nabla \psi_{3b}|^2 + 2\psi_{3b}^* \nabla^2 \psi_{3b} \quad (\text{A.19})$$

Finally, by writing out the definitions from Eqs. (A.5) and (A.6) it is seen that

$$\begin{aligned}
 \mathbf{J}_n(\mathbf{r}) \cdot \mathbf{J}_3(\mathbf{r}) = & -2 \sum_{i \in N} \int d\mathbf{r}_{cv_1} \left(\psi_{3b,\uparrow}^*(\mathbf{r}_{cv_1}, \mathbf{r}) \nabla \psi_{3b,\downarrow}(\mathbf{r}_{cv_1}, \mathbf{r}) \cdot \psi_{i\uparrow}^*(\mathbf{r}) \nabla \psi_{i\downarrow}(\mathbf{r}) \right. \\
 & + \psi_{3b,\downarrow}^*(\mathbf{r}_{cv_1}, \mathbf{r}) \nabla \psi_{3b,\uparrow}(\mathbf{r}_{cv_1}, \mathbf{r}) \cdot \psi_{i\downarrow}^*(\mathbf{r}) \nabla \psi_{i\uparrow}(\mathbf{r}) \\
 & - 2 \sum_{i \in N} \int d\mathbf{r}_{cv_2} \left(\psi_{3b,\uparrow}^*(\mathbf{r}, \mathbf{r}_{cv_2}) \nabla \psi_{3b,\downarrow}(\mathbf{r}, \mathbf{r}_{cv_2}) \cdot \psi_{i\uparrow}^*(\mathbf{r}) \nabla \psi_{i\downarrow}(\mathbf{r}) \right. \\
 & \left. + \psi_{3b,\downarrow}^*(\mathbf{r}, \mathbf{r}_{cv_2}) \nabla \psi_{3b,\uparrow}(\mathbf{r}, \mathbf{r}_{cv_2}) \cdot \psi_{i\downarrow}^*(\mathbf{r}) \nabla \psi_{i\uparrow}(\mathbf{r}) \right) \quad (\text{A.20})
 \end{aligned}$$

Appendix A.2. t_0 and t_3 energy contribution

Here the contribution to the energy from the t_0 part of the core-valence neutron interaction for variation with respect to ψ_{3b}^* is derived. Only the contribution from the interaction between the core and one valence nucleon is calculated, i.e. the contribution from V_{iv_1} . The contribution from the other valence nucleon is the same with a change of coordinates.

The interaction is

$$V_{iv_1}^{(t_0)} = t_0 (1 + x_0 P_\sigma) \delta(\mathbf{r} - \mathbf{r}_{cv_1}). \quad (\text{A.21})$$

The energy is then calculated by multiplying by Ψ from the left and the right, and integrating over all coordinates

$$\begin{aligned}
 E_{t_0} = & t_0 \left(\sum_{i \in N} + \sum_{i \in Z} \right) \int d\mathbf{r} d\mathbf{r}_{cv_1} d\mathbf{r}_{cv_2} \left\{ \right. \\
 & \psi_i^*(\mathbf{r}) \psi_{3b}^*(\mathbf{r}_{cv_1}, \mathbf{r}_{cv_2}) \delta(\mathbf{r} - \mathbf{r}_{cv_1}) (1 + x_0 P_\sigma(i, v_1)) \\
 & \left. \times [\psi_i(\mathbf{r}) \psi_{3b}(\mathbf{r}_{cv_1}, \mathbf{r}_{cv_2}) - \psi_i(\mathbf{r}_{cv_1}) \psi_{3b}(\mathbf{r}, \mathbf{r}_{cv_2}) \delta_{q_i, q_{v_1}}] \right\}, \quad (\text{A.22})
 \end{aligned}$$

where the last δ function is to ensure exchange is only included when core and valence nucleon is of the same type. The calculation is also split into the sum over neutrons and protons. Here it is assumed the valence nucleons are neutrons, but the derivation for protons is identical. The situation is simplified greatly by the δ function in the Skyrme force, as only $|S = 0\rangle$ contributes when core and valence nucleon are the same type.

So for neutrons, the contribution is

$$\begin{aligned}
 E_{t_0}^{(N)}(|S = 0\rangle) = & t_0 \sum_{i \in N} \int d\mathbf{r}_{cv_1} d\mathbf{r}_{cv_2} \left\{ \frac{(1 - x_0)}{2} \right. \\
 & \times [\psi_{i\uparrow}^*(\mathbf{r}_{cv_1}) \psi_{3b,\downarrow}^*(\mathbf{r}_{cv_1}, \mathbf{r}_{cv_2}) - \psi_{i\downarrow}^*(\mathbf{r}_{cv_1}) \psi_{3b,\uparrow}^*(\mathbf{r}_{cv_1}, \mathbf{r}_{cv_2})] \\
 & \left. \times 2 [\psi_{i\uparrow}(\mathbf{r}_{cv_1}) \psi_{3b,\downarrow}(\mathbf{r}_{cv_1}, \mathbf{r}_{cv_2}) - \psi_{i\downarrow}(\mathbf{r}_{cv_1}) \psi_{3b,\uparrow}(\mathbf{r}_{cv_1}, \mathbf{r}_{cv_2})] \right\} \\
 = & t_0 \int d\mathbf{r}_{cv_1} d\mathbf{r}_{cv_2} \left\{ (1 - x_0) \right. \\
 & \left. \times [n_{n\uparrow}(\mathbf{r}_{cv_1}) |\psi_{3b,\downarrow}(\mathbf{r}_{cv_1}, \mathbf{r}_{cv_2})|^2 + n_{n\downarrow}(\mathbf{r}_{cv_1}) |\psi_{3b,\uparrow}(\mathbf{r}_{cv_1}, \mathbf{r}_{cv_2})|^2] \right\} \quad (\text{A.23})
 \end{aligned}$$

With a neutron as valence nucleon, there is no exchange when interacting with a core proton. Therefore both $|S = 0\rangle$ and $|S = 1\rangle$ contributes. For $|S = 0\rangle$ the contribution

is

$$E_{t_0}^{(Z)} (|S = 0\rangle) = t_0 \int d\mathbf{r}_{cv_1} d\mathbf{r}_{cv_2} \frac{1-x_0}{2} [n_{p\uparrow}(\mathbf{r}_{cv_1}) |\psi_{3b,\downarrow}(\mathbf{r}_{cv_1}, \mathbf{r}_{cv_2})|^2 + n_{p\downarrow}(\mathbf{r}_{cv_1}) |\psi_{3b,\uparrow}(\mathbf{r}_{cv_1}, \mathbf{r}_{cv_2})|^2], \quad (\text{A.24})$$

while for $|S = 1\rangle$ the contribution consists of three components

$$E_{t_0}^{(Z)} (|S = 1, S_z = 0\rangle) = t_0 \int d\mathbf{r}_{cv_1} d\mathbf{r}_{cv_2} \frac{1+x_0}{2} [n_{p\uparrow}(\mathbf{r}_{cv_1}) |\psi_{3b,\downarrow}(\mathbf{r}_{cv_1}, \mathbf{r}_{cv_2})|^2 + n_{p\downarrow}(\mathbf{r}_{cv_1}) |\psi_{3b,\uparrow}(\mathbf{r}_{cv_1}, \mathbf{r}_{cv_2})|^2], \quad (\text{A.25})$$

$$E_{t_0}^{(Z)} (|S = 1, S_z = 1\rangle) = t_0 \int d\mathbf{r}_{cv_1} d\mathbf{r}_{cv_2} (1+x_0) n_{p\uparrow}(\mathbf{r}_{cv_1}) |\psi_{3b,\uparrow}(\mathbf{r}_{cv_1}, \mathbf{r}_{cv_2})|^2, \quad (\text{A.26})$$

$$E_{t_0}^{(Z)} (|S = 1, S_z = -1\rangle) = t_0 \int d\mathbf{r}_{cv_1} d\mathbf{r}_{cv_2} (1+x_0) n_{p\downarrow}(\mathbf{r}_{cv_1}) |\psi_{3b,\downarrow}(\mathbf{r}_{cv_1}, \mathbf{r}_{cv_2})|^2. \quad (\text{A.27})$$

Combining both neutron and proton contributions and using Eq. (A.14) the contribution to the energy is

$$\begin{aligned} E_{t_0} &= t_0 \int d\mathbf{r}_{cv_1} d\mathbf{r}_{cv_2} \left\{ |\psi_{3b,\uparrow}(\mathbf{r}_{cv_1}, \mathbf{r}_{cv_2})|^2 [(1-x_0)n_{n\downarrow}(\mathbf{r}_{cv_1}) + n_{p\downarrow}(\mathbf{r}_{cv_1}) + (1+x_0)n_{p\uparrow}(\mathbf{r}_{cv_1})] \right. \\ &\quad \left. + |\psi_{3b,\downarrow}(\mathbf{r}_{cv_1}, \mathbf{r}_{cv_2})|^2 [(1-x_0)n_{n\uparrow}(\mathbf{r}_{cv_1}) + n_{p\uparrow}(\mathbf{r}_{cv_1}) + (1+x_0)n_{p\downarrow}(\mathbf{r}_{cv_1})] \right\} \\ &= t_0 \int d\mathbf{r}_{cv_1} d\mathbf{r}_{cv_2} |\psi_{3b}(\mathbf{r}_{cv_1}, \mathbf{r}_{cv_2})|^2 \left[\left(1 + \frac{1}{2}x_0\right) n_c(\mathbf{r}_{cv_1}) - \left(\frac{1}{2} + x_0\right) n_n(\mathbf{r}_{cv_1}) \right] \\ &= \int d\mathbf{r}_{cv_1} d\mathbf{r}_{cv_2} |\psi_{3b}(\mathbf{r}_{cv_1}, \mathbf{r}_{cv_2})|^2 [t_{01}n_c(\mathbf{r}_{cv_1}) - t_{02}n_n(\mathbf{r}_{cv_1})]. \quad (\text{A.28}) \end{aligned}$$

An identical t_0 contribution would arise from the interaction between the second valence nucleon and the core, only with a change of coordinates. If the valence nucleon is a proton the only difference would be a change of subscript, $n_n \leftrightarrow n_p$.

The calculation of the t_3 contribution to the energy is identical only including a factor of $(n_c + n_3)^\alpha/6$ from the interaction. The result is

$$E_{t_3} = \frac{1}{6} \int d\mathbf{r}_{cv_1} d\mathbf{r}_{cv_2} |\psi_{3b}(\mathbf{r}_{cv_1}, \mathbf{r}_{cv_2})|^2 (n_c(\mathbf{r}_{cv_1}) + n_3(\mathbf{r}_{cv_1}))^\alpha [t_{31}n_c(\mathbf{r}_{cv_1}) - t_{32}n_n(\mathbf{r}_{cv_1})]. \quad (\text{A.29})$$

It should be noted that the t_3 term in V_{ij} from Eq. (15) also depends on n_3 . However, this is just the regular t_3 contribution [37] with $n_c^\alpha \rightarrow (n_c + n_3)^\alpha$. This contribution is then

$$E_{t_3}^{(c)} = \frac{1}{12} \int d\mathbf{r} (n_c(\mathbf{r}) + n_3(\mathbf{r}))^\alpha [t_{31}n_c(\mathbf{r})^2 - t_{32}(n_n(\mathbf{r})^2 + n_p(\mathbf{r})^2)]. \quad (\text{A.30})$$

Appendix A.3. t_1 energy contribution

The contribution to the energy from the t_1 term is slightly more complicated because of the derivatives, but the procedure is the same. The t_1 interaction is

$$\begin{aligned} V_{iv_1}^{(t_1)} &= \frac{1}{2}t_1 (1 + x_1 P_\sigma) (\mathbf{k}'^2 \delta(\mathbf{r}_{cv_1} - \mathbf{r}) + \delta(\mathbf{r}_{cv_1} - \mathbf{r}) \mathbf{k}^2) \\ &= \frac{-t_1}{8} (1 + x_1 P_\sigma) \left((\nabla'_{v_1} - \nabla')^2 \delta(\mathbf{r}_{cv_1} - \mathbf{r}) + \delta(\mathbf{r}_{cv_1} - \mathbf{r}) (\nabla_{v_1} - \nabla)^2 \right), \end{aligned} \quad (\text{A.31})$$

and the contribution to the energy is then

$$\begin{aligned} E_{t_1} &= -\frac{1}{8}t_1 \left(\sum_{i \in N} + \sum_{i \in Z} \right) \int d\mathbf{r} d\mathbf{r}_{cv_1} d\mathbf{r}_{cv_2} \psi_i^*(\mathbf{r}) \psi_{3b}^*(\mathbf{r}_{cv_1}, \mathbf{r}_{cv_2}) (1 + x_1 P_\sigma(i, v_1)) \\ &\quad \times \left((\nabla'_{v_1} - \nabla')^2 \delta(\mathbf{r}_{cv_1} - \mathbf{r}) + \delta(\mathbf{r}_{cv_1} - \mathbf{r}) (\nabla_{v_1} - \nabla)^2 \right) \\ &\quad \times [\psi_i(\mathbf{r}) \psi_{3b}(\mathbf{r}_{cv_1}, \mathbf{r}_{cv_2}) - \psi_{3b}(\mathbf{r}, \mathbf{r}_{cv_2}) \psi_i(\mathbf{r}_{cv_1}) \delta_{q_i, q_{v_1}}]. \end{aligned} \quad (\text{A.32})$$

The general procedure is the same as for t_0 . That is; divide the derivation into the sum over neutrons and the sum over protons, separate into $S = 1$ and $S = 0$ components, calculate all the derivatives, restructure using partial integration, apply the assumptions from [Appendix A.1](#), regroup to comply with definitions from the beginning of [Appendix A](#), and finally simplify the expressions.

Using Eqs. [\(A.14\)](#) to [\(A.19\)](#) the neutron contribution to the energy from the second term in Eq. [\(A.31\)](#) is then

$$\begin{aligned} E_{t_1}^{(N)} &= -\frac{1-x_1}{8} t_1 \sum_{i \in N} \int d\mathbf{r}_{cv_1} d\mathbf{r}_{cv_2} \left\{ [\psi_{i\uparrow}^* \psi_{3b,\downarrow}^* - \psi_{i\downarrow}^* \psi_{3b,\uparrow}^*] \right. \\ &\quad \times [\psi_{i\uparrow} \psi_{3b,\downarrow}'' - \psi_{i\downarrow} \psi_{3b,\uparrow}'' + \psi_{i\uparrow}'' \psi_{3b,\downarrow} - \psi_{i\downarrow}'' \psi_{3b,\uparrow} + 2(\psi_{i\downarrow}' \psi_{3b,\uparrow}' - \psi_{i\uparrow}' \psi_{3b,\downarrow}')] \left. \right\} \\ &= -\frac{1-x_1}{8} t_1 \int d\mathbf{r}_{cv_1} d\mathbf{r}_{cv_2} \left\{ \frac{3}{4} \nabla^2 n_n |\psi_{3b}|^2 - \frac{1}{2} n_n |\nabla \psi_{3b}|^2 - \frac{1}{2} \tau_n |\psi_{3b}|^2 \right. \\ &\quad \left. + i \mathbf{J}_n \cdot \sum_{\sigma\sigma'} \psi_{3b,\sigma}^* \nabla \psi_{3b,\sigma'} \times \langle \sigma | \sigma | \sigma' \rangle \right\}. \end{aligned} \quad (\text{A.33})$$

The same is done for the proton contribution. This is again divided into $|S = 0\rangle$ and $|S = 1\rangle$. The $|S = 0\rangle$ contribution is half what it was for the neutron contribution because of the missing exchange term, and the $|S = 1\rangle$ contribution is calculated similarly. The total contribution from the proton is then

$$\begin{aligned} E_{t_1}^{(Z)} &= -\frac{1+x_1}{8} t_1 \int d\mathbf{r}_{cv_1} d\mathbf{r}_{cv_2} \left\{ \frac{9}{8} \nabla^2 n_p |\psi_{3b}|^2 - \frac{3}{4} \tau_p |\psi_{3b}|^2 \right. \\ &\quad \left. - \frac{3}{4} n_p |\nabla \psi_{3b}|^2 - i \frac{1}{2} \mathbf{J}_p \cdot \sum_{\sigma\sigma'} \psi_{3b,\sigma}^* \nabla \psi_{3b,\sigma'} \times \langle \sigma | \sigma | \sigma' \rangle \right\}. \end{aligned} \quad (\text{A.34})$$

Combining Eqs. [\(A.33\)](#) and [\(A.34\)](#) gives the energy contribution from the second term in Eq. [\(A.31\)](#). The first term in Eq. [\(A.31\)](#) results in the same contribution because

of symmetry. The total energy contribution from the t_1 term for the interaction between the core and one of the valence neutrons is then

$$\begin{aligned}
 E_{t_1} = & \int d\mathbf{r}_{cv_1} d\mathbf{r}_{cv_2} \left\{ i \frac{t_1}{8} \right. \\
 & (x_1 \mathbf{J}_c(\mathbf{r}_{cv_1}) - \mathbf{J}_n(\mathbf{r}_{cv_1})) \cdot \sum_{\sigma\sigma'} \psi_{3b,\sigma}^*(\mathbf{r}_{cv_1}, \mathbf{r}_{cv_2}) \nabla_{v_1} \psi_{3b,\sigma'}(\mathbf{r}_{cv_1}, \mathbf{r}_{cv_2}) \times \langle \sigma | \sigma | \sigma' \rangle \\
 & + \frac{t_{11}}{4} \left(-\psi_{3b}^*(\mathbf{r}_{cv_1}, \mathbf{r}_{cv_2}) \nabla_{v_1} (n_c(\mathbf{r}_{cv_1}) \nabla_{v_1} \psi_{3b}(\mathbf{r}_{cv_1}, \mathbf{r}_{cv_2})) \right. \\
 & + \tau_c(\mathbf{r}_{cv_1}) |\psi_{3b}(\mathbf{r}_{cv_1}, \mathbf{r}_{cv_2})|^2 - \frac{3}{2} \nabla_{v_1}^2 n_c(\mathbf{r}_{cv_1}) |\psi_{3b}(\mathbf{r}_{cv_1}, \mathbf{r}_{cv_2})|^2 \Big) \\
 & - \frac{t_{12}}{4} \left(-\psi_{3b}^*(\mathbf{r}_{cv_1}, \mathbf{r}_{cv_2}) \nabla_{v_1} (n_n(\mathbf{r}_{cv_1}) \nabla_{v_1} \psi_{3b}(\mathbf{r}_{cv_1}, \mathbf{r}_{cv_2})) \right. \\
 & \left. \left. + \tau_n(\mathbf{r}_{cv_1}) |\psi_{3b}(\mathbf{r}_{cv_1}, \mathbf{r}_{cv_2})|^2 - \frac{3}{2} \nabla_{v_1}^2 n_n(\mathbf{r}_{cv_1}) |\psi_{3b}(\mathbf{r}_{cv_1}, \mathbf{r}_{cv_2})|^2 \right) \right\}. \quad (\text{A.35})
 \end{aligned}$$

There is an identical contribution from the interaction with the other valence neutron, only where the coordinate dependence is \mathbf{r}_{cv_2} instead of \mathbf{r}_{cv_1} in n_i and τ_i .

Appendix A.4. t_2 energy contribution

The t_2 interaction is

$$\begin{aligned}
 V_{iv_1}^{(t_2)} = & t_2 (1 + x_2 P_\sigma) \mathbf{k}' \delta(\mathbf{r}_{cv_1} - \mathbf{r}) \mathbf{k} \\
 = & \frac{1}{4} t_2 (1 + x_2 P_\sigma) (\nabla'_{v_1} - \nabla') \delta(\mathbf{r}_{cv_1} - \mathbf{r}) (\nabla_{v_1} - \nabla). \quad (\text{A.36})
 \end{aligned}$$

The contribution to the energy is therefore

$$\begin{aligned}
 E_{t_2} = & \frac{1}{4} t_2 \left(\sum_{i \in N} + \sum_{i \in Z} \right) \int d\mathbf{r} d\mathbf{r}_{cv_1} d\mathbf{r}_{cv_2} \left\{ \right. \\
 & \psi_i^*(\mathbf{r}) \psi_{3b}^*(\mathbf{r}_{cv_1}, \mathbf{r}_{cv_2}) (\nabla'_{v_1} - \nabla') [1 + x_2 P_\sigma(i, v_1)] \delta(\mathbf{r}_{cv_1} - \mathbf{r}) \\
 & \left. \times (\nabla_{v_1} - \nabla) [\psi_i(\mathbf{r}) \psi_{3b}(\mathbf{r}_{cv_1}, \mathbf{r}_{cv_2}) - \psi_{3b}(\mathbf{r}, \mathbf{r}_{cv_2}) \psi_i(\mathbf{r}_{cv_1}) \delta_{q_i, q_{v_1}}] \right\} \quad (\text{A.37})
 \end{aligned}$$

The derivation of the t_2 contribution to the energy proceeds exactly as in the previous sections, and the final result is

$$\begin{aligned}
 E_{t_2} = & \int d\mathbf{r}_{cv_1} d\mathbf{r}_{cv_2} \left\{ i \frac{t_2}{8} \right. \\
 & (\mathbf{J}_n(\mathbf{r}_{cv_1}) + x_2 \mathbf{J}_c(\mathbf{r}_{cv_1})) \cdot \sum_{\sigma\sigma'} \psi_{3b,\sigma}^*(\mathbf{r}_{cv_1}, \mathbf{r}_{cv_2}) \nabla_{v_1} \psi_{3b,\sigma'}(\mathbf{r}_{cv_1}, \mathbf{r}_{cv_2}) \times \langle \sigma | \sigma | \sigma' \rangle \\
 & + \frac{t_{21}}{8} \left(-2\psi_{3b}^*(\mathbf{r}_{cv_1}, \mathbf{r}_{cv_2}) \nabla_{v_1} (n_c(\mathbf{r}_{cv_1}) \nabla_{v_1} \psi_{3b}(\mathbf{r}_{cv_1}, \mathbf{r}_{cv_2})) \right. \\
 & + 2|\psi_{3b}(\mathbf{r}_{cv_1}, \mathbf{r}_{cv_2})|^2 \tau_c(\mathbf{r}_{cv_1}) + |\psi_{3b}(\mathbf{r}_{cv_1}, \mathbf{r}_{cv_2})|^2 \nabla_{v_1}^2 n_c(\mathbf{r}_{cv_1}) \Big) \\
 & + \frac{t_{22}}{8} \left(-2\psi_{3b}^*(\mathbf{r}_{cv_1}, \mathbf{r}_{cv_2}) \nabla_{v_1} (n_n(\mathbf{r}_{cv_1}) \nabla_{v_1} \psi_{3b}(\mathbf{r}_{cv_1}, \mathbf{r}_{cv_2})) \right. \\
 & \left. \left. + 2|\psi_{3b}(\mathbf{r}_{cv_1}, \mathbf{r}_{cv_2})|^2 \tau_n(\mathbf{r}_{cv_1}) + |\psi_{3b}(\mathbf{r}_{cv_1}, \mathbf{r}_{cv_2})|^2 \nabla_{v_1}^2 n_n(\mathbf{r}_{cv_1}) \right) \right\}. \quad (\text{A.38})
 \end{aligned}$$

Again there is an identical contribution from the interaction with the other nucleon, only where n_c , n_n , \mathbf{J}_c , and \mathbf{J}_n depends \mathbf{r}_{cv_2} instead of \mathbf{r}_{cv_1} , and the gradients are also with respect to \mathbf{r}_{cv_2} .

Appendix A.5. W_0 energy contribution

As in a regular Skyrme-Hartree-Fock calculation the spin-orbit part is much simpler to calculate. In this case, using a prime notation to indicate a complex conjugated operator acting to the right, makes the calculation slightly more intuitive. The interaction can be written out explicitly as

$$\begin{aligned}
 V_{jv_1}^{(SO)} &= \frac{i}{4} W_0 (\boldsymbol{\sigma}_j + \boldsymbol{\sigma}_{v_1}) \cdot [(\boldsymbol{\nabla}'_j - \boldsymbol{\nabla}'_{v_1}) \times \delta(\mathbf{r}_j - \mathbf{r}_{cv_1}) (\boldsymbol{\nabla}_j - \boldsymbol{\nabla}_{v_1})] \\
 &= \frac{i}{4} W_0 [\boldsymbol{\sigma}_j \cdot \boldsymbol{\nabla}'_j \times \delta \boldsymbol{\nabla}_j - \boldsymbol{\sigma}_j \cdot \boldsymbol{\nabla}'_{v_1} \times \delta \boldsymbol{\nabla}_j - \boldsymbol{\sigma}_j \cdot \boldsymbol{\nabla}'_j \times \delta \boldsymbol{\nabla}_{v_1} \\
 &\quad + \boldsymbol{\sigma}_j \cdot \boldsymbol{\nabla}'_{v_1} \times \delta \boldsymbol{\nabla}_{v_1} + \boldsymbol{\sigma}_{v_1} \cdot \boldsymbol{\nabla}'_j \times \delta \boldsymbol{\nabla}_j - \boldsymbol{\sigma}_{v_1} \cdot \boldsymbol{\nabla}'_{v_1} \times \delta \boldsymbol{\nabla}_j \\
 &\quad - \boldsymbol{\sigma}_{v_1} \cdot \boldsymbol{\nabla}'_j \times \delta \boldsymbol{\nabla}_{v_1} + \boldsymbol{\sigma}_{v_1} \cdot \boldsymbol{\nabla}'_{v_1} \times \delta \boldsymbol{\nabla}_{v_1}], \tag{A.39}
 \end{aligned}$$

To rewrite this expression a number of common vector identities will be used, along with the assumption of time-reversal symmetry, and the fact that (see Ref. [37])

$$\sum_{i\sigma\sigma'} \psi_{i\sigma}^*(\mathbf{r}) \langle \sigma | \boldsymbol{\sigma} | \sigma' \rangle \psi_{i\sigma'}(\mathbf{r}) = \sum_i \psi_i^*(\mathbf{r}) \boldsymbol{\sigma} \psi_i(\mathbf{r}) = 0, \tag{A.40}$$

where the second equality is just a shorthand notation. The idea is then to eliminate any $\boldsymbol{\nabla}'$ using partial integration, and rewrite the terms into the form $\boldsymbol{\nabla}_A \cdot \boldsymbol{\nabla}_B \times \boldsymbol{\sigma}_B$.

The first term can be rewritten as

$$\begin{aligned}
 \boldsymbol{\sigma}_j \cdot \boldsymbol{\nabla}'_j \times \delta \boldsymbol{\nabla}_j &= -\boldsymbol{\sigma}_j \cdot \boldsymbol{\nabla}'_{v_1} \times \delta \boldsymbol{\nabla}_j - \boldsymbol{\sigma}_j \cdot \boldsymbol{\nabla}_j \times \delta \boldsymbol{\nabla}_j - \boldsymbol{\sigma}_j \cdot \boldsymbol{\nabla}_{v_1} \times \delta \boldsymbol{\nabla}_j \\
 &= -2\delta \boldsymbol{\nabla}_{v_1} \cdot \boldsymbol{\nabla}_j \times \boldsymbol{\sigma}_j, \tag{A.41}
 \end{aligned}$$

as $\boldsymbol{\nabla}_j \cdot \boldsymbol{\nabla}_j \times \boldsymbol{\sigma}_j = 0$, and $-\boldsymbol{\sigma}_j \cdot \boldsymbol{\nabla}'_{v_1} \times \delta \boldsymbol{\nabla}_j = -\boldsymbol{\sigma}_j \cdot \boldsymbol{\nabla}_{v_1} \times \delta \boldsymbol{\nabla}_j$ because of time-reversal symmetry. The second term in Eq. (A.39) follows by the same time-reversal argument.

The third term is rewritten using Eq. (A.40) as

$$\begin{aligned}
 -\boldsymbol{\sigma}_j \cdot \boldsymbol{\nabla}'_j \times \delta \boldsymbol{\nabla}_{v_1} &= \boldsymbol{\sigma}_j \cdot \boldsymbol{\nabla}'_{v_1} \times \delta \boldsymbol{\nabla}_{v_1} + \boldsymbol{\sigma}_j \cdot \boldsymbol{\nabla}_j \times \delta \boldsymbol{\nabla}_{v_1} + \boldsymbol{\sigma}_j \cdot \boldsymbol{\nabla}_{v_1} \times \delta \boldsymbol{\nabla}_{v_1} \\
 &= -\delta \boldsymbol{\nabla}_{v_1} \cdot \boldsymbol{\nabla}_j \times \boldsymbol{\sigma}_j. \tag{A.42}
 \end{aligned}$$

Finally, the fourth term is just zero because of Eq. (A.40). The next four terms follow by symmetry.

After integration over \mathbf{r} , ψ_{3b} depends on $(\mathbf{r}_{cv_1}, \mathbf{r}_{cv_2})$ and ψ_i depends on (\mathbf{r}_{cv_1}) . Using the definitions from Eqs. (A.1), and (A.5), along with Eqs. (A.16) and (A.18) the contribution to the energy from the spin-orbit term becomes

$$\begin{aligned}
 E_{SO} &= -iW_0 \sum_i \int d\mathbf{r}_{cv_1} d\mathbf{r}_{cv_2} \left\{ \right. \\
 &\quad \left. \psi_i^* \psi_{3b}^* (\boldsymbol{\nabla}_{v_1} \cdot \boldsymbol{\nabla}_j \times \boldsymbol{\sigma}_j + \boldsymbol{\nabla}_j \cdot \boldsymbol{\nabla}_{v_1} \times \boldsymbol{\sigma}_{v_1}) \psi_i \psi_{3b} (1 + \delta_{q_i, n}) \right\} \tag{A.43} \\
 &= -\frac{1}{2} W_0 \int d\mathbf{r}_{cv_1} d\mathbf{r}_{cv_2} \left\{ |\psi_{3b}(\mathbf{r}_{cv_1}, \mathbf{r}_{cv_2})|^2 [\boldsymbol{\nabla}_{v_1} \cdot \mathbf{J}_c(\mathbf{r}_{cv_1}) + \boldsymbol{\nabla}_{v_1} \cdot \mathbf{J}_n(\mathbf{r}_{cv_1})] \right\}
 \end{aligned}$$

$$+ i \left[\nabla_{v_1} n_c(\mathbf{r}_{cv_1}) + \nabla_{v_1} n_n(\mathbf{r}_{cv_1}) \right] \cdot \psi_{3b}^*(\mathbf{r}_{cv_1}, \mathbf{r}_{cv_2}) \nabla_{v_1} \psi_{3b}(\mathbf{r}_{cv_1}, \mathbf{r}_{cv_2}) \times \boldsymbol{\sigma}_{v_1} \Big\},$$

with an identical contribution from the other valence neutron only where n_c , n_n , \mathbf{J}_c , and \mathbf{J}_n depends on \mathbf{r}_{cv_2} instead of \mathbf{r}_{cv_1} , and the gradients are also with respect to \mathbf{r}_{cv_2} .

Appendix A.6. Three-body Schrödinger equation

Having derived the energy contribution from the various terms in the Skyrme interaction in the previous sections, and given that the energy must be stationary under individual variation of both the core and three-body wave function, the Schrödinger equation for the three-body part follows from Eqs. (A.28,A.29,A.30,A.35,A.38,A.43). Given that ψ_{3b}^* intentionally has been isolated to the left in all the equations, the variation is trivial.

The three-body Schrödinger equation becomes

$$E_3 \psi_{3b}(\mathbf{r}_{cv_1}, \mathbf{r}_{cv_2}) = \left[T_x + T_y + V_{cv}(\mathbf{r}_{cv_1}) + V_{cv}(\mathbf{r}_{cv_2}) + V_{v_1v_2}(\mathbf{r}_{cv_1}, \mathbf{r}_{cv_2}) + V_3(\mathbf{r}_{cv_1}, \mathbf{r}_{cv_2}) \right] \psi_{3b}(\mathbf{r}_{cv_1}, \mathbf{r}_{cv_2}), \quad (\text{A.44})$$

where T_x and T_y are the kinetic energy operators related to the three-body equation, V_{cv} are the core - valence neutron interaction, $V_{v_1v_2}$ is the interaction between the two valence neutrons, and V_3 is the three-body interaction. The core - valence neutron interaction contains ordinary central, V_{cen} and spin-orbit, V_{SO} terms as well as effective masses, V_{grad} in the form of gradient terms

$$V_{cv}(\mathbf{r}) = V_{cen}(\mathbf{r}) + V_{SO}(\mathbf{r}) + V_{grad}(\mathbf{r}) \quad (\text{A.45})$$

$$V_{cen}(\mathbf{r}) = n_{eff}(\mathbf{r}) + n_{H_c}(\mathbf{r}) + V^C(\mathbf{r}), \quad (\text{A.46})$$

$$V_{SO}(\mathbf{r}) = -i \mathbf{n}_J(\mathbf{r}) \cdot \nabla_r \times \boldsymbol{\sigma}, \quad (\text{A.47})$$

$$V_{grad}(\mathbf{r}) = \nabla_r \cdot (n_a(\mathbf{r}) \nabla_r), \quad (\text{A.48})$$

where n_{H_c} is specifically from the variation of Eq. (A.30). The parameters entering in the three-body equation are

$$\begin{aligned} n_{eff}(\mathbf{r}) &= t_{01} n_c(\mathbf{r}) + \frac{t_{31}}{6} n_c(\mathbf{r}) \left((n_c(\mathbf{r}) + n_3(\mathbf{r}))^\alpha + \alpha n_3(\mathbf{r}) (n_c(\mathbf{r}) + n_3(\mathbf{r}))^{\alpha-1} \right) \\ &\quad - t_{02} n_n(\mathbf{r}) - \frac{t_{32}}{6} n_n(\mathbf{r}) \left((n_c(\mathbf{r}) + n_3(\mathbf{r}))^\alpha + \alpha n_3(\mathbf{r}) (n_c(\mathbf{r}) + n_3(\mathbf{r}))^{\alpha-1} \right) \\ &\quad + \frac{1}{8} \nabla^2 n_c(\mathbf{r}) (-3t_{11} + t_{21}) + \frac{1}{8} \nabla^2 n_n(\mathbf{r}) (3t_{12} + t_{22}) \\ &\quad + \frac{\tau_c(\mathbf{r})}{4} (t_{11} + t_{21}) + \frac{\tau_n(\mathbf{r})}{4} (t_{22} - t_{12}) - \frac{W_0}{2} [\nabla \cdot \mathbf{J}_c(\mathbf{r}) + \nabla \cdot \mathbf{J}_n(\mathbf{r})], \\ n_{H_c}(\mathbf{r}) &= \frac{\alpha}{12} (n_c(\mathbf{r}) + n_3(\mathbf{r}))^{\alpha-1} [t_{31} n_c(\mathbf{r})^2 - t_{32} (n_p(\mathbf{r})^2 + n_n(\mathbf{r})^2)], \\ n_a(\mathbf{r}) &= \frac{1}{4} n_c(\mathbf{r}) (-t_{11} - t_{21}) + \frac{1}{4} n_n(\mathbf{r}) (t_{12} - t_{22}), \\ \mathbf{n}_J(\mathbf{r}) &= \frac{1}{8} [(t_1 - t_2) \mathbf{J}_n(\mathbf{r}) - (t_1 x_1 + t_2 x_2) \mathbf{J}_c(\mathbf{r}) + 4W_0 (\nabla n_c(\mathbf{r}) + \nabla n_n(\mathbf{r}))]. \end{aligned} \quad (\text{A.49})$$

In the case of valence protons the expressions are similar after exchanging neutrons by protons ($n \leftrightarrow p$).

Appendix A.6.1. Core Schrödinger equation. The previous sections focused on the variation with respect to ψ_{3b}^* . From Eq. (20) it is clear that another variation with respect to ψ_i^* is needed. Fortunately, this is fairly straightforward given the previous derivations. The variation will contain two parts; one part from Eq. (15) and one part from Eq. (16).

The part from Eq. (15) is identical to regular Skyrme-Hartree-Fock [37], only $n_c^\alpha \rightarrow (n_c + n_3)^\alpha$ in the t_3 in the Skyrme interaction. The part from Eq. (16) could be calculated exactly as was done in Appendix A.2 to Appendix A.5. However, the only difference would be that the surviving integral would be with respect to \mathbf{r} instead of \mathbf{r}_{cv_1} and \mathbf{r}_{cv_2} , which means that $|\psi_{3b}|^2 \rightarrow n_3$ and likewise for τ_3 and \mathbf{J}_3 . The core Schrödinger equation then becomes

$$\begin{aligned} \epsilon_{iq}\psi_{iq}(\mathbf{r}) = & \left[-\nabla \cdot \frac{\hbar^2}{2m_q^*(\mathbf{r})} \nabla + U_q(\mathbf{r}) - i\mathbf{W}_q(\mathbf{r}) \cdot (\nabla \times \boldsymbol{\sigma}) \right. \\ & \left. - \nabla \cdot \frac{1}{m_q'^*(\mathbf{r})} \nabla + U_q'(\mathbf{r}) - i\mathbf{W}_q'(\mathbf{r}) \cdot (\nabla \times \boldsymbol{\sigma}) \right] \psi_{iq}(r), \end{aligned} \quad (\text{A.50})$$

where a prime indicates the interaction is due to the valence nucleons. The specific interactions entering in the core equation are

$$\begin{aligned} \frac{\hbar^2}{2m_q^*(\mathbf{r})} &= \frac{\hbar^2}{2m_q} + \frac{1}{4} [(t_{11} + t_{21})n_c(\mathbf{r}) + (t_{22} - t_{12})n_q(\mathbf{r})], \\ U_q(\mathbf{r}) &= t_{01}n_c(\mathbf{r}) - t_{02}n_q(\mathbf{r}) + \frac{1}{4}\tau_c(\mathbf{r})[t_{11} + t_{21}] + \frac{1}{4}\tau_q(\mathbf{r})[t_{22} - t_{12}] \\ &+ \frac{t_{31}}{12} (2(n_c(\mathbf{r}) + n_3(\mathbf{r}))^\alpha n_c(\mathbf{r}) + \alpha n_c(\mathbf{r})^2 (n_c(\mathbf{r}) + n_3(\mathbf{r}))^{\alpha-1}) \\ &- \frac{t_{32}}{6} (n_c(\mathbf{r}) + n_3(\mathbf{r}))^\alpha n_q(\mathbf{r}) \\ &- \frac{t_{32}}{12} \alpha (n_c(\mathbf{r}) + n_3(\mathbf{r}))^{\alpha-1} (n_n(\mathbf{r})^2 + n_p(\mathbf{r})^2) \\ &+ \frac{\nabla^2 n_c(\mathbf{r})}{8} (t_{21} - 3t_{11}) + \frac{\nabla^2 n_q(\mathbf{r})}{8} [3t_{12} + t_{22}] \\ &- \frac{W_0}{2} (\nabla \cdot \mathbf{J}_c(\mathbf{r}) + \nabla \cdot \mathbf{J}_q(\mathbf{r})) + V_c^C \end{aligned} \quad (\text{A.51})$$

$$\mathbf{W}_q(\mathbf{r}) = \frac{1}{2}W_0 (\nabla n_c(\mathbf{r}) + \nabla n_q(\mathbf{r})) + \frac{1}{8} ((t_1 - t_2)\mathbf{J}_q - (t_1x_1 + t_2x_2)\mathbf{J}_c),$$

The core-valence neutron interaction basically amounts to adding n_3 to n_n (only some care has to be taken with the t_3 term), if the valence nucleons are neutrons. So, for core nucleons of the same type as the valence neutrons ($s \in N$), the addition to the interaction becomes

$$\begin{aligned} \frac{1}{m_s'^*(\mathbf{r})} &= \frac{1}{4}n_3(\mathbf{r}) [t_{11} - t_{12} + t_{21} + t_{22}], \\ U_s'(\mathbf{r}) &= n_3(\mathbf{r}) (t_{01} - t_{02}) + \frac{1}{4}\tau_3(\mathbf{r}) [t_{11} - t_{12} + t_{21} + t_{22}] \\ &+ \frac{n_3(\mathbf{r})}{6} \left\{ \alpha (n_c(\mathbf{r}) + n_3(\mathbf{r}))^{\alpha-1} (n_c(\mathbf{r})t_{31} - n_n(\mathbf{r})t_{32}) \right\} \end{aligned}$$

$$\begin{aligned}
 & + (n_c(\mathbf{r}) + n_3(\mathbf{r}))^\alpha (t_{31} - t_{32}) \} \\
 & + \frac{1}{8} \nabla^2 n_3(\mathbf{r}) [t_{21} + t_{22} + 3(t_{12} - t_{11})] - W_0 \nabla \cdot \mathbf{J}_3(\mathbf{r}), \\
 \mathbf{W}'_s(\mathbf{r}) & = W_0 \nabla n_3(\mathbf{r}) + \frac{1}{8} \mathbf{J}_3(\mathbf{r}) [t_1 - t_2 - (t_1 x_1 + t_2 x_2)]. \tag{A.52}
 \end{aligned}$$

Likewise, for core nucleons of a different type than the valence neutrons ($d \in Z$) the interaction simplifies to

$$\begin{aligned}
 \frac{1}{m_d^*(\mathbf{r})} & = \frac{1}{4} n_3(\mathbf{r}) [t_{11} + t_{21}], \\
 U'_d(\mathbf{r}) & = t_{01} n_3(\mathbf{r}) + \frac{1}{4} \tau_3(\mathbf{r}) [t_{11} + t_{21}] + \frac{1}{8} \nabla^2 n_3(\mathbf{r}) [t_{21} - 3t_{11}] \\
 & + \frac{n_3(\mathbf{r})}{6} \alpha (n_c(\mathbf{r}) + n_3(\mathbf{r}))^{\alpha-1} (t_{31} n_c(\mathbf{r}) - t_{32} n_n(\mathbf{r})) \\
 & + \frac{n_3(\mathbf{r})}{6} t_{31} (n_c(\mathbf{r}) + n_3(\mathbf{r}))^\alpha - \frac{1}{2} W_0 \nabla \cdot \mathbf{J}_3(\mathbf{r}), \\
 \mathbf{W}'_d(\mathbf{r}) & = \frac{1}{2} W_0 \nabla n_3(\mathbf{r}) - \frac{1}{8} \mathbf{J}_3(\mathbf{r}) [t_1 x_1 + t_2 x_2]. \tag{A.53}
 \end{aligned}$$

In the case of valence protons the expressions are similar after exchanging neutrons by protons ($n \leftrightarrow p$). In the same way $s \in Z$ and $d \in N$. Also, the Coulomb term should be added in this case to U'_s . The Coulomb interaction within the Slater approximation for the exchange part takes the form [92, 115, 187]

$$V_c^C(\mathbf{r}) = \frac{e^2}{2} \int \frac{n_p(\mathbf{r}')}{|\mathbf{r} - \mathbf{r}'|} d\mathbf{r}' - \frac{e^2}{2} \left(\frac{3}{\pi} \right)^{1/3} n_p(\mathbf{r})^{1/3}, \tag{A.54}$$

and similarly for the Coulomb interaction of the valence protons.

Appendix B. New three-body equations

Due to the almost-local, effective masses in Eq. (22) the usual three-body equations [88] change slightly. This is due to the appearance of the $V_{grad}(\mathbf{r})$ term (A.48) into the nucleon-core interaction $V_{cv}(\mathbf{r})$ in Eq.(A.45). Also, since the core is assumed to be spherical all the density functions in Eq.(A.49), and therefore also the potential V_{grad} , do actually depend only on the distance r .

Taking this into account, the almost-local terms are expressed in terms of the Jacobi coordinates from Eq. (28)

$$\nabla \cdot (n_a(r) \nabla) = \frac{\mu_x}{m} \nabla_x \cdot (n_a(r) \nabla_x) = \frac{\mu_x}{m} \{ \nabla_x \}, \tag{B.1}$$

where $\{ \nabla_x \}$ can also be written as

$$\begin{aligned}
 \{ \nabla_x \} & = \nabla_x \cdot (n_a(r) \nabla_x) = n_a(r) \nabla_x^2 + (\nabla_x n_a(r)) \cdot \nabla_x \\
 & = \{ \nabla_x \}_1 + \{ \nabla_x \}_2. \tag{B.2}
 \end{aligned}$$

Let us focus now on the first part in the equation above, $\{\nabla_x\}_1$, which in spherical coordinates takes the form

$$\{\nabla_x\}_1 = n_a(r) \left(\frac{1}{x^2} \frac{\partial}{\partial x} \left(x^2 \frac{\partial}{\partial x} \right) - \frac{\hat{\ell}_x^2}{x^2} \right), \quad (\text{B.3})$$

where $\hat{\ell}_x$ is the usual angular momentum operator associated with the \mathbf{x} Jacobi coordinate. Translation of this into hyperspherical coordinates leads to

$$\begin{aligned} \{\nabla_x\}_1 = n_a(r) & \left(\sin^2 \alpha \frac{\partial^2}{\partial \rho^2} + \frac{2 + \cos^2 \alpha}{\rho} \frac{\partial}{\partial \rho} + \frac{\cos^2 \alpha}{\rho^2} \frac{\partial^2}{\partial \alpha^2} + \frac{2 \cos^3 \alpha}{\rho^2 \sin \alpha} \frac{\partial}{\partial \rho} \right. \\ & \left. + \frac{2 \sin \alpha \cos \alpha}{\rho} \frac{\partial}{\partial \rho} \frac{\partial}{\partial \alpha} - \frac{\hat{\ell}_x^2}{\rho^2 \sin^2 \alpha} \right). \end{aligned} \quad (\text{B.4})$$

The second term in Eq. (B.2), $\{\nabla_x\}_2$, is much simpler, as n_a only depends on r , and it can be written as

$$\{\nabla_x\}_2 = (\nabla_x n_a(r)) \cdot \nabla_x = \frac{dn_a}{dx} \frac{\partial}{\partial x} = \frac{dn_a}{dx} \left(\sin \alpha \frac{\partial}{\partial \rho} + \frac{\cos \alpha}{\rho} \frac{\partial}{\partial \alpha} \right). \quad (\text{B.5})$$

Combining Eqs. (B.4) and (B.5) the full non-local part of the two-body potential given in Eq. (B.2) can be written as

$$\begin{aligned} \nabla_x \cdot (n_a(r) \nabla_x) = n_a \sin^2 \alpha \frac{\partial^2}{\partial \rho^2} & + \left(n_a \frac{2 + \cos^2 \alpha}{\rho} + \frac{dn_a}{dx} \sin \alpha \right) \frac{\partial}{\partial \rho} \\ & + n_a \frac{\sin 2\alpha}{\rho} \frac{\partial}{\partial \rho} \frac{\partial}{\partial \alpha} + n_a \frac{\cos^2 \alpha}{\rho^2} \frac{\partial^2}{\partial \alpha^2} \\ & + \left(n_a \frac{2 \cos^3 \alpha}{\rho^2 \sin \alpha} + \frac{dn_a \cos \alpha}{dx} \frac{1}{\rho} \right) \frac{\partial}{\partial \alpha} - n_a \frac{\hat{\ell}_x^2}{\rho^2 \sin^2 \alpha}. \end{aligned} \quad (\text{B.6})$$

The expression in Eq. (B.6) can be divided in two parts, $\{\nabla_x\}_{pot}$ and $\{\nabla_x\}_{coup}$, given by

$$\begin{aligned} \{\nabla_x\}_{pot} & = n_a \frac{\cos^2 \alpha}{\rho^2} \frac{\partial^2}{\partial \alpha^2} + \left(n_a \frac{2 \cos^3 \alpha}{\rho^2 \sin \alpha} + \frac{dn_a \cos \alpha}{dx} \frac{1}{\rho} \right) \frac{\partial}{\partial \alpha} - n_a \frac{\hat{\ell}_x^2}{\rho^2 \sin^2 \alpha} \\ \{\nabla_x\}_{coup} & = n_a \sin^2 \alpha \frac{\partial^2}{\partial \rho^2} + \left(n_a \frac{2 + \cos^2 \alpha}{\rho} + \frac{dn_a}{dx} \sin \alpha \right) \frac{\partial}{\partial \rho} \\ & + n_a \frac{\sin 2\alpha}{\rho} \frac{\partial}{\partial \rho} \frac{\partial}{\partial \alpha} \\ & = g_1(\rho, \alpha) \frac{\partial^2}{\partial \rho^2} + g_2(\rho, \alpha) \frac{\partial}{\partial \rho} + g_3(\rho, \alpha) \frac{\partial}{\partial \rho} \frac{\partial}{\partial \alpha}, \end{aligned} \quad (\text{B.8})$$

where g_1 , g_2 , and g_3 have been introduced to simplify the notation.

The first term, $\{\nabla_x\}_{pot}$, does not depend on the derivatives of the hyperradius, and it can be fully included in the two-body potential and treated when solving the angular part of the Faddeev equations. The second term, $\{\nabla_x\}_{coup}$, is more complicated due to the derivatives of ρ , as they give rise to new coupling terms between the radial equations, similar to what the usual P 's and Q 's do [88].

Inserting the expanded three-body wave function from Eq. (36) into Eq. (37) and using Eqs. (B.7) and (B.8) the three-body Schrödinger equation becomes

$$\begin{aligned}
 0 = & \sum_m \left[-\frac{15}{4} \frac{1}{\rho^2} f_m \phi_m + \frac{\partial^2 f_m}{\partial \rho^2} \phi_m + 2 \frac{\partial f_m}{\partial \rho} \frac{\partial \phi_m}{\partial \rho} + f_m \frac{\partial^2 \phi_m}{\partial \rho^2} \right. \\
 & - \frac{2\mu_{cv_1} \rho^{5/2}}{\hbar^2} \{ \nabla_{x_{cv_1}} \}_{coup} \frac{1}{\rho^{5/2}} f_m \phi_m - \frac{2\mu_{cv_2} \rho^{5/2}}{\hbar^2} \{ \nabla_{x_{cv_2}} \}_{coup} \frac{1}{\rho^{5/2}} f_m \phi_m \\
 & \left. + \frac{2m(E - V_3)}{\hbar^2} f_m \phi_m - \frac{f_m}{\rho^2} \left(\hat{\Lambda}^2 + \frac{2m\rho^2}{\hbar^2} (\tilde{V}_{12} + \tilde{V}_{13} + \tilde{V}_{23}) \right) \phi_m \right], \quad (\text{B.9})
 \end{aligned}$$

where μ_{cv_i} is the reduced mass between the core and the i 'th valence nucleon, $\{ \nabla_{x_{cv_i}} \}_{coup}$ is the related new coupling, and the two-body potentials \tilde{V}_{ij} contain the usual central and spin orbit terms as well as the $\{ \nabla_x \}_{pot}$ term discussed above.

It should be noted that the angular functions ϕ_n are defined to be the eigenfunctions of the angular part of the Faddeev equations

$$\left(\hat{\Lambda}^2 + \frac{2m\rho^2}{\hbar^2} (\tilde{V}_{12} + \tilde{V}_{13} + \tilde{V}_{23}) \right) \phi_n(\rho, \Omega) = \lambda_n(\rho) \phi_n(\rho, \Omega), \quad (\text{B.10})$$

in such a way that multiplying Eq. (B.9) from the left by $\phi_n^*(\rho, \Omega)$ and integrating over Ω Eq. (B.9) results in

$$\begin{aligned}
 0 = & \frac{\partial^2 f_n}{\partial \rho^2} - \frac{\lambda_n + \frac{15}{4}}{\rho^2} f_n + \frac{2m(E_3 - V_3)}{\hbar^2} f_n + 2 \sum_m P_{nm} \frac{\partial f_m}{\partial \rho} + \sum_m Q_{nm} f_m \\
 & - \sum_m \left\langle \Phi_n \left| \frac{2\mu_{12} \rho^{5/2}}{\hbar^2} \{ \nabla_{x_{12}} \}_{coup} + \frac{2\mu_{13} \rho^{5/2}}{\hbar^2} \{ \nabla_{x_{13}} \}_{coup} \right| \frac{f_m \Phi_m}{\rho^{5/2}} \right\rangle_{\Omega} \quad (\text{B.11})
 \end{aligned}$$

which except for the last term is the usual coupled set of radial equations [88].

The last line in Eq. (B.11) gives rise to quite a few additional couplings. In the case of two identical valence particles they are the same for both valence nucleons, resulting in a factor of 2. For this particular case the radial equations are

$$\begin{aligned}
 0 = & \frac{\partial^2 f_n}{\partial \rho^2} - \frac{\lambda_n + \frac{15}{4}}{\rho^2} f_n + \frac{2m(E_3 - V_3)}{\hbar^2} f_n + 2 \sum_m P_{nm} \frac{\partial f_m}{\partial \rho} + \sum_m Q_{nm} f_m \\
 & - \sum_m (2C_{nm}^{(12)} + C_{nm}^{(21)} + C_{nm}^{(31)} - \frac{5}{\rho} C_{nm}) \frac{\partial f_m}{\partial \rho} - \sum_m C_{nm} \frac{\partial^2 f_m}{\partial \rho^2} \quad (\text{B.12}) \\
 & - \sum_m (C_{nm}^{(13)} + C_{nm}^{(22)} + C_{nm}^{(32)} + \frac{35}{4\rho^2} C_{nm} - \frac{5}{\rho} C_{nm}^{(12)} - \frac{5}{2\rho} C_{nm}^{(21)} - \frac{5}{2\rho} C_{nm}^{(31)}) f_m,
 \end{aligned}$$

where

$$\begin{aligned}
 C_{nm} &= 2 \frac{2\mu_x}{\hbar^2} \langle \phi_n | g_1(\rho, \alpha) | \phi_m \rangle_{\Omega}, \\
 C_{nm}^{(12)} &= 2 \frac{2\mu_x}{\hbar^2} \left\langle \phi_n \left| g_1(\rho, \alpha) \frac{\partial}{\partial \rho} \right| \phi_m \right\rangle_{\Omega}, \\
 C_{nm}^{(13)} &= 2 \frac{2\mu_x}{\hbar^2} \left\langle \phi_n \left| g_1(\rho, \alpha) \frac{\partial^2}{\partial \rho^2} \right| \phi_m \right\rangle_{\Omega}, \\
 C_{nm}^{(21)} &= 2 \frac{2\mu_x}{\hbar^2} \langle \phi_n | g_2(\rho, \alpha) | \phi_m \rangle_{\Omega},
 \end{aligned}$$

$$\begin{aligned}
 C_{nm}^{(22)} &= 2 \frac{2\mu_x}{\hbar^2} \left\langle \phi_n \left| g_2(\rho, \alpha) \frac{\partial}{\partial \rho} \right| \phi_m \right\rangle_{\Omega}, \\
 C_{nm}^{(31)} &= 2 \frac{2\mu_x}{\hbar^2} \left\langle \phi_n \left| g_3(\rho, \alpha) \left| \frac{\partial \phi_m}{\partial \alpha} \right. \right\rangle_{\Omega}, \\
 C_{nm}^{(32)} &= 2 \frac{2\mu_x}{\hbar^2} \left\langle \phi_n \left| g_3(\rho, \alpha) \frac{\partial}{\partial \rho} \left| \frac{\partial \phi_m}{\partial \alpha} \right. \right\rangle_{\Omega}.
 \end{aligned} \tag{B.13}$$

These new coupling terms can be easily computed. The only problem comes from the C_{nm} , which mixes the second derivatives of the radial functions. However, the non-diagonal C_{nm} terms are very small, and the simplest is to neglect them, in such a way that the coupled set of radial equations to be solved are

$$\begin{aligned}
 0 &= (1 - C_{nm}) \frac{\partial^2 f_n}{\partial \rho^2} - \frac{\lambda_n + \frac{15}{4}}{\rho^2} f_n + \frac{2m(E - V_3)}{\hbar^2} f_n \\
 &+ 2 \sum_m (P_{nm} + P'_{nm}) \frac{\partial f_m}{\partial \rho} + \sum_m (Q_{nm} + Q'_{nm}) f_m,
 \end{aligned} \tag{B.14}$$

$$\begin{aligned}
 Q'_{nm} &= \frac{5}{\rho} C_{nm}^{(12)} + \frac{5}{2\rho} C_{nm}^{(21)} + \frac{5}{2\rho} C_{nm}^{(31)} - C_{nm}^{(13)} - C_{nm}^{(22)} - C_{nm}^{(32)} - \frac{35}{4} \frac{1}{\rho^2} C_{nm}, \\
 P'_{nm} &= \frac{5}{2\rho} C_{nm} - C_{nm}^{(12)} - \frac{1}{2} C_{nm}^{(21)} - \frac{1}{2} C_{nm}^{(31)}.
 \end{aligned} \tag{B.15}$$

References

- [1] Siemens P J and Jensen A S 1987 *Elements of Nuclei, Lecture Notes and Supplements in Physics* Addison-Wesley, Reading Massachusetts
- [2] Bohr A and Mottelson B R 1969 *Nuclear Structure, Vols. 1 and 2.* Benjamin, Reading Massachusetts
- [3] Ioffe B L 2006 *Prog. Part. Nucl. Phys.* **56** 232, 2006.
- [4] Berakdar J and Briggs J S 1994 *Phys. Rev. Lett.* **72** 3799
- [5] Brockmann R and Machleidt R 1990 *Phys. Rev. C* **42** 1965
- [6] Saito S, Okai S, Tamagaki R and Yasuno M 1973 *Prog. Theor. Phys.* **50** 1561
- [7] W.D. Myers and W.J. Swiatecki, *Ann.Phys.* **55** (1969) 595, **84** (1974) 186.
- [8] Langanke K and Martínez-Pinedo G 2003 *Rev. Mod. Phys.* **75** 819
- [9] Fedorov D V, Garrido E and Jensen A S 2003 *Few-body Syst.* **33** 153
- [10] Chernykh M, Feldmeier H, Neff T, von Neumann-Cosel P and Richter A 2007 *Phys. Rev. Lett.* **98** 032501
- [11] Epelbaum E, Krebs H, Lee D and Meißner U- G 2011 *Phys. Rev. Lett.* **106** 192501
- [12] Garrido E, Jensen A S and Fedorov D V 2015 *Phys. Rev. C* **91** 054003
- [13] Čížek J 1966 *J. Chem. Phys.* **45** 4256.
- [14] Bartlett R J and Purvis G D 1978 *Int. J. Quantum Chem.* **14** 561
- [15] Frederico T, Delfino A, Tomio L, and Yamashita M T 2012 *Prog. Part. Nucl. Phys.* **67** 939
- [16] Braaten B and Hammer H- W 2006 *Phys. Rep.* **428** 259
- [17] Hoffman C R *et al* 2009 *Phys. Lett. B* **672** 17
- [18] Caesar Ch *et al* 2013 *Phys. Rev. C* **88** 034313
- [19] Kohley Z *et al* 2013 *Phys. Rev. Lett.* **110** 152501
- [20] Kondo Y *et al* 2016 *Phys. Rev. Lett.* **116** 102503
- [21] Hove D, Garrido E, Sarriguren P, Fedorov D V, Fynbo H O U, Jensen A S and Zinner N T 2017 *Phys. Rev. C* **95** 061301
- [22] Hagen G, Hagen P, Hammer H- W and Platter L 2013 *Phys. Rev. Lett.* **111** 132501

- [23] Feshbach H 1958 *Ann. Phys.* **5** 357
- [24] Harvey M and Khanna F C 1970 *Nucl. Phys. A* **152** 588
- [25] Burgess C P 2007 *Annu. Rev. Nucl. Part. Sci.* **57** 329
- [26] Epelbaum E, Hammer H- W and Meißner U- G 2009 *Rev. Mod. Phys.* **81** 1773
- [27] Machleidt R and Entem D R 2011 *Phys. Rep.* **503** 1
- [28] Hammer H- W, Ji C and Phillips D R 2017 *J. Phys. G: Nucl. Part. Phys.* **44** 103002
- [29] Goepfert Mayer M 1950 *Phys. Rev.* **78** 16
- [30] Goepfert Mayer M 1950 *Phys. Rev.* **78** 22
- [31] Barrett B R, Navrátil P and Vary J P 2013 *Progr. Part. Nucl. Phys.* **69** 131
- [32] Nogga A, Navrátil P, Barrett B R and Vary J P 2006 *Phys. Rev. C* **73** 064002
- [33] Caurier E, Martínez-Pinedo G, Nowacki F, Poves A and Zuker A P 2005 *Rev. Mod. Phys.* **77** 427
- [34] Bogner S, Kuo T T S, Coraggio L, Covello A and Itaco N 2002 *Phys. Rev. C* **65** 051301
- [35] Sebe T and Harvey M 1968 *At. Energy of Canada Ltd., Chalk River Rep. No.* **3007**
- [36] Nilsson S G 1955 *Mat Fys. Medd. Dan. Vid. Selsk.* **29** 2
- [37] Vautherin D and Brink D M 1972 *Phys. Rev. C* **5** 626
- [38] Schrieffer J R 1964 *Theory of superconductivity.* Benjamin, New York
- [39] Bender M, Heenen P- H and Reinhard P- G 2003 *Rev. Mod. Phys.* **75** 121
- [40] Goriely S, Hilaire S, Girod M and Péru S 2009 *Phys. Rev. Lett.* **102** 242501
- [41] Vary J P, Sauer P U and Wong C W 1973 *Phys. Rev. C* **7** 1776
- [42] Barrett B R and Kirson M W 1973 *Adv. Nucl. Phys.* **6** 219
- [43] Brown G E, Kuo T T S, Holt J W and Lee S 2010 *The Nucleon-Nucleon Interaction and the Nuclear Many-Body Problem: Selected Papers of Gerald E. Brown and TTS Kuo.* World Scientific, 2010.
- [44] Navrátil P, Quaglioni S, Stetcu I and Barrett B R 2009 *J. Phys. G: Nucl. Part. Phys.* **36** 083101
- [45] Faddeev L D 1961 *Sov. Phys. JETP* **12** 1014
- [46] Yakubovsky O A 1967 *Sov. J. Nucl. Phys.* **5** 937
- [47] Jensen A S, Riisager K, Fedorov D V and Garrido E 2004 *Rev. Mod. Phys.* **76** 215
- [48] Riisager K 2013 *Phys. Scr. T* **152** 014001
- [49] Adhikari H, Frederico T and Goldman I D 1995 *Phys. Rev. Lett.* **74** 487
- [50] Frederico T, Tomio L, Delfino A, Hadizadeh M R and Yamahita M T 2011 *Few-body Syst.* **51** 87
- [51] Wheeler J A 1937 *Phys. Rev.* **52** 1083
- [52] Wheeler J A 1937 *Phys. Rev.* **52** 1107
- [53] Griffin J J and Wheeler J A 1957 *Phys. Rev.* **108** 311
- [54] Hill D L and Wheeler J A 1953 *Phys. Rev.* **89** 1102
- [55] Tang Y- C, LeMere M and Thompsom D R 1978 *Phys. Rep.* **47** 167
- [56] Brink D M and Weiguny A 1968 *Nucl. Phys. A* **120** 59
- [57] Thompson D R, LeMere M and Tang Y C 1977 *Nucl. Phys. A* **286** 53
- [58] Hesse M, Roland J and Baye D 2002 *Nucl. Phys. A* **709** 184
- [59] Pieper S C and Wiringa R B 2001 *Annu. Rev. Nucl. Part. Sci.* **51** 53
- [60] Shimizu N, Abe T, Tsunoda Y, Utsuno Y, Yoshida T, Mizusaki T, Honma M and Otsuka T 2012 *Progr. Theor. Exp. Phys.* **2012** 01A205
- [61] Hisashi H 1991 *Nucl. Phys. A* **522** 257
- [62] Kanada-Enyo Y, Horiuchi H and Ono A 1995 *Phys. Rev. C* **52** 628
- [63] Feldmeier H 1990 *Nucl. Phys. A* **515** 147
- [64] Aichelin J and Stoecker H 1986 *Phys. Lett. B* **176** 14
- [65] Kanada-En'yo Y, Kimura M and Horiuchi H 2003 *C. R. Physique* **4** 497
- [66] Feldmeier H, Bieler K and Schnack J 1995 *Nucl. Phys. A* **586** 493
- [67] Neff T and Feldmeier H 2004 *Nucl. Phys. A* **738** 357
- [68] Kanada-En'yo Y 1998 *Phys. Rev. Lett.* **81** 5291
- [69] Kanada-En'yo Y and Horiuchi H 2001 *Prog. Theor. Phys. Suppl.* **142** 205
- [70] Leidemann W and Orlandini G 2013 *Progr. Part. Nucl. Phys.* **68** 158

- [71] Coester F 1958 *Nucl. Phys.* **7** 421
- [72] Coester F and Kümmel H 1960 *Nucl. Phys.* **17** 477
- [73] Bogner S K, Thomas Kuo T T S and Schwenk A 2003 *Phys. Rep.* **386** 1
- [74] Wiringa R B, Stoks V G J and Schiavilla R 1995 *Phys. Rev. C* **51** 38
- [75] Machleidt R 2001 *Phys. Rev. C* **63** 024001
- [76] Weinberg S 1990 *Phys. Lett. B* **251** 288
- [77] Epelbaum E, Gloeckle W and Meißner U- G 1998 *Nucl. Phys. A* **637** 107
- [78] Hagen G, Hjorth-Jensen M, Jansen G R and Papenbrock T 2016 *Phys. Scr.* **91** 063006
- [79] Hagen G, Papenbrock T, Hjorth-Jensen M and Dean D J 2014 *Rep. Prog. Phys.* **77** 096302
- [80] Michel N, Nazarewicz W, Płoszajczak M and Vertse T 2008 *J. Phys. G: Nucl. Part. Phys.* **36** 013101
- [81] Hagen G, Dean D J, Hjorth-Jensen M, Papenbrock T 2007 *Phys. Lett. B* **656** 169
- [82] Hagen G, Hjorth-Jensen M, Jansen G R, Machleidt R, Papenbrock T 2012 *Phys. Rev. Lett.* **108** 242501
- [83] Wegner F 1994 *Ann. Phys. (Berlin)* **506** 77
- [84] Głazek S D and Wilson K G 1993 *Phys. Rev. D* **48** 5863
- [85] Tsukiyama K Bogner S K and Schwenk A 2011 *Phys. Rev. Lett.* **106** 222502
- [86] Hergert H, Bogner S K, Morris T D, Schwenk A and Tsukiyama K 2016 *Phys. Rep.* **621** 165
- [87] Hove D, Garrido E, Jensen A S, Sarriguren P, Fynbo H O U, Fedorov D V and Zinner N T 2017 *Few-body Syst.* **58** 33
- [88] Nielsen E, Fedorov D V, Jensen A S and Garrido E 2001 *Phys. Rep.* **347** 373
- [89] Vautherin D 1973 *Phys. Rev. C* **7** 296
- [90] Schunck N, Dobaczewski J, McDonnell J, Moré J, Nazarewicz W, Sarich J and Stoitsov M V 2010 *Phys. Rev. C* **81** 024316
- [91] Bonneau L, Quentin P and Möller P 2007 *Phys. Rev. C* **76** 024320
- [92] Chabanat E, Bonche P, Haensel P, Meyer J and Schaeffer R 1998 *Nucl. Phys. A* **635** 231
- [93] Decharge J, Girod M and Gogny D 1975 *Phys. Lett. B* **55** 361
- [94] Flocard H, Quentin P, Kerman A K and Vautherin D 1973 *Nucl. Phys. A* **203** 433
- [95] Macek J 1968 *J. Phys. B: At. Mol. Phys.* **1** 831
- [96] Macek J H 2002 *Few-body Syst.* **31** 241
- [97] Hove D, Fedorov D V, Jensen A S, Riisager K and Zinner N T 2014 *Eur. Phys. J. A* **50** 181
- [98] Garrido E, Fedorov D V and Jensen A S 1997 *Nucl. Phys. A* **617** 153
- [99] Garrido E, Fedorov D V and Jensen A S 1999 *Nucl. Phys. A* **650** 247
- [100] Thomas L H 1935 *Phys. Rev.* **47** 903
- [101] Efimov V 1970 *Phys. Lett. B* **33** 563
- [102] Garrido E and Moya De Guerra E 1999 *Nucl. Phys. A* **650** 387
- [103] Dechargé J and Gogny D 1980 *Phys. Rev. C* **21** 1568
- [104] Fedorov D V and Jensen A S 1996 *Phys. Lett. B* **389** 631
- [105] Noble J V 1970 *Phys. Lett. B* **31** 253
- [106] Bartel J, Quentin Ph, Brack M, Guet C and Håkansson H- B 1982 *Nucl. Phys. A* **386** 79
- [107] Beiner M, Flocard H, Van Giai N and Quentin Ph 1975 *Nucl. Phys. A* **238** 29
- [108] Hagino K and Sagawa H 2016 *Phys. Rev. C* **93** 034330
- [109] Zinser M *et al* 1997 *Nucl. Phys. A* **619** 151
- [110] Garrido E, Fedorov D V and Jensen A S 1996 *Phys. Rev. C* **53** 3159
- [111] Garrido E, Fedorov D V and Jensen A S 2001 *Nucl. Phys. A* **695** 109
- [112] Garrido E, Fedorov D V and Jensen A S 1999 *Phys. Rev. C* **59** 1272
- [113] Garrido E, Fedorov D V and Jensen A S 2002 *Nucl. Phys. A* **700** 117
- [114] Hove D, Jensen A S Riisager K 2013 *Phys. Rev. C* **88** 064329
- [115] Erler J, Klüpfel P and Reinhard P G 2011 *J. Phys. G: Nucl. Part. Phys.* **38** 033101
- [116] Bhattacharya M and Gangopadhyay G 2005 *Phys. Rev. C* **72** 044318
- [117] Hove D, Garrido E, Sarriguren P, Fedorov D V, Fynbo H O U, Jensen A S and Zinner N T 2018

- Phys. Rev. Lett.* **120** 052502
- [118] Riisager K, Jensen A S and Møller P 1992 *Nucl. Phys. A* **548** 393
- [119] Misu T, Nazarewicz W and Åberg S 1997 *Nucl. Phys. A* **614** 44
- [120] Zhongzhou R and Gongou X 1990 *Phys. Lett. B* **252** 311
- [121] Fedorov D V and Jensen A S 1993 *Phys. Rev. Lett.* **71** 4103
- [122] Jensen A S and Fedorov D V 2003 *Europhys. Lett.* **62** 336
- [123] Garrido E, Fedorov D V and Jensen A S 2006 *Phys. Rev. Lett.* **96** 112501
- [124] Mazumdar I and Bhasin V S 1997 *Phys. Rev. C* **56** R5
- [125] Mazumdar I, Arora V and Bhasin V S 2000 *Phys. Rev. C* **61** 051303
- [126] Zhongzhou R 1994 *Phys. Rev. C* **49** 1281
- [127] Zhongzhou R, Otsuka T, Sakurai H and Ishihara M 1997 *J. Phys. G: Nucl. Part. Phys.* **23** 597
- [128] Meng J, Toki H, Zeng J Y, Zhang S Q and Zhou S- G 2002 *Phys. Rev. C* **65** 041302
- [129] Garrido E, Fedorov D V, Fynbo H O U and Jensen A S 2007 *Nucl. Phys. A* **781** 387
- [130] Garrido E, Fedorov D V, Jensen A S and Fynbo H O U 2006 *Nucl. Phys. A* **766** 74
- [131] Zaccanti M, Deissler B, D'Errico C, Fattori M, Jona-Lasinio M, Müller S, Roati G, Inguscio M and Modugno G 2009 *Nat. Phys.* **5** 586–591
- [132] Gullans M U, Diehl S, Rittenhouse S T, Ruzic B P, D'Incao J P, Julienne P, Gorshkov A V and Taylor J M 2017 *Phys. Rev. Lett.* **119** 233601
- [133] Wallace R K and Woosley So E 1981 *Astrophys. J. Suppl. Ser.* **45** 389
- [134] Mathews G J and Ward R A 1985 *Rep. Prog. Phys.* **48** 1371
- [135] Bartlett A, Görres J, Mathews G J, Otsuki K, Wiescher M, Frekers D, Mengoni A and Tostevin J 2006 *Phys. Rev. C* **74** 015802
- [136] Burbidge E M, Burbidge G R, Fowler W A and Hoyle F 1957 *Rev. Mod. Phys.* **29** 547
- [137] Arnould M and Goriely S 2003 *Phys. Rep.* **384** 1
- [138] Rauscher T, Dauphas N, Dillmann I, Fröhlich C, Fülöp Zs and Gyürky Gy 2013 *Rep. Prog. Phys.* **76** 066201
- [139] Reifarh R, Lederer C and Käppeler 2014 *J. Phys. G: Nucl. Part. Phys.* **41** 053101
- [140] Wallerstein G *et al* 1997 *Rev. Mod. Phys.* **69** 995
- [141] Schatz H, Aprahamian A, Barnard V, Bildsten L, Cumming A, Ouellette M, Rauscher T, Thielemann F- K and Wiescher M 2001 *Phys. Rev. Lett.* **86** 3471
- [142] Schatz H *et al* 1998 *Phys. Rep.* **294** 167
- [143] Wöhr A *et al* 2004 *Nucl. Phys. A* **742** 349
- [144] Robertson R G H and Austin S M 1974 *Phys. Rev. C* **9** 1801
- [145] Baumann P *et al* 1994 *Phys. Rev. C* **50** 1180
- [146] Piqueras I *et al* 2003 *Eur. Phys. J. A* **16** 313
- [147] Schury P *et al* 2007 *Phys. Rev. C* **75** 055801
- [148] Tu X L *et al* 2011 *Phys. Rev. Lett.* **106** 112501
- [149] Hove D, Jensen A S, Fynbo H O U, Zinner N T, Fedorov D V and Garrido E 2016 *Phys. Rev. C* **93** 024601
- [150] De Diego R, Garrido E, Fedorov D V and Jensen A S 2011 *Phys. Lett. B* **695** 324
- [151] Hove D, Garrido E, Jensen A S, Sarriguren P, Fynbo H O U, Fedorov D V and Zinner N T 2017 *preprint arXiv:1709.01270*
- [152] Hove D, Garrido E, Jensen A S, Fynbo H O U, Fedorov D V and Zinner N T 2017 *Few-body Syst.* **58** 13
- [153] Del Santo M *et al* 2014 *Phys. Lett. B* **738** 453
- [154] Audi G, Wang M, Wapstra A H, Kondev F G, MacCormick M, Xu X and Pfeiffer B 2012 *Chinese Phys. C* **36** 1287
- [155] Garrido E 2015 *Few-body Syst.* **56** 829
- [156] Iliadis C 2015 *Nuclear physics of stars* John Wiley & Sons
- [157] Nichols A J *et al* 2014 *Phys. Lett. B* **733** 52
- [158] Neseraja C D 2014 *Nucl. Data Sheets* **115** 1

- [159] McCutchan E A 2012 *Nucl. Data Sheets* **113** 1735
- [160] Grigorenko L V, Johnson R C, Mukha I G, Thompson I J and Zhukov M V 2001 *Phys. Rev. C* **64** 054002
- [161] Álvarez-Rodríguez R, Fynbo H O U, Jensen A S and Garrido E 2008 *Phys. Rev. Lett.* **100** 192501
- [162] Grigorenko L V and Zhukov M V 2005 *Phys. Rev. C* **72** 015803
- [163] Chekanov S *et al* 2007 *Eur. Phys. J. C* **51** 289
- [164] Garrido E, Fedorov D V, Jensen A S and Fynbo H O U 2005 *Nucl. Phys. A* **748** 27
- [165] Brink D M and Boeker E 1967 *Nucl. Phys. A* **91** 1
- [166] Berger J F, Girod M and Gogny D 1984 *Nucl. Phys. A* **428** 23
- [167] Chappert F, Girod M and Hilaire S 2008 *Phys. Lett. B* **668** 420
- [168] Chappert F, Pillet N, Girod M and Berger J- F 2015 *Phys. Rev. C* **91** 034312
- [169] Rodríguez-Guzmán R, Sarriguren P and Robledo L M 2010 *Phys. Rev. C* **82** 061302
- [170] Rodríguez-Guzmán R, Sarriguren P and Robledo L M 2010 *Phys. Rev. C* **82** 044318
- [171] Rodríguez-Guzmán R, Sarriguren P and Robledo L M 2011 *Phys. Rev. C* **83** 044307
- [172] Pérez-Martín S and Robledo L M 2008 *Phys. Rev. C* **78** 014304
- [173] Maruhn J and Greiner W 1972 *Z. Physik* **251** 431
- [174] Gherghescu R A 2003 *Phys. Rev. C* **67** 014309
- [175] Díaz-Torres A 2008 *Phys. Rev. Lett.* **101** 122501
- [176] Yamashita M T, Fedorov D V and Jensen A S 2010 *Phys. Rev. A* **81** 063607
- [177] Yamashita M T, Fedorov D V and Jensen A S 2011 *Few-body Syst.* **51** 135
- [178] Jensen A S, Fedorov D V and Garrido E 2010 *J. Phys. G: Nucl. Part. Phys.* **37** 064027
- [179] Garrido E, Jensen A S and Fedorov D V 2014 *Few-body Syst.* **55** 101
- [180] Romero-Redondo C, Garrido E, Barletta P, Kievsky A and Viviani M 2011 *Phys. Rev. A* **83** 022705
- [181] Timofeyuk N K and Johnson R C 1999 *Phys. Rev. C* **59** 1545
- [182] Cobis A, Fedorov D V and Jensen A S 1997 *J. Phys. G: Nucl. Part. Phys.* **23** 401
- [183] Zinner N T and Jensen A S 2005 *J. Phys. G: Nucl. Part. Phys.* **40** 053101
- [184] Hansen P G and Jonson B 1987 *Eurphys. Lett.* **4** 409
- [185] Kraemer T *et al* 2006 *Nature* **440** 315
- [186] Kunitski M *et al* 2015 *Science* **348** 551
- [187] Gu H Q, Liang H, Long W H, Van Giai N and Meng J 2013 *Phys. Rev. C* **87** 041301